Carl von Ossietzky Universität Oldenburg

Doctoral Thesis

Spatial and Temporal Correlations in Human Cortical Dynamics: Implications for Cognition and Epilepsy Management

Author:
Paul Manuel Müller
Date of Birth:
29.03.1996
Place of Birth:
Hanau, DE

Supervisors:
Prof. Dr. Thilo Gross
PD Dr. med. Christian Meisel

A thesis submitted in partial fulfillment of the requirements for the degree and title of Doctor of Science (Doctor rer. nat.) at the

School of Mathematics and Sciences,
Carl von Ossietzky Universität Oldenburg

by

Paul Manuel Müller,
Research Group Biodiversity Theory,
Institute for Chemistry and Biology of the Marine Environment

in cooperation with the

Research Group Computational Neurology,
Charité - Universitätsmedizin Berlin.

Gutachter:
Prof. Dr. Thilo Gross
PD Dr. med. Christian Meisel

Weitere Mitglieder der Prüfungskommission:
Prof. Dr. Alexander Hartmann

Tag der Disputation: 04.04.2025

Eidesstattliche Erklärung

Hiermit erkläre ich, Paul Manuel Müller, an Eides statt, dass ich diese Dissertationsschrift, „Spatial and Temporal Correlations in Human Cortical Dynamics: Implications for Cognition and Epilepsy Management“, selbstständig und ohne fremde unzulässige Hilfe und ohne Benutzung anderer als der angegebenen Hilfsmittel angefertigt und die aus fremden Quellen direkt oder indirekt übernommenen Gedanken als solche kenntlich gemacht habe.

Der Inhalt der Dissertation wurde nicht schon überwiegend für eine eigenen Bachelor-, Master-, Diplom- oder ähnliche Prüfungsarbeit verwendet.

Ich erkläre weiter, dass mir die Grundsätze zur Sicherung guter wissenschaftlicher Praxis an der Carl von Ossietzky Universität Oldenburg bekannt sind und dass ich die dort niedergelegten Prinzipien wissenschaftlicher Arbeit und Veröffentlichung befolgt habe.

Ich habe im Zusammenhang mit dem Promotionsvorhaben keine kommerziellen Vermittlungs- oder Beratungsdienste (Promotionsberatung) in Anspruch genommen.

Unterschrift:

_____

Ort, Datum:

_____

Abstract

Spatial and Temporal Correlations in Human Cortical Dynamics: Implications for Cognition and Epilepsy Management

People with epilepsy often suffer from cognitive impairment, reducing their quality of life. These impairments and their severity are heterogeneous between individuals, e.g., about 30% retain close to normal cognitive function. Despite established associations with disease and treatment-related factors, a comprehensive understanding of the underlying principles for these cognitive impairments is missing.

Brain criticality is the theoretical principle that optimal cognitive function emerges when cortical dynamics are in the vicinity of a phase transition, e.g., between vanishing and runaway excitation. A balanced network structure is essential to achieving brain criticality, and long-range spatial and temporal correlations (SCs and TCs) are maximized at criticality. These correlations are established measures of information integration, which is essential for cognitive function. However, due to experimental limitations like short recording durations or coarse spatiotemporal resolution, the link between criticality, SCs, TCs, and cognitive function remains elusive. Additionally, cortical network dynamics and cognition-affecting mechanisms, such as antiseizure medication or slow-wave activity, introduce variability into the measurements.

To address these limitations, this thesis combines neuronal model simulations, multi-day intracranial electroencephalography (iEEG) recordings from 104 persons with epilepsy, magnetic resonance imaging (MRI) from 127 persons with epilepsy, and 16 cognitive measures. Specifically, we investigated the variability of SCs and TCs in computational and cortical network dynamics, i.e., in iEEG, and gray matter thickness changes with respect to cognitive performance.

We found that SCs and TCs exhibited substantial co-variability and declined during slow-wave activity and under antiseizure medication. Interictal epileptiform discharges led to shorter TCs but increased SCs. Further, TCs increased with the functional hierarchy, showing their importance for more complex computations. Ultimately, we found a correlation between shorter TCs and cognitive impairments. Additionally, we found that groups with more severe cognitive impairments exhibited broader gray matter changes compared to healthy controls. These changes were predictive of the risk of cognitive worsening after epilepsy surgery.

In short, our model simulations and experimental findings support brain criticality as a unifying framework to explain cognitive function. They also suggest that deviations from criticality, potentially induced by network structure changes, could be a critical factor in understanding the variability in cognitive impairments.

Zusammenfassung

Spatial and Temporal Correlations in Human Cortical Dynamics: Implications for Cognition and Epilepsy Management

Menschen mit Epilepsie leiden häufig unter kognitiven Beeinträchtigungen, die ihre Lebensqualität mindern. Diese Beeinträchtigungen und ihr Schweregrad sind personenabhängig, z. B. haben etwa 30 % der Betroffenen nahezu normale kognitive Fähigkeiten. Ein umfassendes Verständnis der diesen kognitiven Beeinträchtigungen zugrunde liegenden Prinzipien fehlt trotz etablierter Zusammenhänge mit krankheits- und behandlungsbedingten Faktoren.

Die Kritikalität des Gehirns ist das theoretische Prinzip, dass optimale kognitive Funktion auftritt, weil sich die kortikale Dynamik in der Nähe eines Phasenübergangs befindet, z. B. zwischen verschwindender und übermäßiger Aktivität. Eine ausgewogene Netzwerkstruktur ist für die Kritikalität des Gehirns entscheidend und am kritischen Punkt sind räumliche und zeitliche Korrelationen (SCs und TCs) maximal. Diese SCs und TCs sind ein bewährtes Maß für Informationsintegration, welche für kognitive Funktionen wichtig ist. Aufgrund von experimentellen Einschränkungen wie kurzer Aufzeichnungsdauer oder nicht hinreichender räumlicher und zeitlicher Auflösung ist der Zusammenhang zwischen Kritikalität, SCs, TCs und kognitiver Funktion jedoch weiterhin unklar. Darüber hinaus führen Mechanismen, die die Dynamik des kortikalen Netzwerks und die kognitiven Fähigkeiten beeinflussen, wie z. B. Antikonvulsiva oder Tiefschlaf, zu erhöhter Variabilität in den Messungen.

Um diese Einschränkungen zu adressieren, kombiniert diese Arbeit neuronale Modellsimulationen, mehrtägige intrakranielle Elektroenzephalographie (iEEG) Aufzeichnungen von 104 Personen mit Epilepsie, Magnetresonanztomographie (MRT) von 127 Personen mit Epilepsie und 16 kognitive Messungen. Insbesondere untersuchten wir die Variabilität von SCs und TCs in der Dynamik von simulierten und kortikalen Netzwerken (im iEEG), sowie Dickeveränderungen der grauen Substanz in Bezug auf die kognitive Leistung.

Wir fanden eine starke Kovariabilität von SCs und TCs sowie die Abnahme von SCs und TCs während Slow-Wave-Aktivität und unter Antikonvulsiva. Interiktale epileptiforme Entladungen führten zu kürzeren TCs, aber erhöhten SCs. Außerdem nahmen TCs entlang der funktionellen Hierarchie zu, was ihre Bedeutung für komplexere Berechnungen verdeutlicht. Schließlich fanden wir eine Korrelation zwischen kürzeren TCs und kognitiven Beeinträchtigungen. Zudem stellten wir fest, dass Gruppen mit schwereren kognitiven Beeinträchtigungen im Vergleich zu gesunden Kontrollpersonen viele Veränderungen der grauen Gehirnsubstanz aufwiesen. Diese Veränderungen waren prädiktiv für das Risiko einer kognitiven Verschlechterung nach einer Epilepsieoperation.

Zusammenfassend unterstützen unsere Modellsimulationen und experimentellen Ergebnisse die Kritikalität des Gehirns als vereinheitlichenden Rahmen zur Erklärung

von Kognition. Sie deuten auch darauf hin, dass Abweichungen von der Kritikalität, z.B. verursacht durch Netzwerkstrukturveränderungen, ein entscheidender Faktor für das Verständnis der Variabilität kognitiver Beeinträchtigungen sein könnten.

Acknowledgements

I want to express my deepest gratitude to all the individuals who supported me on my academic path and throughout my life. You all were integral to the completion of this thesis.

First, I want to thank my supervisors:

- Christian Meisel, you always found the time to discuss the *Science* behind my projects, provided continuous feedback, and always pushed me to never stop thinking.
- Thilo Gross, thank you for giving me the opportunity to pursue this thesis and share your insights and ideas about my project and the scientific field.

Furthermore, my thank goes to all my colleagues and friends in the Computational Neurology Lab at Charité who supported me, provided feedback and loved brainstorming with me:

- I want to thank Gadi Miron, with whom I worked for a long and fruitful time. I appreciate every discussion we had, as it always helped me understand and brought together the clinical and theoretical points of view. While your academic advice was invaluable, your emotional support might have been even more so. Thank you for being there for me through the lows and highs.
- My special thanks also go to Simon Vock. I am unable to count the times we stood in front of a whiteboard and just tried to make sense of our results and thoughts together. I enjoyed every single one of these encounters, as I also did every one of our coffee and cake breaks.

Further, I want to extend my thanks to all my other collaborators and the research environment at Charité:

- Martin Holtkamp ensured we could get all the needed data and provided important clinical feedback.
- I want to acknowledge the HPC for Research cluster of the Berlin Institute of Health and the Scientific Computing of the IT Division at the Charité - Universitätsmedizin Berlin for providing computational resources that have contributed to the research results reported in this thesis.

I also want to thank everybody who proofread my thesis: Alexander Nelde, Bethany Stieve, Chiara Mielau, Christina Biermann-Müller, Gadi Miron, Laura Krumm, Lucas Kluge, Maximilian Schöls, Robert Salzwedel, Robert Terziev, Simon Vock, and Tobias Müller. Without you, this document would be unreadable and confusing.

Finally, thank you to my friends and family for their continuous support. I know I can count on you, and you will always be there for me.

- In particular, I want to thank my mother, Christina, you will always hold the title for supporting me for the longest time in my life, and I am extremely grateful for it.
- Further, I want to thank Bethany for the intense emotional over the last 3 years and the endless hours of talks and phone calls necessary for this.
- Lastly, I need to thank my eight wonderful niblings, Nuri, Alwin, Yanka, Tilla, Leonora, Fridolin, Esra, and Keke, who were the absolute best at distracting me from my thesis and thus gave me the breaks I needed to recharge.

Contents

List of Figures

List of Tables

List of Publications

- ◦ Miron, G., **Müller, P. M.**, & Holtkamp, M. (2022). Diagnostic and prognostic value of EEG patterns recorded on foramen ovale and epidural peg electrodes. Clinical Neurophysiology, 143, 107–115. https://doi.org/10.1016/j.clinph.2022.08.027

- ◦ Miron, G.*, **Müller, P. M.***, Holtkamp, M., & Meisel, C. (2023). Prediction of epilepsy surgery outcome using foramen ovale EEG – a machine learning approach. Epilepsy Research, 107111. https://doi.org/10.1016/j.eplepsyres.2023.107111

- • **Müller, P. M.**, & Meisel, C. (2023). Spatial and temporal correlations in human cortex are inherently linked and predicted by functional hierarchy, vigilance state as well as antiepileptic drug load. PLOS Computational Biology, 19(3), e1010919. https://dx.plos.org/10.1371/journal.pcbi.1010919

- • Miron, G.*, **Müller, P. M.***, Hohmann, L., Oltmanns, F., Holtkamp, M., Meisel, C.*, & Chien, C.* (2024). Cortical Thickness Patterns of Cognitive Impairment Phenotypes in Drug-Resistant Temporal Lobe Epilepsy. Annals of Neurology, 95(5), 984–997. https://doi.org/10.1002/ana.26893

- ◦ Kashyap, A., **Müller, P.**, Miron, G., & Meisel, C. (2024). Critical dynamics and interictal epileptiform discharge: A comparative analysis with respect to tracking seizure risk cycles. Frontiers in Network Physiology, 4, 1420217. https://doi.org/10.3389/fnetp.2024.1420217

- • **Müller, P. M.***, Miron, G.*, Holtkamp, M., & Meisel, C. (2024). Critical dynamics predict cognitive performance and are disrupted by epileptic spikes, antiseizure medication and slow-wave activity. In Revision at Proceedings of the National Academy of Sciences of the United States of America. Preprint at https://doi.org/10.1101/2024.08.19.24312223

* Equal contribution

Bold text marks my own authorship in the publication.

• mark the publication which were included in this thesis.

◦ mark all other publications I authored during my time as a PhD candidate.

List of Abbreviations

ACC	**A**nterior **C**ingulate **C**ortex
ASM	**A**nti-**S**eizure **M**edication
DFA	**D**etrended **F**luctuation **A**nalysis
DRE	**D**rug-**R**esistant **E**pilepsy
EEG	**E**lectro**e**ncephalo**g**raphy
FI	**F**ocal **I**mpairment
fMRI	**F**unctional **M**agnetic **R**esonance **I**maging
GABA	**G**amma-**A**mino**b**utyric **A**cid
HCP	**H**uman **C**onnectome **P**roject
IED	**I**nterictal **E**pileptifrom **D**ischarge
IC-CoDE	**I**nternational **C**lassification of **Co**gnitive **D**isorders in **E**pilepsy
iEEG	**I**nvasive **E**lectroenc**e**phalo**g**raphy
ILAE	**I**nternational **L**eague **A**gainst **E**pilepsy
MDI	**M**ulti-**D**omain **I**mpairment
MEG	**M**agneto**e**ncephalo**g**raphy
MI	**M**inimal **I**mpairment
MRI	**M**agnetic **R**esonance **I**maging
MT	**M**edial **T**emporal Areas in Visual Cortex
NREM	**N**on-**R**apid **E**ye **M**ovement **S**leep
LIP	**L**ateral **I**ntra**P**arietal Area in Visual Cortex
LPFC	**L**ateral **Pref**rontal **C**ortex
OFC	**O**rbito**f**rontal **C**ortex
PwDRE	**P**atients **w**ith **D**rug-**R**esistant **E**pilepsy
PwE	**P**atients **w**ith **E**pilepsy
REM	**R**apid **E**ye **M**ovement **S**leep
ROI	**R**egion **O**f **I**terest
SCs	**S**patial **C**orrelations
SOC	**S**elf-**O**rganized **C**riticality
SOZ	**S**eizure **O**nset **Z**one
SUDEP	**S**udden **U**nexpected **D**eath in **E**pilepsy
SWA	**S**low-**W**ave **A**ctivity
SWS	**S**low-**W**ave **S**leep
TCs	**T**emporal **C**orrelations
TLE	**T**emporal **L**obe **E**pilepsy

Chapter 1

Introduction

The human brain is a highly advanced and flexible information-processing system that excels at solving complex problems. It analyzes, combines, and contextualizes countless inputs and stimuli to interpret its environment and make decisions. Therefore, it must integrate much information across time and space. At the same time, the brain remains flexible and is not restricted to well-defined tasks alone. The human brain can solve a seemingly infinite number of different tasks. In short, the brain solves complex and specific problems without over-specialization.

Naturally, one wonders how the brain maintains this remarkable capacity for complex computations. Specifically, which general principles allow the brain to integrate vast amounts of information over time and space? To explore the underlying principles, researchers have brought forward different hypotheses combining ideas, among others, from neurology, neuroscience, and branches of physics, like dynamical systems theory. This interdisciplinary approach offers promising insights into understanding the brain's computational abilities.

Consequently, this thesis also sits at the intersection between fields, i.e., neuroscience, neurology, and physics. It aims to first provide insights into how cortical dynamics are correlated via space and time. Therefore, it will analyze a neuronal network model and human intracranial EEG data in the context of the brain criticality hypothesis which makes predictions for cortical dynamics and cognition. Ultimately, the goal of this thesis is to link theoretically driven measures of cortical networks and their dynamics to cognitive performance.

Brain Criticality

The brain criticality hypothesis predicts that cortical networks are in the vicinity of a critical point that optimizes information processing (Beggs, 2022a; Chialvo, 2004; Shew & Plenz, 2013). Experimental findings of long-ranged correlations and power-law distributions have been supporting this hypothesis (Beggs & Plenz, 2003; Linkenkaer-Hansen et al., 2001; Shew et al., 2009, 2011).

Optimal Information Processing at Criticality

A delicate balance of the dynamics close to a phase transition, e.g., between static and chaotic activity, characterizes this critical state. In models, the critical state has been proven to optimize information capacity and transmission (Beggs & Plenz, 2003; Langton, 1990; Shew et al., 2011), dynamical range (Kinouchi & Copelli, 2006; Shew et al., 2009), or the number of metastable states (Haldeman & Beggs, 2005).

In a seminal study, Langton, 1990 analyzed the properties of criticality in a deterministic model. Langton, 1990 showed that the model's dynamics could be tuned between static and chaotic activity. Albeit static activity was stable and thus could conserve information well; it was not flexible, and information could not travel through the network. Conversely, chaotic activity changed quickly so that information could travel. However, repeated interactions disturbed the information and led to the failure of information conservation. Between these two extremes Langton, 1990 identified a critical point, i.e., the phase transition between stasis and chaos. He found that the trade-off between information conservation, transmission, and interactions at the critical point could optimize information processing.

Extending upon this deterministic model, researchers explored stochastic models that yielded similar results. For instance, the branching process also optimizes information theoretical measures at the critical point (Beggs, 2022a; Beggs & Plenz, 2003; Haldeman & Beggs, 2005). In branching-like models, the connection strength between units and the probability of one unit exciting another determine the dynamics and can be tuned to criticality (Beggs & Plenz, 2003; Haldeman & Beggs, 2005; Harris, 1964), (Section 2.1.2). This emphasizes the importance of an adequate neuronal network structure for critical dynamics.

These models lay the foundation for the hypothesis that cortical networks operates at or close to the critical point. Criticality could help to understand the remarkable information-processing capabilities of the human brain. While being close to the critical point would allow cortical networks to perform complex tasks and stay flexible, deviations could lead to cognitive deficits (Zimmern, 2020).

Self-Organized Criticality

Even though theory showed that criticality optimizes information processing, the critical state is a finely balanced state that may be hard to achieve and maintain, particularly for large and complex systems like the human brain. Adaptive self-organization provides plausible mechanisms for the emergence of criticality without system-wide control (Bak et al., 1988; Bornholdt & Röhl, 2003), (Section 2.1.3). Such self-organized criticality (SOC) can rely only on local rules. For example, a neuron grows a synapse if its state remains unchanged or loses one if it changes in a specific time (Bornholdt & Röhl, 2003). Such a system can evolve its structure to the critical point and maintain it there, making criticality plausible even in large complex systems, like the human brain (Bornholdt & Röhl, 2003; Hesse & Gross, 2014). Conversely, the failure of SOC

might be linked to malignant neuronal dynamics, like seizure generation (Meisel et al., 2012).

Experimental Evidence for Criticality

While the critical point is well-defined in theoretical models, researchers looked for experimental evidence in the form of specific characteristics in neuronal data. In particular, power laws are an essential characteristic of criticality, leading to scale-free behavior and perturbations decaying geometrically instead of exponentially fast (Goldenfeld, 1992), (Section 2.1.1).

On the one hand, Beggs and Plenz, 2003 found such power laws in the distribution of cascades of activated electrodes and called these cascades neuronal avalanches (Section 2.1.4). Since then, many researchers identified power law distributions of neuronal avalanches in cortical slices (Beggs & Plenz, 2004; Friedman et al., 2012; Klaus et al., 2011; Shew et al., 2009, 2011; Yang et al., 2012), rats (Ribeiro et al., 2010; Shew et al., 2011), awake monkeys (Petermann et al., 2009; Shew et al., 2011), or humans (Priesemann et al., 2013).

On the other hand, perturbations decaying according to a power law lead to long-range correlation both in time and across network sites (Goldenfeld, 1992; Langton, 1990). For example, long-range temporal correlations were identified in human scalp electroencephalography (EEG) (Berthouze et al., 2010; Linkenkaer-Hansen et al., 2001; Meisel, Bailey, et al., 2017) and intracranial EEG (iEEG) (Worrell et al., 2002), (Section 2.1.5). Thus, this research proved the importance of long-range correlations as a hallmark for criticality (Jensen, 2021).

In short, the brain criticality hypothesis suggests that the brain's proximity to a critical point can explain its information-processing and thus cognitive capabilities. The critical point is achieved for balanced network structures, and long-ranged correlations and power-law distributions provide experimental evidence for it.

Cognitive Impairment in Epilepsy

Brain criticality might help to understand cognitive impairments which are a common comorbidity in neuropsychiatric disorders. Particularly, persons with epilepsy (PwE) often show cognitive deficits, which can adversely impact their quality of life (Lin et al., 2012). However, there is considerable variability in the degree of cognitive impairment between PwE, and up to 30% retain cognition close to the healthy population (McDonald et al., 2023). The causes for these impairments can be multifactorial. Impacting factors include the underlying etiology of the disease, such as mesial temporal sclerosis, epileptic activity like interictal epileptiform discharges (IEDs), mediated disturbances, like disrupted sleep patterns, or even treatment-induced influences like antiseizure medication (ASM) (Elger et al., 2004; Wodeyar et al., 2024). While these

factors and their impacts on cognition are well established, the neuronal basis for cognitive function and the cognitive heterogeneity in PwE remains largely unexplored.

However, the brain criticality framework offers a unifying explanation for this cognitive heterogeneity in PwE. If cortical network dynamics are close to a critical point which optimizes information processing then deviations from the critical point could result in cognitive impairment. Specifically, both neuronal network structure and dynamics have been proven crucial components for cognition (Bassett & Sporns, 2017; Friston, 2009; Sporns, 2010) and criticality (Beggs & Plenz, 2003; Haldeman & Beggs, 2005; Larremore et al., 2011). Thus, deviations of either network structure or cortical dynamics could induce drifts away from criticality and lead to impaired cognition. These relationships to cognition will be investigated in this thesis.

Limitations of Previous Research on Brain Criticality

Despite the theoretical arguments and experimental evidence for brain criticality, some challenges validating brain criticality and its advantages for human cortical network dynamics remain. For instance, although theory proved the advantages of brain criticality for cognition, experimental evidence remains sparse. Studies investigating this connection were often limited to single cognitive tests, short recording duration, low temporal resolution, or coarse spatial coverage (Kardan et al., 2023; Mahjoory et al., 2019; Palva et al., 2013; Wasmuht et al., 2018). For example, short scalp EEG recordings can neither record high-frequency components nor track long-term changes in cortical dynamics, and they are often more prone to muscle artifacts. Alternatively, single cognitive tests might not adequately assess general cognitive function.

Particularly, the issue of short recording duration parallels one common critique when analyzing brain criticality related measures. Short recording durations allow only the assessment of a snapshot of the cortical state and, consequently, one point in the parameter space with respect to criticality. However, first, cortical networks might not always maintain the same spot in this parameter space, and second, tuning cortical network dynamics through the parameter space is essential to draw more robust conclusions on its proximity to criticality (Beggs, 2022b; Beggs & Timme, 2012; Mariani et al., 2022).

Variations of Spatial and Temporal Correlations

These limitations also affected research on spatial and temporal correlations (SCs and TCs) which are measures for information integration and a hallmark of criticality (Cavagna et al., 2010; Jensen, 2021; Linkenkaer-Hansen et al., 2001). SCs and TCs can be extracted solely from time series and positional data and do not require the careful setting of a threshold discerning active from inactive activity as necessary for neuronal avalanche analysis (Beggs & Plenz, 2003; Touboul & Destexhe, 2010).

While SCs and TCs were mostly studied independently over a short time, some studies have identified multiple mechanisms altering specifically TCs on longer time

scales. First, TCs were found to change as a function of the sleep-wake cycle and were especially hemmed by slow-wave activity (SWA) (Meisel, Bailey, et al., 2017; Meisel, Klaus, et al., 2017; Xu et al., 2024). Second, external factors, like antiseizure medication (ASM), were proven to perturb TCs (Meisel, 2020). Nonetheless, how SCs change under these mechanisms and how SCs and TCs are interlinked remains unexplored. Other factors could impact SCs and TCs as well. For example, epileptic activity like interictal epileptiform discharges (IEDs) have been linked to cognitive deficits (Ciliento et al., 2023; Devulder et al., 2024; Kleen & Kirsch, 2017; Kleen et al., 2013; Lam et al., 2017), which might be explained by IEDs altering SCs and TCs. However, the distinct impact of IEDs on SCs and TCs and their relationship to criticality requires further investigation.

Furthermore, TCs were found to be heterogeneous across the cortex. Notably, research in non-human primates showed that TCs increase along the functional information processing hierarchy, i.e., from single sensory stimulus evaluation over input integration to complex tasks and decision-making (Murray et al., 2014). Even though for humans, there is evidence for TCs increasing along the functional hierarchy from magnetoencephalography (MEG) (Golesorkhi, Gomez-Pilar, Tumati, et al., 2021) and functional MRI (fMRI)(Raut et al., 2020), definitive evidence in iEEG is still missing (Golesorkhi, Gomez-Pilar, Zilio, et al., 2021).

1.1 Research Hypothess

To extend previous research and overcome its limitations, like the singular assessment of SCs or TCs in short recordings, this thesis investigates the co-variability of and perturbative impacts on SCs and TCs. Specifically, it evaluates the following hypotheses in both neuronal network simulations (Chapter 4) and in iEEG data from persons with drug-resistant epilepsy (PwDRE) (Chapter 5):

1. SCs and TCs co-vary over time.
2. In humans, TCs increase along the functional hierarchy, as proven for non-human primates (Murray et al., 2014).
3. SCs and TCs are disrupted by the sleep-wake cycle, especially slow-wave activity.
4. Interictal epileptiform discharges perturb SCs and TCs.
5. Antiseizure medications lead to a decline of SCs and TCs.

Verifying these hypotheses could lead to an increased understanding of the interplay of SCs and TCs with each other and with perturbative mechanisms. This could provide valuable insights into the brain's relative proximity to criticality in different states and consequently help to investigate the link between brain criticality and cognitive function. To explicitly explore the connection between cortical structure, network dynamics and cognition this thesis will additionally investigate the following hypotheses (Chapter 6):

6. Groups with more severe cognitive impairments show distinct and more widespread cortical thickness abnormalities.

7. Shorter TCs predict cognitive impairment.

Establishing such connections between structure, dynamics, and cognition could help to understand if brain criticality underlies cortical function as a unifying principle. Additionally, answering these questions could also help to improve diagnostics and management in neurological disorders such as epilepsy, for example prediction of the risk of epilepsy surgery (Chapter 6).

1.2 Research Methodology

To address the experimental limitations of previous studies and the critique concerning brain criticality, we will investigate multi-day high-resolution iEEG recordings from 104 persons with drug-resistant epilepsy (PwDRE) and cortex-wide structural magnetic resonance imaging (MRI) from 124 PwDRE, together with a large cognitive test battery of up to 16 measures from five cognitive domains, e.g., the language or attention domain.

Our analysis is guided by a neuronal network model (Chapter 4) consisting of excitatory and inhibitory binary neurons with distance-dependent connectivity. This model can be tuned with respect to criticality and introduces mechanisms for slow-wave activity, interictal epileptiform discharges, and antiseizure medication. In this model SCs and TCs can be extracted directly from the neuronal activity. The model will be used to justify the predictions of hypotheses 1-5. These predictions are then tested for SCs and TCs extracted from multi-day iEEG data (Chapter 5). Specifically, SCs and TCs are derived from the broadband high-γ power, as this has been proven to be a proxy for the underlying neuronal network activity (Buzsáki et al., 2012; Manning et al., 2009; Miller, 2010; Whittingstall & Logothetis, 2009). TCs are then analyzed from regions along the visual pathway as in Murray et al., 2014 (research question 2). Slow-wave activity and interictal epileptiform discharges are scored by validated algorithms (Reed et al., 2017) & (Quon et al., 2022) and compared to the SCs and TCs fluctuations (research hypotheses 3 and 4). Further, antiseizure medication (ASMs) data was gathered from the available patient data and SCs and TCs were analyzed with respect to the ASM (hypothesis 5).

To test if cortical structure deviations correlate with cognitive impairment (hypothesis 6), cortical gray matter thicknesses are extracted from MRI in PwDRE and aligned with a large cognitive test battery (Chapter 6). To characterize the severity of cognitive impairment, the PwDREs are grouped into cognitive phenotypes according to International Classification of Cognitive Disorders in Epilepsy (IC-CoDE) criteria (McDonald et al., 2023). This framework provides a comprehensive assessment of the cognitive impairment going further than single tests by grouping patients into minimal, focal, or multi-domain impaired phenotypes. Then, for each phenotype, cortical

thickness deviations are analyzed. If the healthy cortical network structure leads to criticality and thus optimizes cognition, cognitive impairment might show as deviations from this structure. Independently, we will investigate if the cortical thickness changes of these PwDRE can predict the risk of cognitive deterioration after epilepsy surgery.

To link cortical dynamics with cognitive performance (hypothesis 7), TCs are measured in PwDRE and aligned with a large cognitive test battery (Chapter 6). Particularly, brain criticality predicts that long TCs are a sign of proximity to the critical point and, hence, good cognitive performance. In contrast, shorter TCs could indicate deviations from criticality, leading to impaired cognition, e.g., attention impairment.

In short, this thesis has two main goals. The first goal is to provide a comprehensive, model-guided analysis of SCs and TCs in cortical dynamics. The second goal is to connect both changes in cortical structure and SCs and TCs to cognitive impairment. Brain criticality guides the investigation and provides a unifying framework for the mechanisms affecting cognition.

This thesis is structured as follows. Chapter 2 summarizes the theoretical and literature background to brain criticality and epilepsy. Chapter 3 introduces the methods and data used throughout this thesis. The focus of Chapter 4 is to investigate SCs and TCs in a neuronal network model. Further, SWA, IEDs, and ASMs are added as perturbative mechanisms on the dynamics and, consequently, SCs and TCs. Chapter 5 tests the model's predictions and characterizes SCs and TCs in human iEEG recordings. The investigation focuses on the co-variability of SCs and TCs, the hierarchical ordering of TCs, and the impact of perturbative mechanisms on them. To test the predictions from brain criticality about cognition, Chapter 6 investigates cognitive impairment in PwDRE. First, we investigate the association between cortical thickness variations and the severity of cognitive impairment. Second, TCs are correlated with cognitive domain impairments. Both Chapter 5 and Chapter 6 end with a section putting the results into context with existing literature and explaining the limitations of the respective analyses. The main discussion, particularly in the context of brain criticality, is in Chapter 7. At the end of Chapter 7, a section provides an outlook on potential implications for clinical applications and future research.

Chapter 2

Foundational Concepts and Literature Review

This chapter introduces the theoretical and experimental environment in which this thesis is set. The first part covers brain criticality as the underlying theoretical framework. The second part focuses on epilepsy, as the data analyzed later originates from persons with epilepsy (PwE).

2.1 The Brain Criticality Hypothesis

In order to understand the brain criticality hypothesis, we first need to establish what a critical point is. First, this is illustrated in a simple but tractable system (Section 2.1.1). Second, the critical point's unique benefits for information processing are discussed within the branching processes (Section 2.1.2). The branching process will set the stage for the model simulations in this thesis (Chapter 4). Third follows a summary of important contributions to the field, i.e., how self-organization could lead to criticality (Section 2.1.3), the emergence of neuronal avalanches (Section 2.1.4), and how distant time points become correlated (Section 2.1.5). Then, the criticality discussion ends in Section 2.2 with three specific contributions that inspired the investigations in this thesis (Chapter 5).

2.1.1 Criticality in a One-Dimensional System

To set the stage, we will investigate a simple non-linear system following the line of thought by Gross, 2021. The system may be described by only one variable $x(t)$, which changes over time t. To improve readability, we omit the explicit time dependency from now on and only write x. In the context of cortical network dynamics, x could be the average neuronal activity.

In the absence of an external stimulus, x evolves over time, and its rate of change can be written as

$$\frac{d}{dt}x = f(x, p) \ . \tag{2.1}$$

Here, f is a non-linear function describing how the current state of x influences its change $\frac{d}{dt}x$. Further, p is a so-called control parameter. In the brain context, p could be interpreted as the excitation-inhibition balance between the neurons, which is thought essential for controlling activity propagation in cortical networks (Poil et al., 2012). For example, if excitation outweighs inhibition, activity will grow. If inhibition dominates, activity wanes eventually.

When cortical networks are in their resting state activity neither explodes nor is completely absent. While it is an oversimplification to say the average resting activity is constant, it is helpful to assume so for illustrative purposes, i.e., the system is at a fixed point x^*. At the fixed point, no change over time can be observed

$$\frac{d}{dt}x^* = 0 \,. \tag{2.2}$$

Consequently, the fixed point can be found by solving

$$f(x^*, p) = 0 \,. \tag{2.3}$$

In an ideal scenario, the system would stay indefinitely at this fixed point if it is not perturbed. However, the brain is constantly exposed to external stimuli and internal changes. Therefore, we will investigate how the system behaves if subjugated to a small perturbation δ from the fixed point. Inserting the perturbation around the fixed point $x^* + \delta$ into Eq. (2.1) yields

$$\frac{d}{dt}(x^* + \delta) = f(x^* + \delta, p) \,, \tag{2.4}$$

$$\frac{d}{dt}\delta = f(x^* + \delta, p) \,. \tag{2.5}$$

The time derivative of the fixed point x^* is zero due to Eq. (2.2).

To analyze this, $f(x^* + \delta, p)$ is Taylor expanded around the fixed point

$$f(x^* + \delta, p) = \underbrace{f(x^*, p)}_{=0,\ Eq.\ (2.3)} + \delta f'(x^*, p) + \frac{1}{2}\delta^2 f''(x^*, p) + O(\delta^3) \,, \tag{2.6}$$

$$f(x^* + \delta, p) \approx \delta f'(x^*, p) \,. \tag{2.7}$$

Higher than first-order terms have been neglected, as they are comparably small as long as the perturbation is small.

For example, $\delta = 0.01 \Rightarrow \delta^2 = 0.0001$ shows that already the quadratic term is considerably smaller than the linear. This assumption is the basis for linear stability analysis in dynamical systems' theory (see for instance (Strogatz, 2015)). Combining Eq. (2.5) and Eq. (2.7) yields

$$\frac{d}{dt}\delta \approx \delta f'(x^*, p) \,. \tag{2.8}$$

This is a linear differential equation in δ, which can be solved using an exponential ansatz, leading to

$$\delta(t) = \delta(0)\mathrm{e}^{t \cdot f'(x^*,p)} \ . \tag{2.9}$$

Here, $\delta(0)$ comes from an integration constant and can be fixed by knowing the initial condition. To interpret this solution we have to ask how $f'(x^*, p)$ behaves:

- If $f'(x^*, p) < 0$, any small perturbation decays exponentially. The system returns to its fixed point, rapidly losing information about the perturbation. This could be understood as the brain returning quickly to its resting state.
- If $f'(x^*, p) > 0$, the system is unstable. Small perturbations grow exponentially, pushing the system away from the fixed point. This scenario seems implausible for a stable brain state as it describes dynamics that do not return to the resting state and thus are unstable.

Critical Slowing Down

In the previous section, we have learned how the system behaves for $f'(x^*, p^*) \neq 0$. The system was stable for $f'(x^*, p) < 0$ and unstable for $f'(x^*, p) > 0$. However, the dynamics become more complex at the transition point between these two regimes, i.e., $f'(x^*, p) = 0$. This point is also called the critical point and will be the subject of the following section.

Let us first assume that such a point exists, and we can choose p so that $f'(x^*, p^*) = 0$. As $f'(x^*, p^*) = 0$, one can no longer neglect the second order term in the Taylor expansion from Eq. (2.6) because the first order term vanishes. Therefore, with Eq. (2.6) and Eq. (2.5) it follows

$$\frac{d}{dt}\delta \approx \frac{1}{2}\delta^2 f''(x^*, p) \ . \tag{2.10}$$

This differential equation can be solved using separation of variables. However, first, we recognize the trivial case of $\delta = 0$, which would solve the equation. This case would not introduce any change to the system around the fixed point and is thus not interesting. Excluding this case, one can write

$$\frac{d\delta}{\delta^2} = \frac{1}{2} dt f''(x^*, p) \ , \tag{2.11}$$

$$\int \frac{d\delta}{\delta^2} = \frac{1}{2} \int dt f''(x^*, p) \ , \tag{2.12}$$

$$\Rightarrow -\frac{1}{\delta} + C = \frac{1}{2} t \cdot f''(x^*, p) \ . \tag{2.13}$$

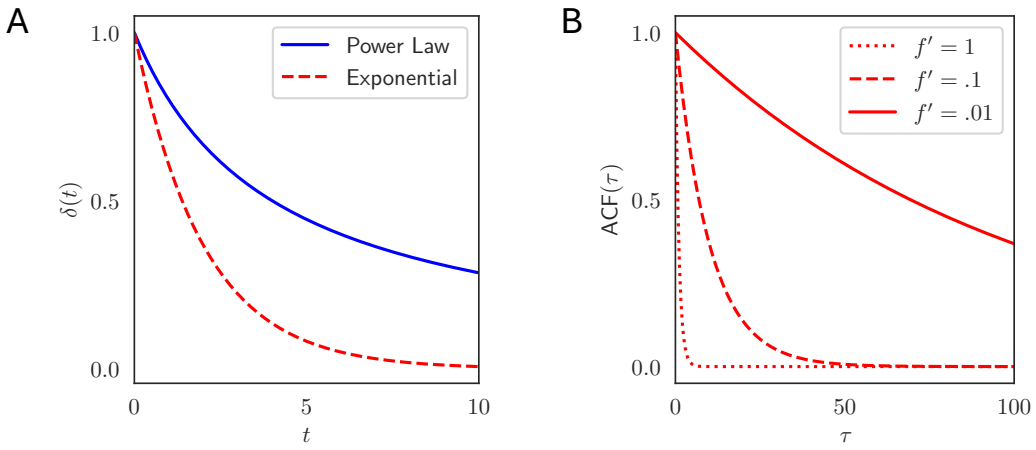

FIGURE 2.1: Dynamics at Criticality: **A** Power law and exponential decay of the perturbation δ as in Eq. (2.9) and Eq. (2.14) respectively. **B** Slowing of the auto-correlation function (ACF) approaching the critical point where f' vanishes (Eq. (2.23)).

Here, C is an integration constant. Now, this can be solved for δ

$$\delta(t) = \frac{1}{C - \frac{1}{2}t \cdot f''(x^*, p)} \,. \tag{2.14}$$

Notably, this solution is no longer an exponential function as Eq. (2.9) but a power law. For $t \gg 0$ it even simplifies to

$$\delta(t) \approx \frac{-2}{t \cdot f''(x^*, p)} \,. \tag{2.15}$$

For large t, this function will always decay considerably slower than Eq. (2.9), illustrated in Fig. 2.1 A. Thus, the information about said perturbations, or at least parts of the information, stays in the system for a longer time. This power law decay at the critical point is at the root of the phenomenon referred to as "Critical Slowing Down", which describes the slow decay of perturbations in the vicinity of the critical point (M. Scheffer et al., 2009). Furthermore, this power law is the root of many power laws encountered at the critical point (Gross, 2021). We will see more examples of power laws at the critical point in Section 2.1.4.

This example gave us an idea of the dynamics at the critical point and how perturbations stay in the system for a longer time, thus leading to long-ranged correlations. We will revisit the critical point in a more illustrative model in Section 2.1.2, discussing further properties of the critical point and why it could be beneficial for cortical dynamics. Before doing so, we want to have another look at the dynamics, not exactly at, but close to the critical point.

Auto-Correlation Close to Criticality

While perturbations persist for a long time at the critical point, one can already observe if a system approaches the critical point. One method for this is to look at the signal's auto-correlation function (ACF). The ACF assesses how similar a signal is with a time-delayed version of itself. For a stationary process, it is defined as

$$\mathrm{ACF}(\tau) = \mathrm{E}[x(t) \cdot x(t+\tau)] \,. \tag{2.16}$$

Here, τ is a time delay, and $\mathrm{E}[\cdot]$ denotes the expectation value concerning time t.

We will now analyze the ACF of the perturbation in the vicinity of the critical point and assume that the system is stable first, i.e., $f'(x^*, p) < 0$. Therefore, we will plug Eq. (2.9) into the definition of the ACF and later analyze what happens if $f'(x^*, p)$ approaches zero.

$$\mathrm{ACF}(\tau) = \mathrm{E}[\delta(t)\delta(t+\tau)] \,. \tag{2.17}$$

$$= \mathrm{E}\left[\delta(0)\mathrm{e}^{t\cdot f'(x^*,p)}\delta(0)\mathrm{e}^{(t+\tau)\cdot f'(x^*,p)}\right] \,, \tag{2.18}$$

$$= \mathrm{E}\left[\delta(0)^2\mathrm{e}^{f'(x^*,p)(2t+\tau)}\right] \,, \tag{2.19}$$

$$= \mathrm{E}\left[\delta(0)^2\mathrm{e}^{f'(x^*,p)2t}\mathrm{e}^{f'(x^*,p)\tau}\right] \,. \tag{2.20}$$

The last exponential function term does not explicitly depend on t but only on τ. Hence, one can pull it out of the expectation value

$$\mathrm{ACF}(\tau) = \mathrm{e}^{f'(x^*,p)\tau}\mathrm{E}\left[\delta(0)^2\mathrm{e}^{f'(x^*,p)2t}\right] \,, \tag{2.21}$$

$$= \mathrm{e}^{f'(x^*,p)\tau}\mathrm{E}\left[\left(\delta(0)\mathrm{e}^{f'(x^*,p)t}\right)^2\right] \,, \tag{2.22}$$

$$= \mathrm{e}^{f'(x^*,p)\tau}\mathrm{E}\left[\delta(t)^2\right] \,. \tag{2.23}$$

The term $\mathrm{E}[\delta(t)^2]$ does not depend on τ and thus is a constant. As τ only remains in the exponential, the ACF decays exponentially with the time delay τ. However, the closer the system gets to the critical point, i.e., the closer $f'(x^*, p)$ gets to zero, the slower this decay becomes. This is illustrated in Fig. 2.1 B. Note that the approximation only to use first-order terms fails at the critical point.

In short, we have established another signature of critical slowing down, i.e., the auto-correlation function decaying slower near a critical point. M. Scheffer et al., 2009 showed this similarly for a discrete system by showing the auto-correlation after one

iteration increases as the system approaches the critical point. Another signature for critical slowing down is an increase in signal variability (M. Scheffer et al., 2009). Such markers of a system approaching the critical point have been successfully applied in many fields, e.g., prediction of climate tipping points (Dakos et al., 2008), or markers for epileptic seizure risk (Maturana et al., 2020; Meisel & Kuehn, 2012).

While this simple model can provide more, we will now be satisfied with having understood that close to a critical point, perturbations and the ACF decay slowly, leading to long-ranged correlations. A more thorough discussion, for example, on which type of transition cortical networks might go through could be found in (Gross, 2021). In the next section, we will transfer these insights onto a more complex model, which is easier to interpret in the context of cortical dynamics, the branching process.

2.1.2 The Branching Process

While the previous example was simple enough to allow for some formalism, it might not be the most intuitive model. Describing the human brain with just one variable, as we did in the previous section, is undoubtedly an oversimplification. Therefore, we will now introduce a slightly more complex model that has successfully described cortical dynamics: the branching process. This section will focus on qualitatively discussing this model's dynamics and its implications for information processing. This discussion largely follows the line of thought elegantly presented by John Beggs in the first chapter of his book *The Cortex and the Critical Point* (Beggs, 2022a).

The model consists of a set of units representing neurons in the brain's context. At each discrete time step, each active neuron can activate a number of connected neurons in the subsequent step. Consequently, activity can branch out from a neuron, hence the name branching process. Generally, the activation of the neurons occurs probabilistically. The probability of activation, $p_i(t)$, at step t is determined based on the sum of inputs a neuron receives

$$p_i(t) = \sum_j w_{ij} \cdot s_j(t-1)\,. \tag{2.24}$$

w_{ij} is the synaptic connection strength between neuron i and j, and $s_j(t-1)$ is neuron j's previous state, e.g., one if it was active and zero if it was inactive. Generally, the probabilistic approach allows the model to capture the stochastic nature of neuronal firing without exactly needing to model all inputs.

A key parameter in this model is the branching ratio, σ, which represents the average number of neurons activated by each active neuron at each time step. It can be formulated as the fraction of the number of offspring, $n_{\text{active}}(t+1)$, to the number of previously active neurons, $n_{\text{active}}(t)$, averaged over all steps, t, (Haldeman & Beggs, 2005)

$$\sigma = \left\langle \frac{n_{\text{active}}(t+1)}{n_{\text{active}}(t)} \right\rangle_t\,. \tag{2.25}$$

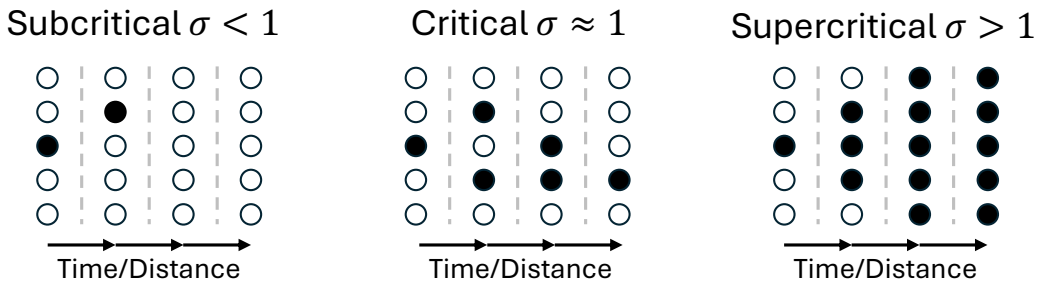

FIGURE 2.2: Branching Process: Illustration of the branching process in the subcritical, critical, and supercritical regimes. In the subcritical regime ($\sigma < 1$), activity gradually decreases as it progresses through the network, leading to a lack of correlation between distant sites/times. In the supercritical regime ($\sigma > 1$), activity rapidly saturates, losing specific information about the initial stimulus. In the critical regime ($\sigma = 1$), activity neither vanishes nor saturates. This allows for distinct activity patterns and, consequently, information flow through the network.

This ratio fundamentally characterizes the general dynamics of the system. The branching ratio, in particular, allows us to characterize different regimes of network behavior, ranging from rapid decay of activity to explosive growth. In the following sections, we will explore these dynamical regimes in more detail.

The Subcritical Regime

First, we consider the regime where $\sigma < 1$. In that regime, each active neuron leads to, on average, less than one active neuron. In this scenario, the dynamics will eventually halt as the number of active units progressively decreases until none remain active (left-hand side of Fig. 2.2).

To understand the implications for information processing, consider the initial number of active neurons as the input or stimulus to the system. Regardless of the initial input, the dynamics will converge to zero active neurons which is a problem for information processing. If all stimuli map to the same output (in this case, no activity), it becomes impossible to discern different stimuli based on the system's response. Consequently, all information about the initial input dissipates over time.

This behavior is analogous to the exponentially fast vanishing perturbation far from the critical point in our one-dimensional model discussed in Section 2.1.1. In both cases, the system rapidly loses information about its initial state. This particular regime of the branching model is called its subcritical regime.

The Supercritical Regime

Second, we examine the opposite extreme: the supercritical regime where $\sigma > 1$. In this scenario, each active neuron produces, on average, more than one active neuron in the subsequent time step. As a result, neural activity rapidly propagates and amplifies throughout the network (right-hand side of Fig. 2.2).

In the supercritical state, the stimuli get quickly amplified until most or all of the neurons are activated. Thus, the neuronal network effectively saturates.

While this might amplify inputs, it poses a problem for information processing. Similar to the subcritical case, all stimuli ultimately lead to the same outcome - in this instance, a fully activated system. Consequently, distinguishing between initial inputs becomes more difficult as the system saturates.

In the context of the one-dimensional model discussed in Section 2.1.1, this would be a perturbation that grows uncontrollably, masking any structure in the initial conditions. Thus, the supercritical regime ($\sigma > 1$) represents another extreme which is unsuitable for information processing. While it does not "forget" like the subcritical regime, it instead "over-reacts", losing specific information through chaotic interaction and excitation of the whole system.

The Critical Regime

Last, the critical regime can be found for $\sigma = 1$. In this state, each neuron excites, on average, one neuron in the subsequent time step (center of Fig. 2.2). This creates a balance between the two previously discussed extremes.

In an ideal critical system, neural activity neither vanishes completely (subcritical regime) nor saturates the network (supercritical regime). Instead, the critical state exhibits ongoing activity with complex activation patterns.

These characteristics can be beneficial for information processing. When a stimulus is introduced into the system, it follows a trajectory distinct from other stimulis' trajectories. This allows the system to discern various inputs even after many time steps. Consequently, the system maintains some "memory" of the initial stimuli over an extended period. Critical systems preserve input characteristics for prolonged durations, unlike the rapid information loss in subcritical systems or the information-obscuring saturation in supercritical systems. The system generally remains responsive to new inputs without overreacting.

The critical state closely corresponds to the critical point in our one-dimensional model discussed in Section 2.1.1. In that context, we can think of a stimulus as a perturbation to the system. The closer the system is to the critical point, the slower the information decay from this perturbation.

The critical regime, $\sigma = 1$, offers a delicate balance where the system is neither too "forgetful" nor too "chaotic". Hence, the critical system is well suited for maintaining and processing complex information patterns. If the human brain also operates close to criticality, it could explain the brain's unique information-processing capabilities.

The Spatial Picture

While we have previously considered the propagation of activations over time, we can also think of this process from a spatial perspective by asking how activity propagates across the network. For example, each step could be conceptualized as a new layer in

a feed-forward architecture. The question could be which is the last activated layer or which output neurons are activated. This spatial view provides additional insights into how information traverses the network in the different regimes.

In the subcritical regime ($\sigma < 1$), where each neuron in one layer excites on average less than one neuron in the following layer, activity gradually diminishes as it progresses through the network (left-hand side in Fig. 2.2). Consequently, information about the initial stimulus cannot reach distant layers as the activity vanishes before traversing the entire network. This results in a lack of correlation between distant sites in the network.

Conversely, in the supercritical regime ($\sigma > 1$), each neuron activates more than one neuron in the subsequent layer on average (right-hand side in Fig. 2.2). In sufficiently deep networks, this leads to a rapid saturation of activity, with all neurons in later layers becoming excited regardless of the initial input. While activity persists, the specific information about the initial stimulus is lost due to this saturation. As a result, the correlation between distant sites remains low, albeit for different reasons than in the subcritical case.

The critical regime ($\sigma = 1$) presents a balanced scenario where each neuron excites approximately one neuron in the next layer (center of Fig. 2.2). In this state, activity neither vanishes nor saturates as it propagates through the network. Consequently, different stimuli in the input layer can produce distinct output patterns. Thus, information is maintained over the network, leading to correlations between distant sites.

In the critical regime, activity can traverse the entire network. However, it often remains more localized for finite networks. For example, if an activity ends in a particular pathway, which particularly can occur in finite-sized systems. The pattern of such localization is extensively studied when investigating neuronal avalanches - cascades of activity that vary in size and duration. The properties of these avalanches, including their size distribution and lifetimes, provide crucial insights into the network's dynamics. We will explore this phenomenon in more detail, along with the first experimental observations of neuronal avalanches, in Section 2.1.4.

The spatial perspective adds to the picture of the branching processes in neural networks, particularly how information propagates and is maintained across both time and space. It underscores the unique properties of the critical regime in maintaining a delicate balance that allows for complex, sustained patterns of activity and information flow throughout the network. Extensive research has been performed for branching networks, which showed that many properties that govern information processing are optimal at the critical state. This included the maximization of metastable states (Haldeman & Beggs, 2005), transmitted information (Beggs & Plenz, 2003), dynamical range (Shew et al., 2009), and information capacity (Shew et al., 2011).

These insights into branching processes will be particularly interesting when the model used in this thesis is discussed in Chapter 4. In particular, spatial and temporal correlations (SCs and TCs) will be analyzed close to the critical point.

2.1.3 Self-Organized Criticality

In the previous sections, we have discussed simple models and how information processing can be optimized at their critical point. However, how cortical networks could achieve such a finely balanced critical state is not fully understood. One plausible framework is the concept of self-organized criticality (SOC) on adaptive networks which requires only local rules to tune a system towards a critical state.

Self-organized criticality, a concept from complex systems theory, was first introduced by Bak et al., 1988. The fundamental idea is that local rules, rather than global processes, tune a system towards a critical state. This makes SOC a plausible mechanism for cortical network dynamics, as it requires only unit-level and local neighborhood-level rules rather than system-wide coordination.

While the original SOC model involved sand piles, more illustrative examples exist in the context of neural networks. One example is the model proposed by Bornholdt and Rohlf, 2000, demonstrating self-organized criticality of a neuronal network.

In their model, neurons can be in one of two states, $s_i(t) = \pm 1$. The state of each neuron is updated based on inputs from other neurons according to the equation

$$s_i(t+1) = \text{sign}\left[\sum_j c_{ij} s_j(t)\right] . \tag{2.26}$$

Here, c_{ij} represents the connections between neurons, which can be $c_{ij} = \pm 1$ or $c_{ij} = 0$ (no connection). The network is iterated until it reaches an attractor or a maximum number of time steps.

After the run is completed and before a new run is started, rewiring rules are applied to drive the system towards criticality. Hence, the model has dynamics on the neuronal network in each run and dynamics of the network structure which evolves through update rules between runs. The key to these rules is that they are local and consider only the history of individual neurons without requiring global network information. Specifically for the model by Bornholdt and Rohlf, 2000, they are:

1. A neuron gains a random new link if it was in the same state throughout the run.

2. A neuron loses a link if its state changed during the run.

3. Random noise occasionally flips the sign of a link, simulating extrinsic perturbations.

Rule 1 and 2 are illustrated in Fig. 2.3 A and B, respectively. This simple algorithm drives the system to its critical state regardless of its initial configuration. In Fig. 2.3 C

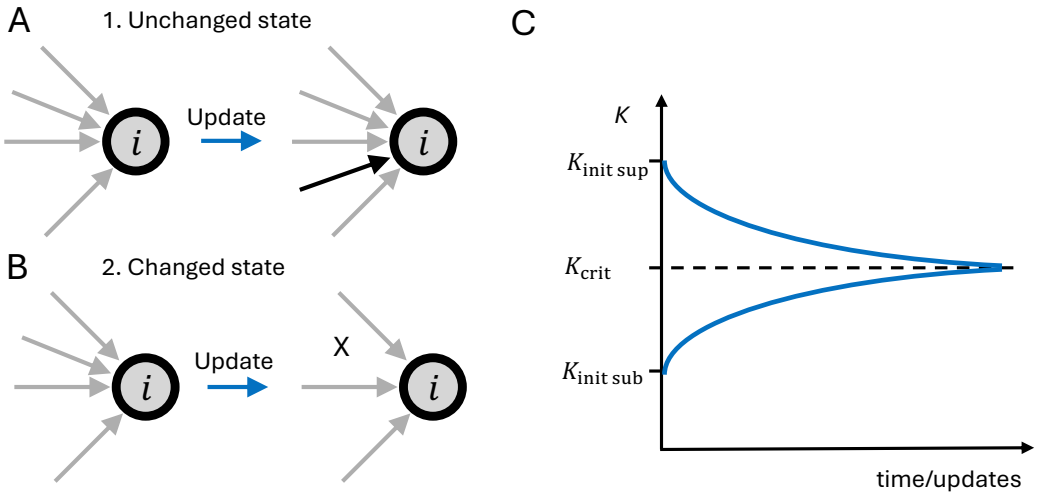

FIGURE 2.3: Self-Organized Criticality: **A** Update rule 1: A neuron with an unchanged state gains a link (bold black). **B** Update rule 2: A neuron with changed state loses a link. **C** Illustration of the average connectivity K evolution (blue lines) to a critical value K_{crit} (dashed line) irrespective of the initial connectivity being subcritical $K_{\text{init sub}}$ or supercritical $K_{\text{init sup}}$.

this is illustrated where independent of the average initial connectivity K_{init}, the average connectivity K evolves to the same value. This value has been identified as the critical value K_{crit} by Bornholdt and Rohlf, 2000. Importantly, each neuron only needs information about its state, making it a plausible model for biological systems. The model by Bornholdt and Rohlf, 2000 is just one example of self-organizing systems in neural contexts. For example, other models may incorporate information from neighboring neurons (Bornholdt & Röhl, 2003) or include integrate-and-fire dynamics (Meisel & Gross, 2009). However, they all share that local rules drive a system towards a critical state, making it plausible that such processes in the human brain could govern neuronal network plasticity and guide the system to a critical set point.

Therefore, the framework of self-organized criticality provides a compelling explanation for how complex biological systems like the brain might naturally maintain themselves near a critical point, optimizing their capacity for information processing and adaptation.

2.1.4 Neuronal Avalanches

The critical point in neural systems offers significant benefits for information processing, as we have seen in the previous discussion of simple models. To understand how criticality manifests in neural networks, we need to introduce the concept of "neuronal avalanches" - distinct patterns of neural activity that vary significantly in size and duration. Generally, neuronal avalanches consist of subsequent neuronal activations that are separated to the next avalanche by quiescent periods (Fig. 2.4 A). Neuronal

avalanches are closely linked to the critical dynamics in neural systems and provide a means to empirically investigate the presence of criticality in the brain.

In particular, the distribution of neuronal avalanches can indicate if a system is critical because the distribution follows a power law for critical systems (Harris, 1964; Zapperi et al., 1995). This implies that critical systems can have extensively large avalanches with a non-zero but decreasing probability. These power law distributions are scale-free, meaning the avalanches have no characteristic size or length. Formally, the probability of observing an avalanche of size S scales as

$$P(S) \propto S^{-\alpha} \, . \tag{2.27}$$

α is the power law exponent. For a critical branching process, theory predicts specific values for these exponents: $\alpha = 1.5$ for the avalanche size distribution and $\alpha = 2$ for the avalanche duration distribution (Harris, 1964; Zapperi et al., 1995). This power law behavior breaks down as the system deviates from criticality, with long avalanches being unable to propagate in a subcritical (under-connected) network and large avalanches becoming more frequent in a supercritical system, as seen in the previous section on branching processes (Section 2.1.2).

Neuronal avalanches exhibit additional distinctive features that provide further evidence of criticality. These include the collapse of avalanche temporal profiles onto a single universal shape when normalized for size and duration and the emergence of a third scaling exponent that couples the size and duration distribution exponents (Sethna et al., 2001). These characteristics help identify criticality in neural systems.

Beggs and Plenz, 2003 were the first to find critical avalanche scaling in an experimental setting. They demonstrated that both size and duration distributions of neural activity patterns closely matched the theoretical exponents (Fig. 2.4 B), (Beggs & Plenz, 2003). Their work inspired brain criticality research across various experimental paradigms. Subsequent studies have confirmed the presence of avalanches in vitro (Beggs & Plenz, 2004; Klaus et al., 2011; Shew et al., 2009, 2011; Yang et al., 2012), in rats (Ribeiro et al., 2010; Shew et al., 2011), cats (Hahn et al., 2010), monkeys (Petermann et al., 2009; Shew et al., 2011), and even humans (Priesemann et al., 2013).

Beggs and Plenz, 2003 also revealed the sensitivity of avalanche distributions to pharmacological interventions, showing that the power laws break down when chemicals perturb neural tissue. This finding underscores the delicate balance required for critical behavior. It provides a method for perturbing the system away from criticality, an approach we will explore later in this thesis using a different modality to characterize critical points in human neural activity.

While this thesis does not directly investigate neuronal avalanches, it does investigate the SCs and TCs both in model simulations (Chapter 4) and then human

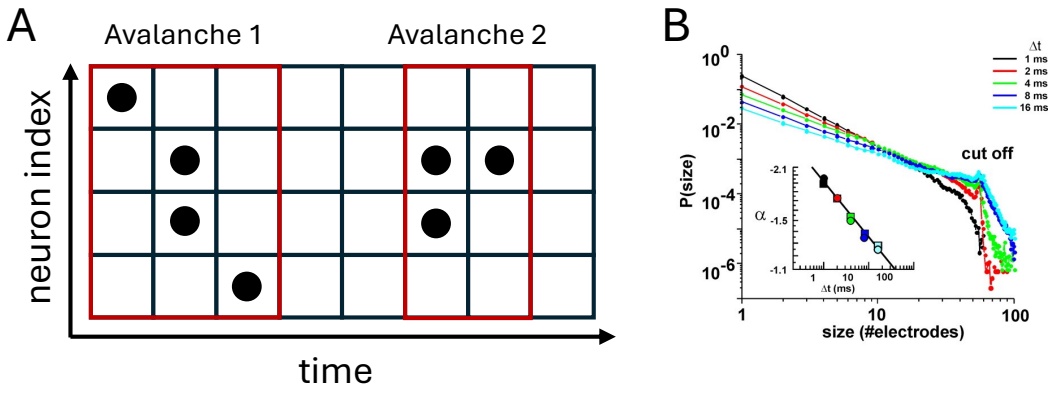

FIGURE 2.4: Neuronal Avalanches: **A** Neuronal avalanches, as timely, closely coordinated neuron firing (black dots), are separated by quiescent periods. **B** First results by Beggs and Plenz showed power law behavior for the avalanche size distribution irrespective of time bin size. Panel B adapted from (Beggs & Plenz, 2003) Copyright 2003 Society for Neuroscience.

intracranial EEG data (Chapter 5). Thinking of the potential for avalanches to propagate across extensive portions of a network and persist over extended time periods provides an intuitive example of which patterns of critical dynamics can lead to stronger correlations between distant sites and prolonged TCs, which will be the focus of the following parts.

2.1.5 Temporal Correlations

In the simple model in Section 2.1.1, we observed that perturbations decay according to a power law at the critical point. This absence of a dominant timescale indicates scale-free behavior, mirroring the avalanche dynamics where events could occur at any size up to the system limit, with decreasing but non-zero probability. In the temporal domain, this scale-free nature implies the potential for long-range temporal correlations (TCs) without a characteristic scale.

A seminal study by Linkenkaer-Hansen et al., 2001 investigated whether TCs in human brain signals exhibit power law behavior, as expected in scale-free, critical systems. Their research used magnetoencephalography (MEG) and scalp electroencephalography (EEG) data, with emphasis on the α-frequency band (8 Hz - 13 Hz). This frequency range is prominently observed during wakefulness and closed eyes.

At the center of their analysis was the examination of the auto-correlation function (ACF) of the signal. The ACF quantifies how similar a signal is to itself at different time lags. Their hypothesis posited that if the system exhibits scale-free critical dynamics, the ACF should decay following a power law rather than an exponential decay characteristic of systems with a dominant timescale (see Section 2.1.1).

The results from Linkenkaer-Hansen et al., 2001 indeed showed that the ACF of the α-band amplitude fluctuations was well-fitted by a power law both in MEG and

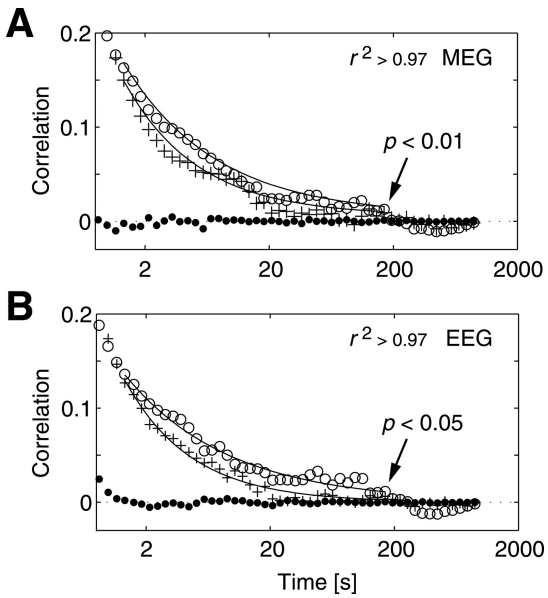

FIGURE 2.5: Temporal Correlations: **A** Auto-correlation functions of human α-band power (empty dots and crosses) follow a power law (solid lines) in MEG and **B** EEG data. Surrogate data (black dots) does not show this behavior. Reprinted with from (Linkenkaer-Hansen et al., 2001) [CC BY 4.0].

scalp EEG data (Fig. 2.5 A and B respectively). This finding provided evidence that scale-free dynamics might govern human brain dynamics, as one would expect at a critical point, and that long-range TCs emerge naturally in this state.

Linkenkaer-Hansen et al., 2001 employed detrended fluctuation analysis (DFA) as a complementary method to further validate their ACF findings. DFA helps identify long-range correlations in time series data by analyzing the self-similarity parameter, which characterizes the degree of correlation over different time scales and has been proven to be more robust if non-stationarities can be found in the data. The study's DFA results corroborated the ACF findings, confirming the presence of robust power law scaling in α oscillations across different subjects and conditions. A more detailed explanation of DFA can be found in the review by Hardstone et al., 2012.

While Linkenkaer-Hansen et al.'s study provided robust evidence of temporal scaling in brain activity through ACF analysis, they also highlighted the need for more fine-grained intracranial EEG data to better understand spatial and temporal correlations. They suggested that high-resolution techniques such as intracranial recordings would be necessary to capture the spatial dynamics and how they interact with temporal structures across different brain regions (Linkenkaer-Hansen et al., 2001).

Building on these results, this thesis will further investigate TCs using ACFs. Our approach in Chapter 5 will examine the decay of ACFs without assuming a specific form (power law or exponential), allowing for a more general characterization of the TCs structure. Furthermore, responding to call of Linkenkaer-Hansen et al., 2001 for spatiotemporally high-resolved data, we will also investigate the decay of spatial

correlations (SCs) and TCs in human brain dynamics in Chapter 5.

2.2 Foundational Studies on Temporal Correlations

The previous sections introduced the concept of brain criticality and its potential to explain the human brain's remarkable information-processing capabilities. We have identified long-range SCs and TCs as hallmarks of a critical state, providing measurable indicators of criticality in neural systems.

In the following sections, we will explore key studies that have employed these measures to investigate brain criticality. These selected publications have been instrumental in shaping our understanding of critical phenomena in neural systems and have directly inspired the questions addressed in this thesis.

2.2.1 Along the Functional Hierarchy

The previous sections addressed criticality and long-range TCs as general properties of the brain. However, the brain is not a homogeneous structure. Expecting a single parameter to fully describe the complexity of cortical dynamics would be an oversimplification.

A study by Murray et al., 2014 provided evidence that TCs are distributed heterogeneously across the cortex. Their research focused on single-neuron spike trains in non-human primates, characterizing the timescale at which the ACF of these spike trains decayed. They call TCs the "intrinsic timescale", obtained from the decay rate of fitting an exponential to the ACF (Murray et al., 2014). Notably, Murray et al., 2014 excluded the first few lag values of the ACF to account for neuronal refractoriness, i.e., the time period a neuron needs to be able to fire again.

In particular, Murray et al., 2014 examined five specific regions along the visual pathway, arranged in order of increasing functional hierarchy (Fig. 2.6 A and B):

1. Medial-temporal area in visual cortex (MT),
2. Lateral intraparietal area in parietal association cortex (LIP),
3. Lateral prefrontal cortex (LFPC),
4. Orbitofrontal cortex (OFC),
5. Anterior cingulate cortex (ACC).

Their key finding was a systematic increase in TCs along this functional hierarchy (Fig. 2.6 C and D). This result demonstrated the heterogeneity of TCs but also revealed the functional hierarchy as an underlying organizational principle for TCs. They also investigated two somatosensory areas with consistent findings (Fig. 2.6).

The authors interpreted their findings in the following way: Lower regions in the hierarchy, responsible for processing dynamic stimuli, need to adjust to rapidly changing inputs. Thus, correlations with previous inputs would not be beneficial. However,

higher regions tasked with integrating diverse inputs and improving signal-to-noise ratios can leverage longer TCs to integrate information over extended periods. In short, areas associated with more complex tasks require longer TCs and short TCs might benefit early processing of fast changing stimuli (Murray et al., 2014).

While Murray et al., 2014 did not explicitly frame their findings in terms of brain criticality, their results align well with the criticality hypothesis. The increase in long-range TCs with increased functional complexity suggests optimized information processing capabilities for complex problems closer to the critical point. In Chapter 5, a similar analysis is performed in human intracranial EEG recordings, and in Chapter 6 TCs are linked to task performance.

2.2.2 Across Vigilance States

While the previous section demonstrated the spatial heterogeneity of TCs across brain regions, a natural follow-up question is whether TCs also exhibit temporal variability. A particularly intriguing aspect of this question concerns the changes in TCs between wakefulness and sleep.

Meisel, Klaus, et al., 2017 addressed this question by examining TCs across different vigilance states in rats. Using multi-unit recordings, they investigated how TCs are modulated during non-rapid eye movement (NREM) sleep, rapid eye movement (REM) sleep, and wakefulness. Their findings show a significant disruption of TCs during NREM sleep compared to wakefulness and REM, but no measurable difference between wakefulness and REM (Fig. 2.7).

Extending their analysis to sleep deprivation, Meisel, Bailey, et al., 2017 showed progressively shorter TCs for prolonged wakefulness. This suggested a relationship between vigilance state and neuronal TCs.

To improve the understanding of the mechanism behind these changes, they investigated slow wave activity (SWA), a characteristic feature of the NREM slow-wave sleep (SWS) (Meisel, Klaus, et al., 2017). They found more frequent SWA during prolonged wakefulness. Furthermore, excluding these slow waves from the data restored TCs to the levels observed during wakefulness. These findings were corroborated by a network model demonstrating TCs collapse when neurons collectively go offline, a phenomenon proposed to underlie the slow-wave signals observed in EEG (Vyazovskiy et al., 2011).

The study by (Meisel, Klaus, et al., 2017) highlights that signatures of criticality, such as long-range TCs, can be disrupted by other neurophysiological mechanisms. This underscores the need for rigorous analysis accounting for confounding factors on TCs, like SWA.

Therefore, this thesis will account for different mechanisms affecting neural dynamics, including SWS. For example, SWA will be incorporated into the model (Chapter 4), and the human iEEG data will be analysed in and out of SWS (Chapter 5).

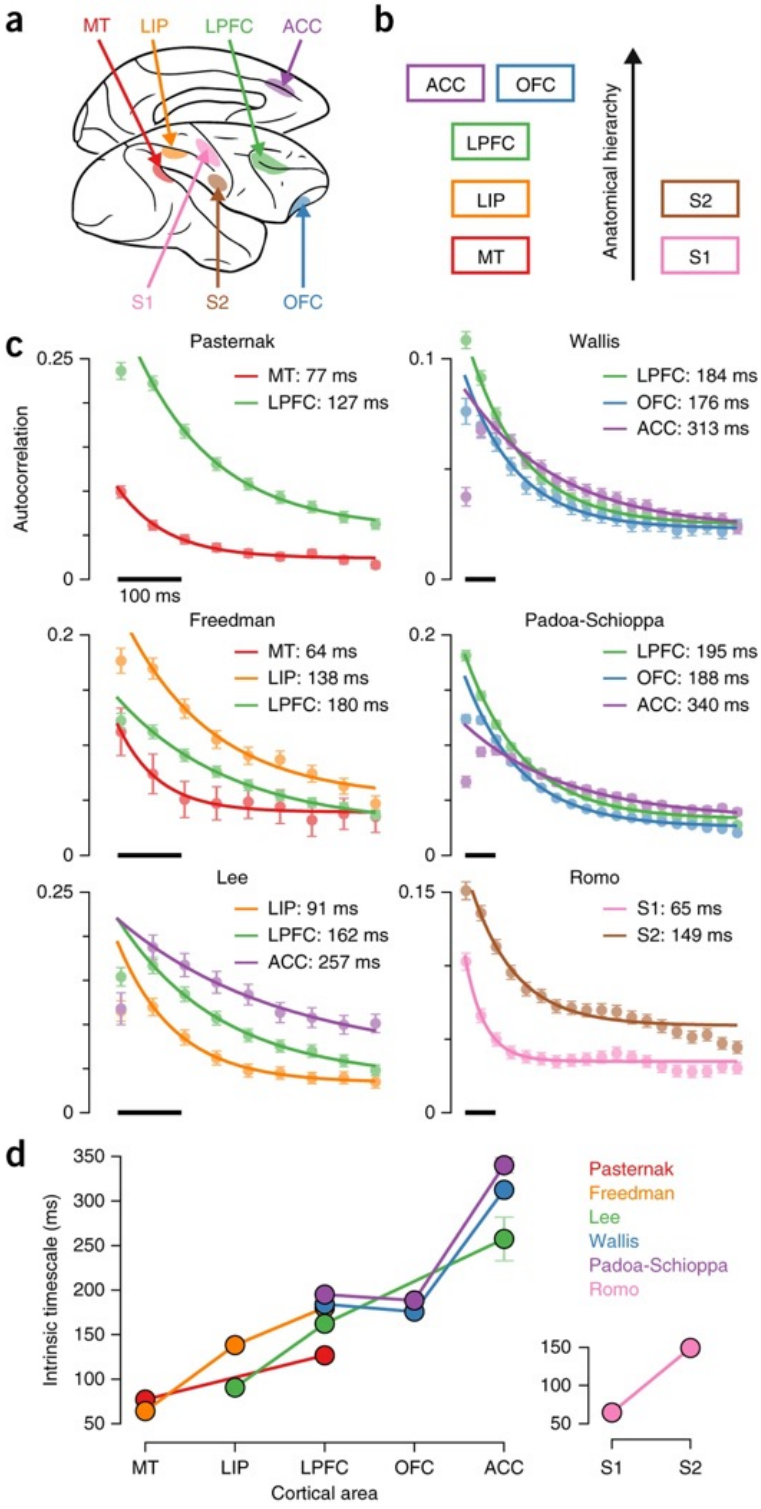

FIGURE 2.6: Temporal Correlations Along the Cortical Hierarchy: **A** The investigated areas in the non-human primate brain. **B** Hierarchical ordering of these regions. **C** Auto-correlation functions for each subject and each area. **D** Summary of TCs (intrinsic timescales) showing increased TCs with increasing functional hierarchy. Reproduced with permission from Springer Nature (Murray et al., 2014).

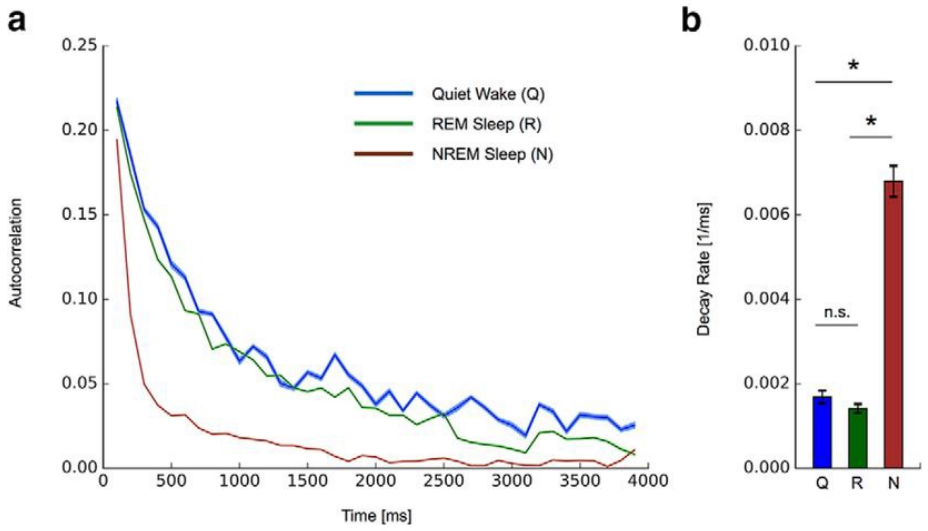

FIGURE 2.7: Temporal Correlations Across Vigilance States: **A** The ACF during NREM sleep visually decays quicker than during REM sleep or wakefulness. **B** This manifests in significantly shorter decay rates of the ACF during NREM. Reprinted from (Meisel, Klaus, et al., 2017) [CC BY 4.0].

2.2.3 Impacts of Antiseizure Medication

In their seminal study Beggs and Plenz, 2003 demonstrated that pharmacological interventions can impact cortical dynamics, shifting them away from the critical point (Section 2.1.4). Shew et al., 2009 later confirmed and extended these findings, showing that the dynamical range of the network is maximal in the pharmacologically unperturbed state. These studies showed that external perturbations could induce shifts away from criticality.

Meisel, 2020 showed this for the first time to human cortical dynamics. Meisel, 2020 investigated intracranial electroencephalography (iEEG) recordings from persons with drug-resistant epilepsy (PwDRE) undergoing antiseizure medication (ASM) tapering, which is standard in the presurgical evaluation for PwDRE (see Section 2.3). This approach allowed Meisel, 2020 to examine the effect of pharmacological changes on TCs and activity cascades in human cortical dynamics.

Meisel, 2020 defined TCs as the half-width at half-maximum of the ACF in the high-γ band (50-100 Hz), a frequency range known to correlate strongly with the underlying neuronal firing (Manning et al., 2009; Miller, 2010; Nir et al., 2007; Whittingstall & Logothetis, 2009). Comparing TCs between days of lowest and highest ASM load showed that higher ASM loads were associated with shorter TCs (Fig. 2.8).

Furthermore, Meisel, 2020 demonstrated that interictal epileptiform discharge (IED) cascades (see Section 2.3.2 for details on IEDs) tended to be shorter during periods of high ASM loads. This suggests that increased ASM levels inhibit activity spread across the neural network.

Meisel, 2020 concluded that ASMs drive brain dynamics toward a subcritical state,

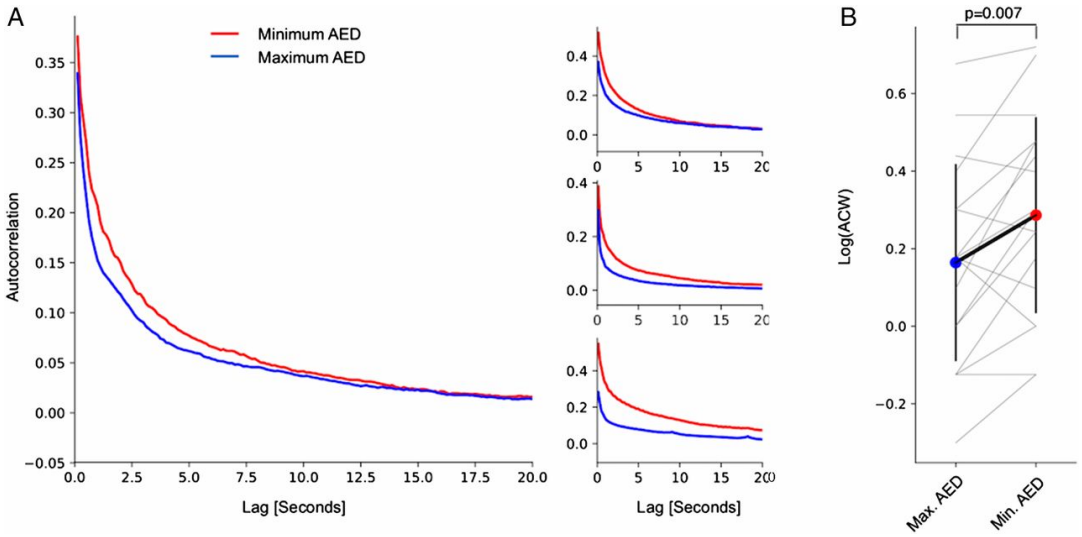

FIGURE 2.8: Temporal Correlations Under Antiseizure Medication: **A** ACF for four patients exhibit quicker decline under higher antiseizure medication load (here AED). **B** In the population, the ACF decay rate was significantly lower under higher ASM loads. Reprinted from (Meisel, 2020) [PNAS license].

and reduce the risk of widespread neuronal excitation. This conclusion was supported by a neuronal network model presented in the same work, which incorporated ASM-like mechanisms that reduced the effective connectivity of the network, leading to dynamics subcritical (Meisel, 2020).

These insights helped to understand how ASMs modulate cortical dynamics and will be incorporated into our network model as well (Chapter 4). Moreover, Chapter 5 aims to confirm and extend (Meisel, 2020) experimental findings on TCs also to SCs, utilizing a significantly larger dataset to provide a more comprehensive understanding of ASM effects on cortical criticality.

2.3 Epilepsy

The following part of the background will focus on epilepsy, as the data used in this thesis stems from persons with epilepsy (PwE). First, a general introduction to epilepsy is given; how it is classified, and which comorbidities or signatures are found in epilepsy. Then, we will turn to the treatment options for epilepsy. The focus will be on antiseizure medication (ASM) and epilepsy surgery with its presurgical monitoring as both will be important to understand the data presented in Chapters 5 and 6.

Epilepsy is a neurological disorder characterized by the tendency of reoccurring, unprovoked seizures, also called ictal events. The international league against epilepsy (ILAE) defines an epileptic seizure as "a transient occurrence of signs and/or symptoms due to abnormal excessive or synchronous neuronal activity in the brain" (Fisher et al., 2014). The ILAE then defines epilepsy as "[...] a disorder of the brain characterized

by an enduring predisposition to generate epileptic seizures [...]" (Fisher et al., 2014) and "[...] requires the occurrence of at least one epileptic seizure [...]" (Fisher et al., 2014). This definition distinguishes epileptic seizures from those caused by acute brain perturbations, such as toxin exposure, stroke, or traumatic brain injury (Asadi-Pooya et al., 2023). These acute seizures are not expected to recur if the underlying causes are removed.

Epilepsy affects approximately 1% of the global population, indepedent of demographic and social boundaries (Fiest et al., 2017). The impact of epilepsy extends beyond seizures, encompassing a range of comorbidities that significantly affect the quality of life of PwE (Asadi-Pooya et al., 2023):

1. Cognitive impairments, e.g., affecting memory, attention, and executive functions.
2. Psychiatric disorders, e.g., higher prevalence of depression, anxiety, and psychosis.
3. Sleep disturbances, e.g., insomnia and sleep apnea, are common.
4. Social challenges, e.g., stigma, reduced employment opportunities, and limitations on driving.
5. Physical health issues, e.g., increased risk of fractures after seizures, cardiovascular diseases, and metabolic disorders.

In particular, this thesis will discuss cognitive impairments together with TCs (Chapter 6).

In addition to these comorbidities, epilepsy is associated with higher mortality rates. A notable example is sudden unexpected death in epilepsy (SUDEP), which occurs at a rate 23 times higher than sudden death in the general population (Saetre & Abdelnoor, 2018). This shows the importance of properly diagnosing epilepsy and providing treatment to the PwE.

The following first introduces specific types of epilepsy and their etiological factors. Second, interictal epileptiform discharges (IEDs) are discussed. IEDs are epileptic activities distinct from seizures. Finally, treatment options are reviewed, beginning with a general overview before delving into more detailed discussions of antiseizure medications and epilepsy surgery. This section aims to provide an overview of epilepsy in the context of the data and analysis employed in this thesis (Chapters 5 and 6). It does not aim to be complete. The interested reader can find an overview of the disease with more detail in Asadi-Pooya et al., 2023 and an extensive view of the human brain's electrical signals and epilepsy, for example, in Zschocke and Hansen, 2023.

2.3.1 Epilepsy Classification

The ILAE provides a guideline for epilepsy diagnosis and characterization into epilepsy syndromes based on seizure types, epilepsy types, and etiology (I. E. Scheffer et al.,

2017) (Fig. 2.9).

Seizure Types

First, seizures are characterized based on their onset (Fisher et al., 2017):

Focal seizures start in only one brain hemisphere. PwE with focal seizures can retain awareness or show impaired awareness. While the onset is localized, these seizures can still develop into seizures affecting both hemispheres.

Generalized seizures involve both hemispheres at seizure detection. The majority of generalized seizures lead to impaired awareness or loss of consciousness.

Unknown onset seizures are labeled all seizures that can not be classified as either focal or generalized, for example, if no record of the seizure onset exists or the onset was obscured by other artifacts

Relation to Brain Criticality: Seizures have been investigated in the context of brain criticality. For example, previous research demonstrated that signs of criticality are lost during seizures, potentially suggesting that seizures are a phase transition into the supercritical regime (Meisel & Kuehn, 2012; Meisel et al., 2012). Additionally, the epileptic tissue has been shown to show extended TCs in interictal dynamics, hinting at the tissue being closer to criticality and thus also closer to a phase transition towards supercritical, potentially seizure, dynamics (Monto et al., 2007).

Epilepsy Types

As the second level, the epilepsy type needs to be classified:

Focal epilepsy: Seizures originate in one or multiple specific brain areas or only involve one hemisphere. In the interictal EEG, one can typically find focal discharges (Section 2.3.2), (Fisher et al., 2017).

Generalized epilepsy: Seizures start and engage both hemispheres, resulting in various seizure types, which mostly include absence, myoclonic, tonic-clonic seizures (Asadi-Pooya et al., 2023). Generalized epilepsy diagnosis can be supported by finding typical interictal EEG discharges, e.g., generalized spike-waves (Fisher et al., 2017).

Combined generalized and focal epilepsy: Both focal and generalized seizures can be found. This is an infrequent type of epilepsy that can be challenging to diagnose and treat (Asadi-Pooya et al., 2023).

Unknown: Used as a type if the epilepsy type could not be determined, typically due to missing information (Asadi-Pooya et al., 2023).

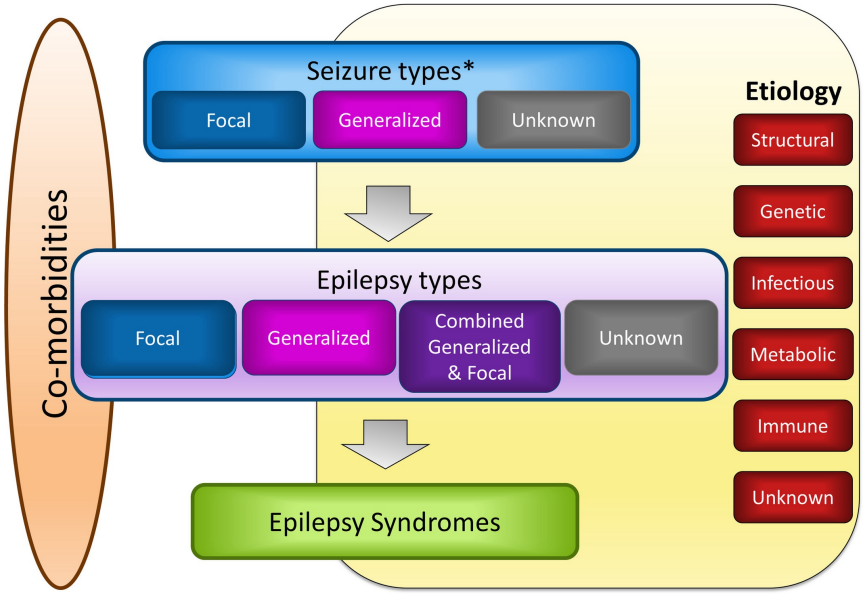

FIGURE 2.9: Epilepsy Diagnosis: The ILAE proposed this pathway in the epilepsy diagnosis. Reprinted with permission from (I. E. Scheffer et al., 2017) Copywright 2017 International League Against Epilepsy.

At the third level, the patient's specific epilepsy syndrome is classified. This classification is based on the seizure type and epilepsy type but also further etiological factors (Fig. 2.9), (I. E. Scheffer et al., 2017). The ILAE provides a comprehensive list of epilepsy syndromes, for example, in I. E. Scheffer et al., 2017.

2.3.2 Interictal Epileptiform Discharges

The interictal, i.e., between seizures, EEG can help identify epilepsy and its type. For example, if a person is referred to a doctor after their first seizure, an EEG recording can help to investigate if there is a risk for reoccurring seizures. If the EEG is abnormal, the risk for reoccurring seizures increases by 40%, and if so-called interictal epileptiform discharges (IEDs) are found, the risk increases by up to 60% making the diagnosis of epilepsy more likely (Fisher et al., 2017).

These IEDs are brief, abnormal electrical events, which are characterized as spikes or sharp waves, which last for (20-70) ms and (70-200) ms respectively (Fig. 2.10), (Tatum, 2022). In scalp EEG, IEDs are characterized by an abrupt changing electrical potential different from the background activity, which then also disrupts the background activity, i.e., pre-IED and post-IED EEG activity is qualitatively different (Kural et al., 2020; Zschocke & Hansen, 2023) (Fig. 2.10 A).

IEDs are found in about a third of the recordings employed for individuals coming for diagnostics after first seizures, making them an important marker for epilepsy (Tatum, 2022). While they can indicate the potential origin of seizures, the location of IEDs does not necessarily coincide with the origin of focal seizures, particularly those observed in scalp EEG (Tatum, 2022). However, IEDs can help to identify the type of epilepsy, e.g., generalized spike-waves are a sign of generalized epilepsy

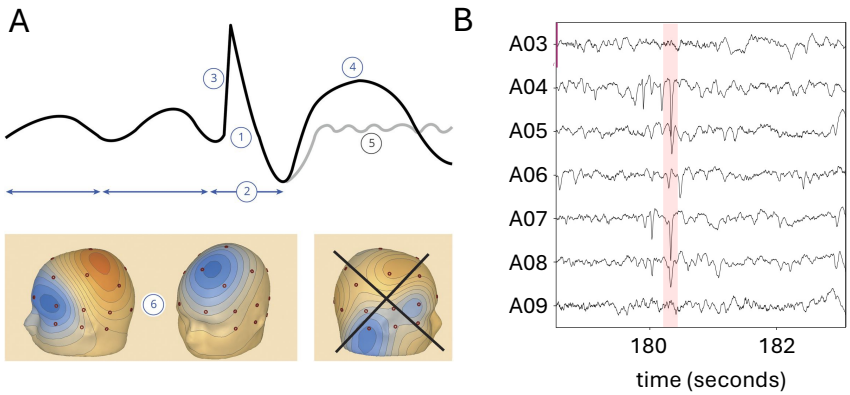

FIGURE 2.10: Interictal Epileptiform Discharges (IEDs): **A** Clinical definition for IEDs in scalp EEG. Reprinted from (Kural et al., 2020) [CC-BY-NC-ND]. **B** Example of an IED in human iEEG (red-shaded area).

in contrast to focal IEDs, which can be associated with focal epilepsy (Asadi-Pooya et al., 2023).

In short, IEDs are short abnormal patterns found in PwE, indicative of the disease. We will later investigate if the disruption of activity through IEDs can impact markers for criticality, i.e., SCs and TCs, by including IED-like activity in the model (Chapter 4), and investigating intracranial EEG data showing IEDs (Chapter 5).

2.3.3 Treatment Options

Epilepsy treatment typically focuses on controlling seizures with the main goal of removing any seizure risk or at least reducing it significantly. The main treatment options include (Asadi-Pooya et al., 2023):

1. Antiseizure medications
2. Surgical interventions
3. Dietary therapies (e.g., ketogenic diet)
4. Neurostimulation devices (e.g., vagus nerve stimulation, deep-brain stimulation)

The choice of treatment depends on factors such as the type and frequency of seizures, the underlying cause of epilepsy, and the individual patient's characteristics. Generally, the goal is to achieve optimal seizure control, improve quality of life, and reduce the risk of SUDEP. ASMs are often the first-line and most common treatment for most epilepsy syndromes as they can achieve seizure control in approximately 70% of PwE (Brodie et al., 2012).

Antiseizure Medication

Antiseizure medications (ASMs) form the cornerstone of epilepsy management. These medications aim to control and prevent seizures while minimizing side effects.

They work through various mechanisms to reduce seizure activity in the brain. While the precise mechanisms are not fully understood for all ASMs, they generally are categorized into three main groups:

Ion channel modulators: These medications reduce neuronal excitability by modulating the function of ion channels in the brain. For example, Carbamazepine and Phenytoin primarily target sodium channels, helping to stabilize neural membranes and prevent the rapid, excessive firing of neurons that occurs during seizures (Bialer & White, 2010; Sankar & Holmes, 2004).

GABAergic drugs: These medications enhance the inhibitory effects of gamma-aminobutyric acid (GABA), the primary inhibitory neurotransmitter in the brain. Drugs like Topiramate and Benzodiazepines fall into this category, dampening excessive neuronal excitation and reducing the likelihood of seizure occurrence (Bialer & White, 2010).

Multiple/unique mechanisms: Some ASMs, such as Levetiracetam, work through multiple or unique mechanisms that do not fit neatly into the above categories. Levetiracetam, for instance, binds to synaptic vesicle protein 2A (SV2A), modulating neurotransmitter release (Lynch et al., 2004).

The ASM choice depends on various factors, including seizure type, epilepsy syndrome, patient age, comorbidities, and potential drug interactions. Treatment typically begins with monotherapy, progressing to alternative medications or polytherapy (Asadi-Pooya et al., 2023).

Besides seizure control, ASMs can impact, for instance, sleep patterns, cognitive function, and mood. For example, some ASMs may cause insomnia, e.g., Lamotrogin, or aggressiveness, e.g., Levetiracetam, while others might impair cognitive functions like memory or language (Aldenkamp & Baker, 2001; Sankar & Holmes, 2004; Strzelczyk & Schubert-Bast, 2022). The tolerability varies among ASMs and individuals, necessitating careful monitoring and potential adjustments to treatment regimens. For example, Valproic acid is avoided in individuals of childbearing age due to risks for the development of their children (Asadi-Pooya et al., 2023).

This thesis will investigate the effect of ASMs on cortical dynamics by introducing them into our model (Chapter 4) and testing their effects on SCs and TCs in human intracranial EEG (Chapter 5). This investigation aims to provide a more comprehensive understanding of how ASMs act in neuronal networks, potentially informing future treatment strategies.

Epilepsy Surgery

Despite advancements in ASM development, drug-resistant epilepsy (DRE) remains a significant challenge in epilepsy management, as approximately one-third of patients with epilepsy continue to experience seizures despite ASM treatment (Brodie et al.,

2012). This fraction of DRE remained stable over the last years despite the introduction of new ASMs with new mechanisms of action, thus emphasizing the complexity of epilepsy and the need for alternative treatment approaches (Asadi-Pooya et al., 2023; Löscher et al., 2020).

For focal epilepsy, epilepsy surgery is recognized as the most cost-effective treatment option (Jehi et al., 2022; Lamberink et al., 2020; Ryvlin et al., 2014). For these individuals, the primary goal of surgery is to eliminate seizures by disconnecting or removing the seizure onset zone (SOZ). However, not all patients with focal epilepsy are suitable candidates for resective surgery, even when the SOZ can be identified. For instance, if the affected area overlaps with critical functional regions, such as those responsible for speech, resection might impair the patient's quality of life. In such cases, the risks of surgery can outweigh the potential benefits.

Also, for generalized epilepsy, surgery can be an option. However, the approach is typically palliative rather than curative, i.e., the aim is to reduce the frequency and severity of seizures and improve the patient's quality of life (Ryvlin et al., 2014). An example of such a surgery is a callosotomy where the corpus callosum, the band of fibers connecting the brain hemispheres, is severed to prevent the spread of seizures between the hemispheres (Ryvlin et al., 2014).

A comprehensive evaluation is required to localize the seizure onset zone (SOZ) and the epileptic network and identify if a PwDRE is a candidate for surgery. Typically, this evaluation involves a series of diagnostic tests and monitoring procedures, referred to as presurgical monitoring. This monitoring can include invasive and non-invasive tests, such as MRI imaging, neuropsychological assessments, and long-term video-iEEG monitoring (Asadi-Pooya et al., 2023). For example, MRI images are used to examine if there are lesions in the brain that could cause the seizures, i.e., epileptogenic lesions. Furthermore, neuropsychological assessments can help to identify cognitive impairments as comorbidities to epilepsy and can track cognitive changes before and after the surgery. Moreover, long-term video-iEEG monitoring, while having major complication rates up to 10% (Jehi et al., 2021), can provide highly resolved data of the brain activity with excellent signal-to-noise ratio and a precise spatial resolution (Parvizi & Kastner, 2018). Additionally, the monitoring can be used to provoke seizures under controlled conditions, for instance, by tapering ASMs, which can give clinicians a better estimate of the origin of the seizures and their progression through the brain.

Epilepsy surgery leads to seizure freedom in about half the patients with focal epilepsy after ten years (De Tisi et al., 2011) and has low mortality rates when performed in specialized centers (Ryvlin et al., 2014). This shows that epilepsy surgery can be a promising solution for PwDRE. However, it remains underutilized due to factors like the lack of awareness by the treating physicians and thus missing referral of the patients to specialized centers (Asadi-Pooya et al., 2022, 2023). Furthermore, epilepsy surgery still has a considerable rate of failure to control seizures completely,

partially due to miss-classified SOZs. Thus, the search of markers for the SOZ (Bartolomei et al., 2008; Gunnarsdottir et al., 2021; A. Li et al., 2021; Lundstrom et al., 2021; Weiss et al., 2015), the success chance of surgery (Fitzgerald et al., 2021; Frauscher, 2020; Lundstrom et al., 2021; Miron et al., 2023), and cognitive risks of the surgery (Baxendale & Thompson, 2020; Busch et al., 2021; Miron et al., 2024) is still in the focus of research.

In this thesis, we will utilize data stemming from the presurgical evaluation. In Chapter 5, we will investigate intracranial EEG data with brain criticality connected markers, i.e., SCs and TCs, to better understand cortical dynamics. We will leverage the ASM tapering in the presurgical monitoring as "active" perturbation of cortical dynamics and additionally investigate how IEDs as epileptic signals affect cortical dynamics. Bringing our research closer to clinically relevant questions, cortical thicknesses detected with MRI will be investigated to identify regions of special interest for predicting cognitive outcomes after surgery. Additionally, we will integrate our insights about TCs with the cognitive profiles of the patients to search for an overarching link between brain dynamics and cognitive performance (Chapter 6). Before investigating this data, the next chapter introduces the datsets and methods used throughout this thesis.

Chapter 3

Materials and Methods

This chapter aims to introduce the datasets and methods used throughout this thesis. First, a branching-process-like neuronal network model which can be tuned around criticality is defined. This model incorporates three mechanisms which in humans can affect cortical dynamics and are known to be linked to cognition: Slow-wave activity (SWA), interictal epileptiform discharges (IEDs), and antiseizure medication (ASM) (Section 3.1.1).

Second, we define spatial and temporal correlations (SCs and TCs) both in the model and for later calculation in human intracranial EEG (iEEG) dynamics (Section 3.3 and Section 3.2).

Third, we describe the two independent iEEG datasets on which the human SCs and TCs structure will be analyzed (Section 3.4). Additionally, the methods to extract SWA, IEDs, and ASMs in the human data are introduced.

Lastly, the methods for two studies investigating the relationship between cognitive performance and cortical data are introduced (Section 3.9) in order to link predictions from brain criticality with cognitive data. The first study includes cortical thickness patterns extracted from MRI data together with different levels of cognitive impairment. The second study aims to test if short TCs are linked to cognitive impairment in patients with epilepsy.

3.1 Model

The model analyzed here is an extension of the model from (Larremore et al., 2014), incorporates parts from (Meisel, 2020; Meisel, Klaus, et al., 2017; Müller & Meisel, 2023) and was previously reported in (Müller et al., 2024). The model consists of $N = 1024$ neurons arranged on a 2-dimensional equidistant grid with periodic boundary conditions (Fig. 3.1 A). The neurons are all-to-all connected, and the initial connection strengths are drawn from a uniform distribution between 0 and 1. Each connection strength w_{ij} between neuron i and neuron j is then scaled by a distance-dependent Gaussian profile

$$\exp^{-\frac{r_{ij}^2}{2\sigma^2}}, \tag{3.1}$$

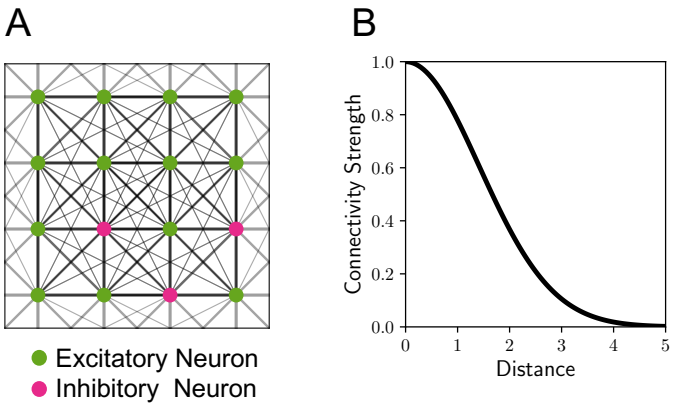

FIGURE 3.1: Network Topology: **A** Excitatory (green) and inhibitory (magenta) neurons are arranged on a 2-d lattice with periodic boundary conditions, i.e., connections leaving on one side come back in on the opposite side. **B** Gaussian profile modifying the connection strength based on the distance between neurons as in Eq. (3.1) for $\sigma = 4$.

where r_{ij} is the distance between the neurons and σ is the scaling width of the profile, which was set to $\sigma = 4$ as in (Müller & Meisel, 2023; Yger et al., 2011; Yu et al., 2014). The Gaussian profile for $\sigma = 4$ is shown in Fig. 3.1 B, and it is balanced between all neurons being disconnected and all neurons being almost equally strongly connected. Furthermore, self-connections are omitted. Lastly, $\alpha = 20\%$ of the neurons are randomly set to be inhibitory by multiplying their outgoing connection strengths with the factor -1. An active inhibitory neuron decreases the firing chance of connected neurons. The other 80% are kept as excitatory neurons (Fig. 3.1 A). An excitatory neuron increases the firing chance of neurons to which it is connected. In general, the network can be tuned from a low to a high connected state by multiplying all connections by the same factor.

The dynamics of the neurons are probabilistic and governed by the inputs they receive from other neurons. Each neuron can at time t either be active $s_i(t) = 1$ or inactive $s_i(t) = 0$. At the next time step, $t + 1$, a neuron will become active based on its inputs with probability

$$s_i(t+1) = \begin{cases} 0, & \sum_j w_{ij} sj(t) < 0 \,, \\ 1, & \sum_j w_{ij} sj(t) > 1 \,, \\ \sum_j w_{ij} sj(t), & \sum_j w_{ij} sj(t) \in [0,1] \,. \end{cases} \tag{3.2}$$

Additionally, one neuron is set to be active in each of the $\max_t = 1000$ time steps as background noise. This background noise could be interpreted as external stimuli or internal brain states that are not explicitly tracked.

3.1.1 Perturbative Mechanisms

Implementing biologically plausible mechanisms that change the dynamics can be valuable addition to the model. These mechanisms can help to generate specific hypotheses that can be tested in experiments. Therefore, we introduce three perturbative mechanisms in our simulations:

1. Introducing random off-periods represents slow-wave activity (SWA) found predominantly in deep sleep stages. In particular, with probability p_{Off} all neurons remain quiescent at a time step similar to the discussion in (Meisel, Klaus, et al., 2017; Vyazovskiy et al., 2011).

2. Interictal epileptiform discharges (IEDs) are introduced in the model as local perturbations by setting a random neuron and its local neighborhood (20% of the network) to be active. This process happens with probability p_{IED}.

3. Antiseizure medications are modelled by reducing the outgoing connections of excitatory neurons by the factor f_{exc}. This mechanism is based on the action mechanism of ion-channel blockers (Meisel, 2020). At the same time, one could also increase the inhibitory connection strength to model GABAergic drugs. Meisel, 2020 has shown that both mechanisms lead to quantitatively similar changes in the dynamics.

All results for a set of parameters are averaged over 1000 simulation runs.

3.2 Quantification of Temporal Correlations

To characterize the models and later the human iEEG dynamics we investigated TCs as they are measures for information maintenance and closely linked to criticality, (Jensen, 2021; Linkenkaer-Hansen et al., 2001; Meisel, Klaus, et al., 2017), (Section 2.1). Generally, TCs characterize the decay speed of the signal's auto-correlation function (ACF). If the ACF decays slowly, information about past states remains for longer times in the system, and thus, TCs are long. In contrast, for a quick decay of the ACF, TCs remain short. TCs are defined as in (Müller et al., 2024).

In detail, to extract TCs in the model, first, the ACF of the average neuron firing in the model is calculated for the entire simulation run (Fig. 3.2 A). Second, the baseline ACF at high lags is extracted, i.e., the median between 1/3 and 1/2 of the whole ACF length. This accounts for potential offsets in the ACF and discards the errors at the end of the ACF originating from the finite time estimation of the ACF. Third, the half maximum between the baseline and the first lag value is calculated, dashed-doted line in Fig. 3.2 A. The zeroth lag value is excluded from the analysis as it is one by definition and not changed by random background noise. This will be particularly important for the iEEG data in Chapter 5 and Chapter 6, which has inherent noise. Last, TCs are defined as the first lag value when the ACF drops below its half maximum (red dot in Fig. 3.2 A). Essentially, TCs are similar to the half

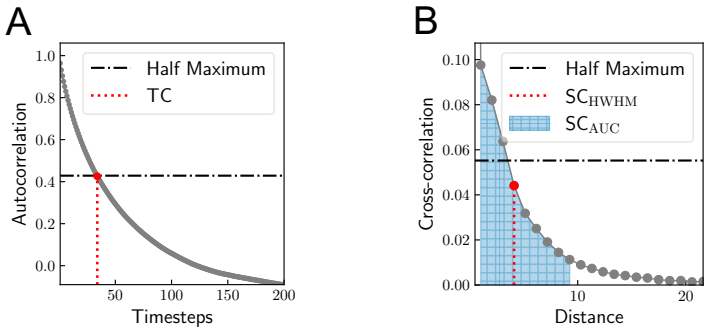

FIGURE 3.2: Definition of Spatial and Temporal Correlations (SCs and TCs): **A** TCs (red dot) are defined as the first lag value when the ACF (gray line) drops between half the value between the first lag and the median between 1/3 and 1/2 of the whole ACF length (dashed-doted line). **B** SCs are defined by the cross-correlation function in two ways. The first is analog to TCs (SC_{HWHM}, red dot), and the second is the area under the curve (AUC) in a predefined distance range (SC_{AUC}, blue shaded area).

width at half maximum of the ACF. Due to the exclusion of the zeroth lag value, the minimal value of TCs is one lag and not zero.

In contrast to the model, TCs in the iEEG data were extracted from the fluctuations of the high-γ power as this has been shown to serve as a proxy for the spatiotemporal population spike rate variation near an electrode (Manning et al., 2009; Miller, 2010; Nir et al., 2007; Whittingstall & Logothetis, 2009).

Following previous work, the channel-wise median high-γ power (56-96 Hz) was calculated every 125 ms using Welch's method with a Hanning window (Honey et al., 2012; Meisel, 2020; Müller & Meisel, 2023; Müller et al., 2024). As high-γ power was approximately log-normally distributed, it was normalized by taking the logarithm (Fig. 3.3).

Auto-correlation functions were then calculated for each channel in 2-minute segments with 90 seconds overlap. Multiple ACFs from different times were aggregated by the median. From these aggregated ACFs, TCs were then extracted similar to the model (Fig. 3.2 A). The baseline of the ACF was calculated as the average value between 1/3 and 1/2 of the 2-minute segment, i.e., 40-60 seconds. Estimation of TCs are qualitatively robust against choosing different baselines as demonstrated in Suppl. Fig. 4 of (Müller & Meisel, 2023). The time resolution of the high-γ power time series was 125 ms, so the smallest lag value, and thus the smallest possible TC value, was also 125 ms.

3.3 Quantification of Spatial Correlations

Similar to sustained information over extended time frames, information needs to travel between distant regions, and thus, correlation between sites is required. This

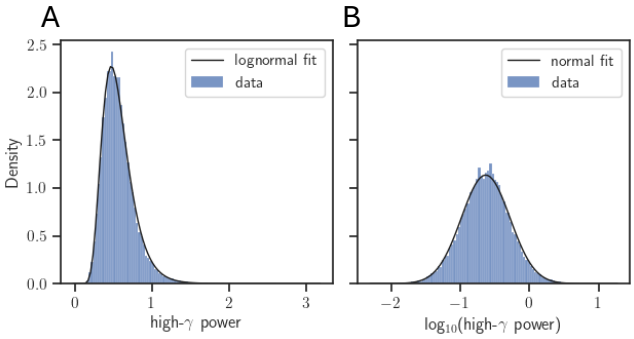

FIGURE 3.3: Distribution of High-γ Power: **A** Raw high-γ power of one exemplary channel with log-normal distribution fitted to the data and **B** $\log_{10}$(high-γ power) with normal distribution fitted to the data.

can be characterized by SCs, which characterize how the information decays over distance. SCs have been linked to criticality and are predicted to be maximal at the critical point, (Cavagna et al., 2010), (Section 2.1). Generally, SCs characterize the decay of the cross-correlation function (CCF) between two neurons or channels with respect to their distance. If the CCF decays slowly, information about the state of one neuron is maintained for longer distances, and thus, SCs are long and vice versa for a quick decay of the CCF. SCs are defined as in (Müller & Meisel, 2023).

In the model, the activity was monitored for 100 random neurons to calculate their cross-correlation. The neuron pair-wise cross-correlation was then averaged for pairs of similar distances to arrive at a distance-dependent CCF. SCs were determined in two ways (Fig. 3.2 B). First, similar to TCs, the first value at which the CCF drops below half the value between the first lag and its baseline. This is essentially a half-width at half maximum; thus, this SC is labeled $\mathrm{SC_{HWHM}}$. Second, SCs are measured as the area under the CCF (AUC), as the first approach depends on the CCF at the shortest distances. These short distances are often unavailable in experimental settings (Chapter 5). Therefore, the mean area under the CCF at a distance between 1 and 10 arbitrary units is assessed and labeled $\mathrm{SC_{AUC}}$. Results were independent of the number of neurons monitored and the choice of evaluated distance between them.

For the iEEG data, only the second method ($\mathrm{SC_{AUC}}$) could be used to evaluate the SCs as electrodes distances were too large to track the fast decay at small distances. The CCF was here calculated from the high-γ power time series in Dataset 2 (Section 3.4) as information on electrode distances was available. Specifically, within 2-minute segments the Pearson cross-correlation was calculated for each pair of electrodes. These correlation values were averaged for pairs with similar distances using equidistant 1 mm wide bins. This resulted in the distance-dependent cross-correlation function (CCF). SCs were then defined as the area under the CCF between 7 mm and 79 mm because for these distances most patients had electrodes (Fig. 3.4).

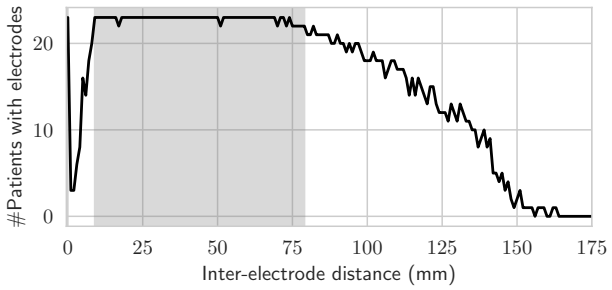

FIGURE 3.4: Electrode Distances for PwDRE: Number of patients which had at least one electrode for each given inter electrode distance.

3.4 Intracranial EEG Datasets

To test the predictions of the model for SCs and TCs we analyzed two independent datasets of persons with drug-resistant epilepsy (PwDRE) who underwent presurgical evaluation, including intracranial EEG (iEEG).

Dataset 1 stems from the Epilepsy Center Berlin-Brandenburg and comprises 81 patients (35 females, average age 32 ± 11 years). All PwDRE had subdural electrodes implanted (average number of electrodes 57 ± 17). Forty-seven PwDRE had temporal lobe epilepsy (TLE), and 34 had extratemporal lobe epilepsy. All PwDRE underwent epilepsy surgery, with 50 achieving a good one-year post-surgical outcome (Engel score = 1). Dataset 1 was previously described in (Müller et al., 2024).

Dataset 2 stems from the epilepsy center at the University of Freiburg and is part of the publicly available Epilepsiae database (Ihle et al., 2012). Dataset 2 included 23 PwDRE (12 female, average age 29 ± 13 years) with subdural and stereo EEG recordings (average number of electrodes 68 ± 27). TLE was diagnosed in 19 PwDRE and extratemporal lobe epilepsy in four. Twenty PwDRE underwent resection, with 14 having a good post-surgical outcome.

Complete patient characteristics for both datasets are in Table 3.1.

3.4.1 Ethics Statement

The analysis of this study was approved by the Institutional Review Board of Charité - Universitätsmedizin Berlin. Due to the study's retrospective nature, patients' informed consent for Dataset 1 was waived. The usage of patient data within Dataset 2 (Epilepsiae database) was approved by the Institutional Review Board of the University of Freiburg, and all patients gave written informed consent that the clinical data might be used and published for research purposes (Ihle et al., 2012).

3.4.2 Antiseizure Medication

Medication information was extracted manually from patient charts for Dataset 1 and was included in Dataset 2. Antiseizure medication (ASM) dosages were normalized by their respective defined daily dosages and summed up for each day. PwDRE

	Dataset 1	Dataset 2
Number of patients	81	23
Sex Female/Male	35/46	12/11
Age	32.3 ± 10.7	28.5 ± 13.2
Epilepsy duration (years)	18.1±12.8	19.3±12.5
History of FBTCS	71	8
Total number of ASMs (previous and current)	5.9±2.6	2.7±1.3
MRI findings		
MTS	12	8
Non-lesional	28	5
FCD	10	7
Others (low grade tumor, vascular lesions, lesions of unclear significance)	31	3
Epilepsy localization		
TLE	47	19
FLE	29	3
OLE/PLE	5	1
Seizure onset side		
Left	48	10
Right	33	5
Bilateral	0	8
Surgical outcome		
Engel 1	50	14
Engel 2-4	24	6
Neuropsychological testing, impaired /not impaired		
Language	54/27	
Verbal Memory	32/49	
Attention	17/64	
Working Memory	37/44	

TABLE 3.1: Patient Characteristics of the IEEG Datasets. FBTCS = focal to bilateral tonic–clonic seizures; MTS = mesial temporal sclerosis; FCD = Focal cortical dysplasia; TLE = temporal lobe epilepsy; FLE = frontal lobe epilepsy; OLE/PLE = Occipital lobe epilepsy/parietal lobe epilepsy. Previously described in (Müller et al., 2024).

routinely underwent ASM tapering during their stay, and days with the lowest and highest summed dosages were identified for analysis. Days with rescue medications (Midazolam, Diazepam, and Lorazepam) were excluded from the study due to their short-term but strong electrophysiological effects. Patients with no dosage change were excluded from all ASM effect analyses.

3.4.3 Electrode Position and Seizure Onset Zone

Clinical needs in both datasets determined electrode placement. Dataset 1 contained only subdural electrodes, while Dataset 2 included subdural and stereo electrodes. For Dataset 1, only lobular information was available without exact coordinates: temporal, frontal, or parietal lobe.

Dataset 2 included electrode coordinates in MNI space. These were extracted by constructing individual brain surfaces from MRI images and warping them into standard MNI-152 template space (Ihle et al., 2012). Electrodes were then assigned to one of five regions of interest (ROI) if they fell within 9.5 mm (euclidean distance) of that ROI using the software *AFNI* (Cox, 1996). This approach provides a trade-off between sample size and positional accuracy. Electrodes assigned to multiple ROIs were excluded. The included ROIs were human equivalents to the regions from (Murray et al., 2014):

MT Medial temporal areas in visual cortex

LIP Lateral intraparietal area in visual cortex

LPFC Lateral prefrontal cortex

OFC Orbitofrontal cortex

ACC Anterior cingulate cortex

These regions are color-coded as in the original paper by Murray et al., 2014 (Fig. 2.6 A & B). They were constructed based on the atlas published by Glasser et al., 2016. A complete list of ROIs and their subregions is in Table 3.2.

Area name as in (Murray et al., 2014)	Zones in humans as in (Glasser et al., 2016)
MT	MST, MT
LIP	VIP, MIP, AIP, LIPd
LPFC	8Ad, 8Av, 9p, 8C, p9-46v, 46, a9-46v, i6-8, s6-8, 8BL, SFL, 44, 45
OFC	OFC, pOFC
ACC	33pr, p24pr, a24pr, a24, d32, p24, a32pr, s32, p32pr

Table 3.2: ROIs Along Functional Hierarchy.

For both datasets, the clinicians annotated each seizure's origin. The seizure onset zone (SOZ) is defined as the set of electrodes that were the origin of at least one seizure during the recording time. All other electrodes were marked as non-seizure onset zone (nSOZ).

3.4.4 Intracranial EEG Preprocessing

The preprocessing pipeline differed slightly between the two datasets due to their distinct characteristics. For Dataset 1, iEEG traces were only available for the first five minutes of each hour, while recordings in Dataset 2 were mainly continuous.

For both datasets, a notch filter was applied to remove power line noise at 50 and 100 Hz, followed by a bandpass filter from 0.1 to 128 Hz to remove slow drifts and high-frequency artifacts. The data was then down-sampled from its original frequency (2048 Hz, 1024 Hz, 512 Hz, or 256 Hz) to a common frequency of 256 Hz. Channels with constant traces were removed as artifacts.

Generally, Dataset 2 was curated for research purposes (Ihle et al., 2012) while Dataset 1 was only extracted retrospectively, which might explain why Dataset 1 tended to have more artifacts. In particular, Dataset 1 required additional preprocessing to remove segments with oscillatory artifacts in the high-γ band. This was achieved by calculating a spectrogram of the high-γ power series and excluding segments with peaks greater than six times the interquartile range over the median segment during recording. This process removed less than 2% of the data.

Visual inspection was performed for both datasets to verify the preprocessing and exclude any additional artifactual channels. Finally, data around seizures, precisely 10 minutes pre- and post-seizure, as well as the seizures themselves, was excluded.

3.5 Slow-Wave Sleep Scoring

To assess the influence of vigilance on SCs and TCs, slow-wave sleep (SWS) was automatically labeled using a validated algorithm (Reed et al., 2017). First, this algorithm calculated a vigilance index for a 30-second segment, which was defined as the band-power ratio (Welch's method, Hanning window)

$$\frac{\theta + \delta}{\alpha + \beta_{\text{high}} + \text{spindle}} .$$

This ratio was high if there was a lot of slow-wave activity (SWA). Therefore, SWA and SWS are used interchangeably from here on. Second, on each day, vigilance indices were z-scored. Third, a segment was defined as SWS if the z-score of its vigilance index was above one. To align the 30-second SWS segments with the 2-minute SCs and TCs segments, a 2-minute segment was labeled as SWS if it contained at least one SWS segment. All other segments were labeled nonSWS.

3.6 Detection of Interictal Epileptic Discharges

Interictal epileptiform discharges (IEDs) are brief abnormal electrical events which disrupt the background activity and thus could have an impact on SCs and TCs (Section 2.3.2). They were identified with a validated algorithm (Quon et al., 2022). The

algorithm first applied a template-matching filter to find candidate IEDs in each channel. In the second step, the iEEG signal around the candidate IEDs was transformed into spectrograms. Last, a pre-trained deep neuronal network rejected or accepted the candidate IEDs. The identified IED times were then aggregated to IED per minute counts. Two-minute segments were classified into four bins: [0,0], (0,1], (1,5], (5-30] IEDs per minute.

3.7 Surrogate Data

In order to test if the results could be explained from the power of the high-γ band alone or if they required the timely coordination of signals, a surrogate analysis with time-shuffled data was performed. In each 2-minute segment, each channel's data points were randomly permuted. This procedure destroyed the temporal coordination of the data points but retained the distribution of their amplitudes. SCs and TCs were then extracted on this surrogate time series and compared to the values from the original time series.

3.8 Statistical Analysis of SCs and TCs

The relationship between SCs and TCs was evaluated using Spearman rank correlation within each patient. P-values on the population were derived through Fisher's method of combination of p-values.

The variation of TCs along the functional hierarchy was evaluated by calculating a Spearman rank correlation ρ and a slope per patient. To get the slope, the regions were assigned numbers from one to five in ascending hierarchical order. We reported both the average ρ and slope. Their significance against no change was evaluated using the Wilcoxon-signed rank test.

The effects of SWS, IED, and ASM were evaluated on the population level using Wilcoxon-signed rank tests. The patient SCs and TCs values were averages of the individual channel results. The channel SCs and TCs were derived from the median CCF and ACF of all time segments per state sub-sampled to the smaller group in the comparison. For example, far fewer segments were classified as SWS than as nonSWS. Consequently, the nonSWS group was randomly sub-sampled to the same number of time points as the SWS group. When comparing more than two groups, all groups were randomly sub-sampled to 50 time points as a trade-off between CCF and ACF robustness and data inclusion. Groups with less than 50 time points were excluded.

Lastly, the trend of TCs over IEDs in the SOZ and nSOZ was evaluated through a linear mixed effects model of the form (notation as in *R*)

$$\mathrm{TC} \sim \mathrm{IED} * \mathrm{SOZ} + (1|\mathrm{patID}) \,. \tag{3.3}$$

In words, TCs were the dependent variable, and both IEDs and SOZ were interacting

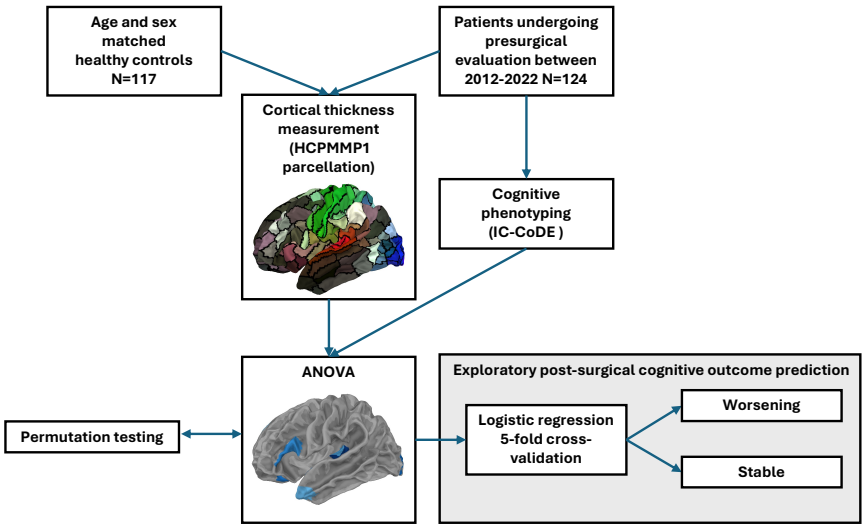

FIGURE 3.5: Study 1 Setup (Structure and Dynamics): Cortical thicknesses distinctively differ for each cognitive phenotype from healthy controls. Reprinted after (Miron et al., 2024) [CC BY-NC 4.0].

independent variables. The PwDREs were treated as random effects on the intercept, represented by (1| patID). Coefficients were reported as mean [95% confidence interval] together with their statistical t-value.

Results were reported as mean ± standard deviation if not stated otherwise.

3.9 Cognitive Impairment related Investigations

To link cortical data with cognitive performance in the context of brain criticality we report two distinct studies. Study 1 investigates distinct cortical thickness pattern in persons with various degrees of cognitive impairments. Study 2 aims to link decreased TCs to cognitive impairment in persons with drug-resistant epilepsy (PwDRE).

3.9.1 Study 1: Structure and Cognition

The aim of this study was to identify abnormal structural pattern in patients with cognitive impairment. Therefore, a new approach to classify cognitive impairment in a coarse grain level was used, i.e., cognitive phenotyping according to the international classification of cognitive disorders in epilepsy (IC-CoDE) criteria (McDonald et al., 2023). For each cognitive phenotype we then aimed to identify the cortical thickness pattern deviating from healthy controls. Ultimately, the aim of this study was to test if these patterns could help to identify cognitive worsening after epilepsy surgery. In Fig. 3.5, an illustration of the outline for this study is provided.

3.9.1.1 Ethics Statement

The institutional review board of Charité - Universitätsmedizin Berlin approved this study (reference number EA2/084_22). Due to the study's retrospective nature, informed patient consent was waived.

3.9.1.2 Participants

The study included 124 PwDRE who underwent pre-surgical evaluation at the Epilepsy-Center Berlin-Brandenburg (63 females, mean age (36.0 ± 12.0) years). The inclusion criteria were drug-resistant temporal lobe epilepsy (TLE) diagnosis, participation in the standard neurological assessment, and a uniform epilepsy MRI protocol. Detailed patient characteristics are provided in Table 3.3.

Additionally, 117 age- and sex-matched healthy controls were acquired from the Human Connectome Project (HCP) to match every individual PwDRE (63 females, age (36.0 ± 12.0) years) (Bookheimer et al., 2019; Van Essen et al., 2013).

3.9.1.3 Cognitive Tests

This study included 16 neuropsychological metrics spanning five distinct cognitive domains (Fig. 3.6).

Verbal learning and memory evaluation was based on a German adaptation of the "Rey Auditory Verbal Learning Test", i.e., the "Verbaler Lern- und Merkfähigkeitstest" (Helmstaedter & Durwen, 1990). The test assessed immediate memory (VLMT1), memory retention at the end of the learning trials (VLMT5), cumulative learning (total of VLMT1-5), and recall abilities after a delay time (VLMT7).

Visual memory and learning were evaluated using the "Diagnostics for Cerebral Brain Injuries" and the "Recurring Figures Test" (Rixecker & Hartje, 1980; Weidlich & Lamberti, 2001). Test scores were the correctly reproduced pattern across trials for the former and figures for the latter.

The **language domain** was assessed with the "Regensburger Wortflüssigkeitstest", which evaluates both semantic and phonetic fluency, including tests with and without category switching (Aschenbrenner et al., 2000).

The **working/short-term memory** domain was tested through "Block Tapping" and "Mottier" tests (Kessels et al., 2000; Welte, 1981).

The **attention domain** was evaluated via the Test Battery for Attentional Performance (TAP; "Testbatterie für Aufmerksamkeitsprüfung"), specifically through its go-no-go and alertness tasks (Zimmermann & Fimm, 1992).

All test outcomes were adjusted for age and sex according to the test manuals to match normative percentiles. If patients missed single tests, the test scores were imputed using *scikit-learn*'s iterative imputer (Pedregosa et al., 2011). The test battery was identical at the one-year follow-up for patients undergoing epilepsy surgery.

	All patients	MDI	FI	MI	P- value
Number of patients	124	66	37	21	
Sex F(M)	63(61)	30(36)	19(18)	14(7)	0.2
Age	36.0±12.0	34.6±11.6	39.4±12.1	34.3±12.3	0.1
Epilepsy duration (years)	18.0±13.2	18.4±14.0	18.4±13.2	14.2±10.5	0.8
Education					0.01*
≤ 12 years	47	31	12	4	
Post-secondary non-tertiary education	41	25	10	6	
Completion of secondary education	12	3	4	5	
Academic education	24	7	11	6	
Presence of FBTCS	96	52(14)	31(6)	13(8)	0.1
Total number of ASMs	5.0±2.2	5.3±2.2	5.1±2.1	4.2±1.6	0.2
MRI findings					0.5
MTS	46	28	11	7	
Non-lesional	55	25	19	11	
Others	23	13	7	3	
Seizure onset side					0.6
Left	65	37	20	8	
Right	49	25	14	10	
Bilateral	10	4	3	3	
Resected, yes (no)	77 (47)	45 (21)	18 (19)	14 (7)	0.1
Surgical outcome					0.8
Engel 1	59	33	15	11	
Engel 2-4	17	12	2	3	

TABLE 3.3: Patient Characteristics of the MRI Dataset. FBTCS = focal to bilateral tonic–clonic seizures; MTS = mesial temporal sclerosis; Others = (focal cortical dysplasia, low grade tumor, vascular lesions, lesions of unclear significance). Previously described in (Miron et al., 2024).

3.9.1.4 Cognitive Phenotyping

Based on the pre-surgical cognitive scores, TLE patients were phenotyped according to the IC-CoDE criteria (McDonald et al., 2023). First, a cognitive impairment on the domain level was diagnosed if at least two tests had scores one standard deviation below the normative average. Second, patients with no impaired domain were classified as minimally impaired (MI). Patients with exactly one impaired domain were classified as focal impaired (FI), and patients with more impaired domains were classified as multi-domain impaired (MDI) (Fig. 3.6).

3.9.1.5 MRI Data

Participants were subjected to 3-Tesla structural MRI scans at Charité – Universitätsmedizin Berlin, Campus Benjamin Franklin, using a Magnetom Skyra (Siemens, Erlangen, Germany) scanner. The protocol included a cerebral 3D T1-weighted sequence optimized for brain imaging (TR/TE = 1900 ms/2.41 ms, TI = 900 ms, flip angle = 9°, voxel size = 0.875/0.875 mm). For comparison, 3D T1-weighted MRIs of healthy controls were sourced from the Human Connectome Project (HCP) S1200 young adult release and the HCP aging and development cohort, employing sequence parameters aligned with established imaging protocols (Bookheimer et al., 2019; Van Essen et al., 2013).

The T1-weighted MRIs from epilepsy patients were converted to NIFTI format using dcm2niix, spatially aligned to the MNI-152 template via fslreorient2std, corrected for intensity non-uniformity using ANTs N4-bias correction, and finally cropped using FSL robustfov (https://fsl.fmrib.ox.ac.uk/fsl/fslwiki/Fslutils) (Jenkinson et al., 2012; X. Li et al., 2016; Tustison et al., 2010). The HCP dataset was already in NIFTI format; however, we performed the same preprocessing and cropping as for the epilepsy dataset to improve comparability. Then, cortical thickness and subregional volumes were parcellated using the CAT12 toolbox, with specific cortical regions delineated according to the HCP Multi-Modal Parcellation atlas (Glasser et al., 2016). This parcellation yielded 360 cortical areas and total intracranial volume, gray matter, and white matter volumes (Dahnke et al., 2013; Glasser et al., 2016).

ANOVA-Based Cortical Thickness Analysis

Type-III ANOVA models were employed to compare MRI regions of interest (ROIs) in the populations of the different cognitive phenotypes to the matched healthy controls. Additional covariates were age, sex, total intracranial volume, and MRI scanner ID to mitigate the impact of technical cofounders. Further clinical covariates included were epilepsy duration (years), total lifetime number of antiseizure medications (ASMs), presence of focal to bilateral tonic-clonic seizures (FBTCS), and seizure onset side.

P-values were corrected for multiple comparisons using Bonferroni correction with n=363 (total number of ROIs and intracranial volume, gray matter, and white matter

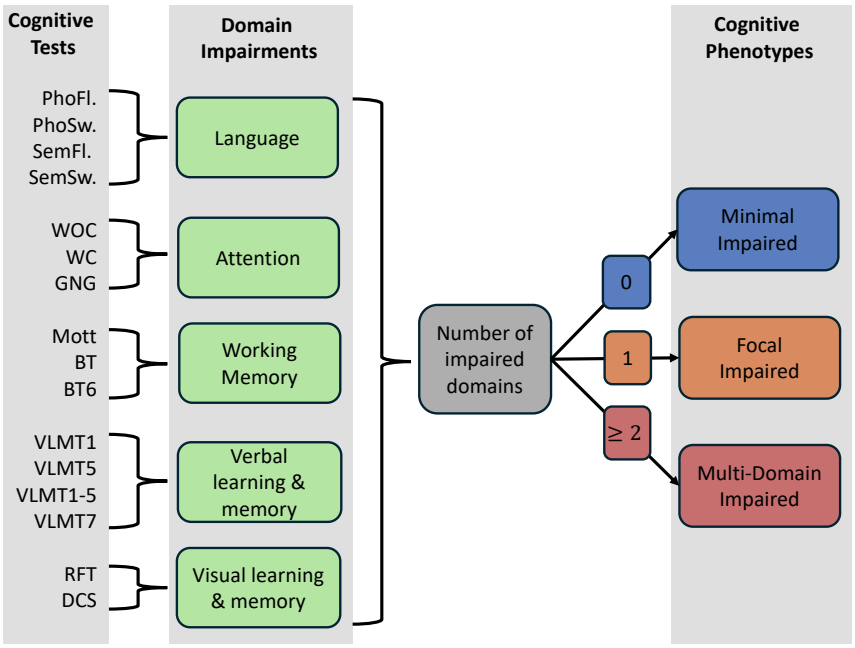

FIGURE 3.6: Cognitive Phenotyping: Phenotyping was performed according to the IC-CoDE criteria (McDonald et al., 2023). First, cognitive tests are clustered into cognitive domains. Second, a domain is counted as impaired if at least two tests in that domain fall one standard deviation below the norm. Third, the cognitive phenotype is derived from the number of impaired domains. PhoFl. = phonetic word fluency; PhoSw. = phonetic category switching; SemFl. = semantic word fluency; SemSw. = semantic category switching; WOC = TAP Alertness subtest without auditory warning cue; TAP = Testbatterie für Aufmerksamkeitsprüfung; WC = TAP Alertness subtest with auditory warning cue; GNG = TAP Go/No-Go subtest; Mott = Mottier test; BT(6) = Block Tapping; VLMT = Verbaler Lern- und Merkfähigkeitstest; RFT = Recurring Figures Test; DCS = Diagnosticum für Cerebralschädigung test.

volume). Only significant (95% F-distribution) differences in cortical thickness between healthy controls and cognitive phenotype were considered for further analysis. The inverse of the F-statistic divided by the average F-statistic was then calculated and labeled as the distance

$$\Delta_i = \frac{\sum_{j=1}^{363} F_j}{363 \cdot F_i} \, . \tag{3.4}$$

Shorter distances reflected a more robust difference between healthy controls and epilepsy patients. Lastly, all ROIs closely associated with MRI scanner ID (distance < 2) were excluded from further analysis.

An additional robustness test was performed by shuffling the labels to the cortical thicknesses on a patient basis and rerunning the ANOVA models. This procedure was repeated 100 times, which provided a baseline p-value-distribution. The empirical p-values needed to fall into the 5th percentile of this permutation-p-value-distribution to be considered significant.

Post-Surgical Cognitive Outcome Prediction

To predict the 1-year post-surgical outcome in each domain, logistic regression models were used to fit the data. Cognitive worsening was defined as a five percent decrease compared to pre-surgical levels. This threshold is a trade-off between robust identification of worsening and keeping group sizes balanced enough to train meaningful predictive models.

The input features were the $n = 13$ ROIs most robustly connected to cognitive phenotypes (distance < 1, Table 6.1) and the clinical features. Different cognitive impairment groups had to be combined; otherwise, the sample size for this approach would have been too small. The patient characteristics for each domain are in Table 3.4.

First, descriptive logistic regression models were fit to the whole dataset. Second, the predictive power of the ROIs' cortical thicknesses was evaluated in a cross-validation scheme (100 times repeated 5-fold nested cross-validation with recursive feature elimination and l2 regularization). Models were built for ROI features, clinical features, and a combination of both. All models were compared by area under the receiver operating curve (ROC-AUC) in the hold-out data within the cross-validation scheme.

Furthermore, all models were tested against two random classifiers. The first random classifier used randomly shuffled worsening labels as predictions. This kept the prevalence constant but destroyed the relationship between variables and labels. The second random classifier drew $n = 13$ random ROIs and used these instead of the 13 ROIs found in the ANOVA cortical thickness analysis.

3.9.2 Study 2: Dynamics and Cognition

The goal of the second study was to investigate the relationship between TCs and cognitive impairment in PwDRE. Therefore, TCs were scored similar as discribed above (Section 3.2). The dataset used for this study is identical to the Dataset 1 (Section 3.4) with detailed patient information in Table 3.1.

Cognitive Data

Cognitive testing was performed before the pre-surgical evaluation, so iEEG recordings parallel to the testing were unavailable. This emphasizes the need to evaluate a broad spectrum of baseline cognitive performance, i.e., many tests spanning many cognitive domains. For this cohort, sufficient cognitive testing was available only for four domains compared to the five domains in Study 1: Verbal learning and memory, language, working/short-term memory, and attention. However, the tests in these domains were identical and are described in Section 3.9.1.3. If single tests were missing for a patient, they were extrapolated with *scikit-learn*'s iterative imputer (Pedregosa et al., 2011). Cognitive impairment was also similarly defined, i.e., if at least two tests in a domain were one standard deviation below the norm. The reduced domain

	Language (N=68)		Working memory (N=66)		Verbal memory (N=64)		Non verbal memory (N=68)	
	Stable (N=51)	Worse (N=17)	Stable (N=54)	Worse (N=12)	Stable (N=40)	Worse (N=24)	Stable (N=49)	Worse (N=19)
Sex								
Female	27 (53%)	7 (41%)	27 (50%)	6 (50%)	20 (50%)	12 (50%)	24 (49%)	10 (53%)
Male	24 (47%)	10 (59%)	27 (50%)	6 (50%)	20 (50%)	12 (50%)	25 (51%)	9 (47%)
Age	32.6±11.8	35.2±11.4	32.6±10.9	31.2±9.5	32.8±9.9	29.9±10.0	33.1±11.8	33.6±11.5
Epilepsy duration	17.8±14.2	16.5±11.4	18.4±13.7	10.8±8.4	17.6±12.6	14.2±12.1	18.5±14.3	14.8±10.7
Total number of ASMs	5.2±2.5*	3.9±1.6	4.8±2.3	4.9±2.0	4.8±2.5	4.8±1.8	5.1±2.4	4.5±2.1
History of FBTCS	37 (73%)	13 (76%)	40 (74%)	10 (83%)	28 (70%)	20 (83%)	36 (73%)	14 (74%)
Pre-surgery percentile	18.5±18.3***	40.2±21.1***	23.0±15.6***	41.8±19.1 ***	27.4±23.6 **	41.9±24.5 **	30.6±22.7***	53.3±19.6***
Cognitive phenotype								
MDI	31 (61%)	6 (25%)	33 (61%)	4 (33%)	23 (58%)	13 (54%)	26 (53%)	11 (58%)
FI	11 (22%)	7 (41%)	11 (20%)	6 (50%)	11 (28%)	5 (21%)	13 (27%)	5 (26%)
MI	9 (17%)	4 (34%)	10 (19%)	2 (17%)	6 (14%)	6 (25%)	10 (20%)	3 (16%)
Resection left	23 (45%)	10 (59%)	26 (48%)	8 (67%)	16 (40%)	16 (67%)	25 (51%)	8 (42%)
Resection right	28 (55%)	7 (41%)	28 (52%)	4 (33%)	24 (60%)	8 (33%)	24 (49%)	11 (58%)
Surgery outcome								
Engel 1	43 (84%)	12 (71%)	43 (80%)	10 (83%)	32 (80%)	19 (79%)	41 (84%)	14 (74%)
Engel 2-4	8 (16%)	5 (29%)	11 (20%)	2 (17%)	8 (20%)	5 (21%)	8 (16%)	5 (26%)
Pathology								
MTS	20 (39%)	3 (18%)	18 (33%)	5 (42%)	13 (33%)	8 (33%)	20 (41%)	3 (16%)
Non-MTS	31 (61%)	14 (82%)	36 (67%)	7 (58%)	27 (67%)	16 (67%)	29 (59%)	16 (84%)

TABLE 3.4: Patient Characteristic for the Post-Surgical Testing: FBTCS = Focal to bilateral tonic clonic seizures; MTS = mesial temporal sclerosis. Previously described in (Miron et al., 2024).

count made cognitive phenotyping less robust. Thus, the analysis for Study 2 remains restricted to the domain impairment level (Fig. 3.6).

3.9.2.1 List of Measures

The main goal of this study was to test if TCs can predict cognition as proposed by brain criticality. However, multiple other measures were evaluated to strengthen the analysis and, thus, the link of TCs to cognitive impairment in the domains.

TCs are defined as in Section 3.2 and characterize the decay of the auto-correlation function of the high-γ band fluctuations (55-95 Hz).

Surrogate TCs are defined as TCs; however, they are extracted from a time-shuffled version of the high-γ band time series as described in Section 3.7.

Band powers are extracted for the standard EEG frequency bands δ (0.5-4 Hz), θ (4-8 Hz), α (8-12 Hz), β (12-30 Hz), γ (30-45 Hz) and high-γ (55-95 Hz) using Welch's method (Hanning window). These measures give information about the power at a given time; however, they neglect the timely coordination of these power fluctuations.

IEDs were found to have a negative effect on TCs (Chapter 5) and have been previously associated with worse cognitive performance (Aldenkamp & Arends, 2004; Ebus et al., 2012; Meekes & Jennekens-Schinkel, 2018). Therefore, they were included as another control measure. IEDs were extracted as described in Section 3.6.

SWS showed a disruption of TCs (Chapter 5). While the data analyzed here was cleaned of SWS segments, the general percentage of SWS during the day was included as a control measure. SWS was extracted as discussed in Section 3.5.

ASMs had a negative effect on TCs (Chapter 5). Thus, the day with the lowest ASM load was analyzed separately. Furthermore, the total ASM load for each day was added as a control measure.

All measures, except SWS and ASM, were extracted in 2-minute windows to align with TCs. SWS and ASM were, by definition, day-wise values. Then, all measures were aggregated per electrode over a day by taking the median measure value during all nonSWS segments. Because patients had different recording lengths, only three distinct days were analyzed: the first, last, and lowest ASM days. The first and last days were the first and last days, which had more than 18 hours of data, respectively.

Statistical Analysis of Cognitive Impairments and TCs

Statistical significance of the association between cognitive impairment and measures was established through Brunner-Munzel tests. Only comparisons with at least $n = 5$ PwDRE group were included as otherwise statistical significance at $p < 0.05$ could not be achieved by definition. The advantage of this non-parametric test is that it does assume neither normality nor homoscadisity, both conditions one would not expect for TCs. P-values were corrected for multiple comparisons through the Benjamini-Hochberg method ($\alpha = 0.05$). To further emphasize that results are unlikely to arise by chance, the distribution of p-values for each measure was compared to a uniform

distribution, which could be expected under the null hypothesis that the groups are equal. The comparison between the groups was then quantified using the Kolmogorov-Smirnov test.

The non-parametric relative effect size was reported to quantify further the difference between the cognitively impaired and not-impaired groups. This effect size describes the probability that if one picks a sample out of each group, the sample of one group would be larger than the other.

3.10 Code Availability

Code for the model simulations is available under https://gitlab.com/computational-neurologie/stc_model_2024. The code for analysis of Dataset 1 is available under https://gitlab.com/computational-neurologie/ieegCD and for Dataset 2 under https://gitlab.com/computational-neurologie/sde_n_cog. The code for analysis of the MRI and cognitive data is available under https://gitlab.com/computational-neurologie/structural_cognitive_TLE.

Chapter 4

Neuronal Network Model

Chapter 2 introduced the brain criticality hypothesis and the branching processes. This review showed that at the critical point, many information theoretical properties are optimized (Shew & Plenz, 2013). Previous work has shown this in models, for example, for the dynamical range (Shew et al., 2009), information capacity and transmission (Langton, 1990; Shew et al., 2011), or the number of metastable states (Haldeman & Beggs, 2005).

This chapter will investigate how spatial and temporal correlations (SCs and TCs) behave around the critical point. Therefore, we analyze the branching-process-like neuronal network model introduced in Section 3.1 and investigate how SCs and TCs change with respect to the connection strength between the neurons. After establishing SCs and TCs around the critical point, we will test how SCs and TCs change under three perturbative mechanisms: slow-wave activity (SWA), interictal epileptiform discharges (IEDs), and antiseizure medications (ASMs). The model results for TCs were previously reported in (Müller & Meisel, 2023; Müller et al., 2024) and the SCs results were partially reported in (Müller & Meisel, 2023).

The aim of simulating these conditions is to provide testable predictions of the interplay between network structure and perturbative mechanism with dynamical measures of brain criticality and, thus, cognitive performance. These predictions will later be tested in data from persons with epilepsy.

4.1 Results

4.1.1 The Connection Strength Governs the Dynamics

Generally, the model studied here is an extension of the model by Larremore et al., 2014. Similarly, it has a parameter regime with ceaseless dynamics due to the inclusion of inhibitory neurons (Fig. 4.1 A). To evaluate this further, we will investigate how the strength of the connection between neurons influences their dynamics. Therefore, the whole connectivity matrix is multiplied by a constant factor. For the original model by Larremore, they showed that the long-term dynamics are dependent on the largest absolute eigenvalue of the connectivity matrix, λ, which scales likewise under multiplication with a constant factor (Larremore et al., 2011, 2014). Therefore, λ is the control parameter for the connection strength. Generally, this discussion is

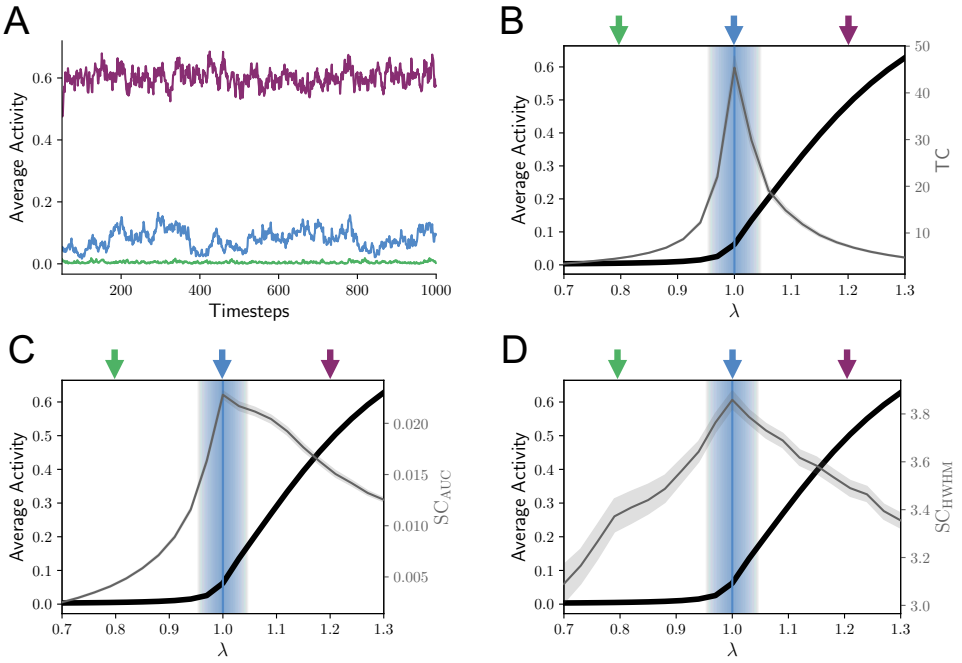

FIGURE 4.1: Connectivity Shapes Network Dynamics, SCs and TCs: **A** Average network activity traces for three regimes of network simulations: subcritical (green), critical (blue), and supercritical (purple). While the integrated network activity (black lines) monotonously increases as function of the largest absolute eigenvalue of the connectivity matrix λ, **B** TCs, **C** SC_{AUC}, and **D** SC_{HWHM} (gray lines) peak at the critical point, $\lambda \approx 1$ (blue arrow).

analogous to the discussion of the branching process (Section 2.1.2).

For very weakly connected networks, $\lambda \ll 1$, the activity does not spread, only a small amount of nodes get engaged, and the dynamics hover around the baseline background activity (green trajectory in Fig. 4.1 A). Generally, the activity stays low, and no excursions can be observed (black line at in Fig. 4.1 B). Because the background noise mainly drives the activity, activities are not correlated in time, and thus, TCs remain low (green arrow in Fig. 4.1 B). Furthermore, as the activity can not spread over the network, SCs measured in both ways are low (green arrows in Fig. 4.1 C, D). In short, the dynamics are subcritical.

For the other extreme case, where the network is very strongly connected, $\lambda \gg 1$, the activity hovers around a higher saturation value as the neurons are generally oversaturated by inputs (purple trajectory in Fig. 4.1 A). Each new noise input quickly travels through the whole network, and thus, the memory of previous inputs is lost quickly, also leading to short TCs (purple arrow in Fig. 4.1 B). While activity can travel quickly through the network, one could think that SCs are high. However, neurons are already oversaturated by the inputs from their closest neighbors. Consequently, even the summed inputs from neurons farther away matter less, and thus, SCs are small too (purple arrows in Fig. 4.1 C, D). In a nutshell, the dynamics are supercritical.

For well-balanced network connectivity, $\lambda \approx 1$, dynamics evolve non trivially (blue

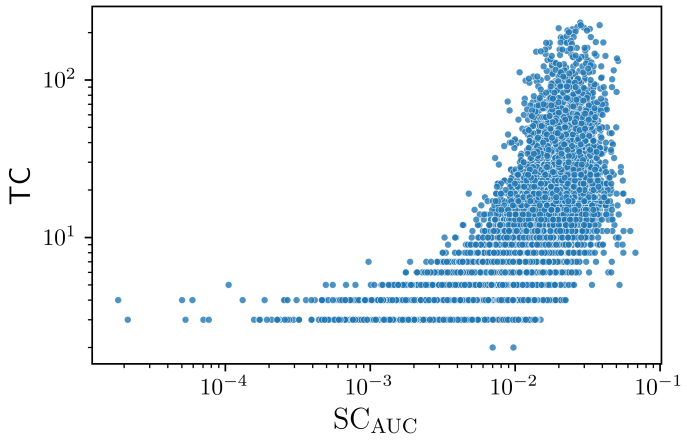

FIGURE 4.2: Correlation of SCs and TCs. Correlation of SC_{AUC} and TC for simulations with different λ in the range as in Fig. 4.1.

trajectory in Fig. 4.1 A). The average activity of the network starts to exhibit larger excursions, and dynamics appear less uniform. These excursions evolve as transients in the network, thus conserving some memory of the initial input over time, leading to long TCs (blue arrow in Fig. 4.1 B). Additionally, these transients engage larger parts of the network, manifesting in cascades, and therefore correlate the activity of distant neurons with each other, which is reflected in longer SCs (blue arrows in Fig. 4.1 C, D). In summary, the system is close to its critical point where a wide range of sustained activity can be observed, and information can travel through network space and time.

Taken together, this shows that under variation of the network's connectivity, SCs and TCs behave similarly, thus leading to a strong co-variation of SCs and TCs for a system whose proximity to criticality changes. This covariation under variation of λ is shown for TCs and SC_{AUC} in Fig. 4.2 (Spearmanr rank correlation: $\rho = 0.77$, $p <$ machine precision). In general, the model results aligns well with the theory on the branching process and the brain criticality hypothesis (Section 2.1.2) and unify previous studies which at the critical point separately showed maximal SCs (Cavagna et al., 2010) and TCs (Jensen, 2021; Meisel, Klaus, et al., 2017).

4.1.2 Perturbations of the Dynamics

While the model can be investigated in different regimes by scaling the connection strength, this approach is less plausible and difficult to achieve in experimental settings, particularly for retrospective data analysis. Rather than actively changing the connectivity, it is more feasible to investigate biological mechanisms that might alter the dynamics, proximity to criticality, and, consequently, SCs and TCs.

Therefore, we introduce three perturbative mechanisms into the model, which will be investigated in the experimental data (Chapter 5). Specifically, the effect of slow-wave activity (SWA) typical for slow-wave sleep (SWS), interictal epileptiform discharges (IEDs), and antiseizure medications (ASMs) on SCs and TCs are evaluated.

Results for TCs and all three perturbations were previously reported in (Müller et al., 2024), and results for SCs with respect to SWS and ASMs were previously reported in (Müller & Meisel, 2023).

4.1.2.1 Slow-Wave Activity

First, off-periods modeling SWA are introduced as the probability p_{Off} that neurons synchronously go offline. In Fig. 4.3 A, two trajectories for a network with $\lambda = 1$ are shown: one with an off period (teal) and one without (gray).

Generally, each off-period disrupts the background activity by setting all neuron states to zero, thus interrupting the dynamics and destroying memory between pre- and post-off-period segments. This explains why TCs gradually decrease with increasing p_{Off} for subcritical and critical networks (Fig. 4.3 B). In the supercritical state, however, the dynamics are already around an upper saturation threshold and inherently have lower memory of past states. Here, an introduced off-period leads to small activity, which then builds up again, thus introducing a transient from zero activation to the saturation boundary. This explains why, for small p_{Off}, TCs are increased in the supercritical state (Fig. 4.3 B). For larger p_{Off}, these transients get disrupted again, leading to decreased TCs. While the off-periods occur randomly and are thus tempo-

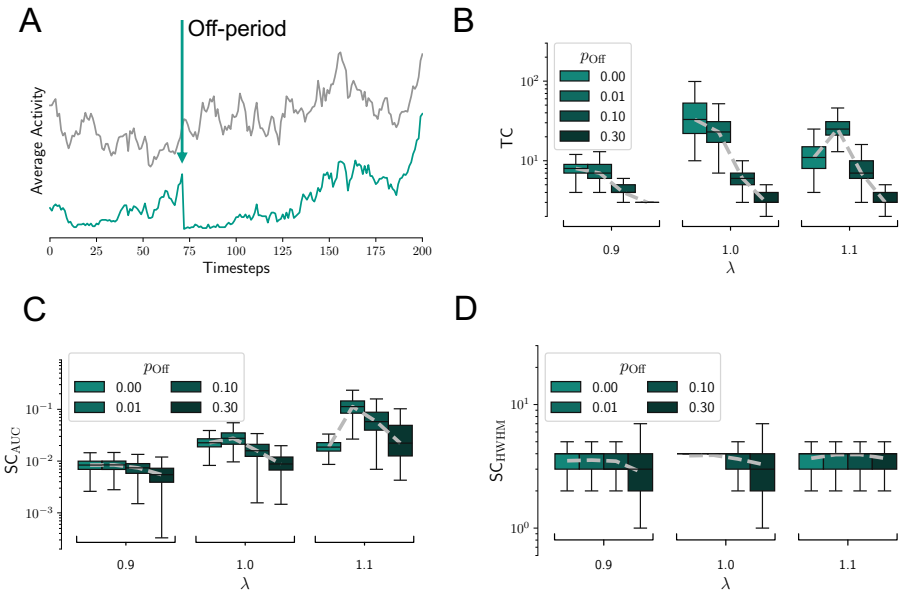

FIGURE 4.3: Slow-Wave Activity in the Model: **A** One trajectory with an off-period, where all neurons are deactivated, (teal) and one trajectory without (gray) for a critical connected network **B** TCs tend to gradually decrease with increasing probability for off-periods p_{Off}. **C** SC_{AUC} and **D** SC_{HWHM} increase with small p_{Off}, however, for larger p_{Off} they decrease again.

rally uncorrelated, they set all neurons into the same state. This can artificially create stronger cross-correlations between neurons. In particular, in the supercritical state, each off-period is priming a new transient with stronger correlations between neurons

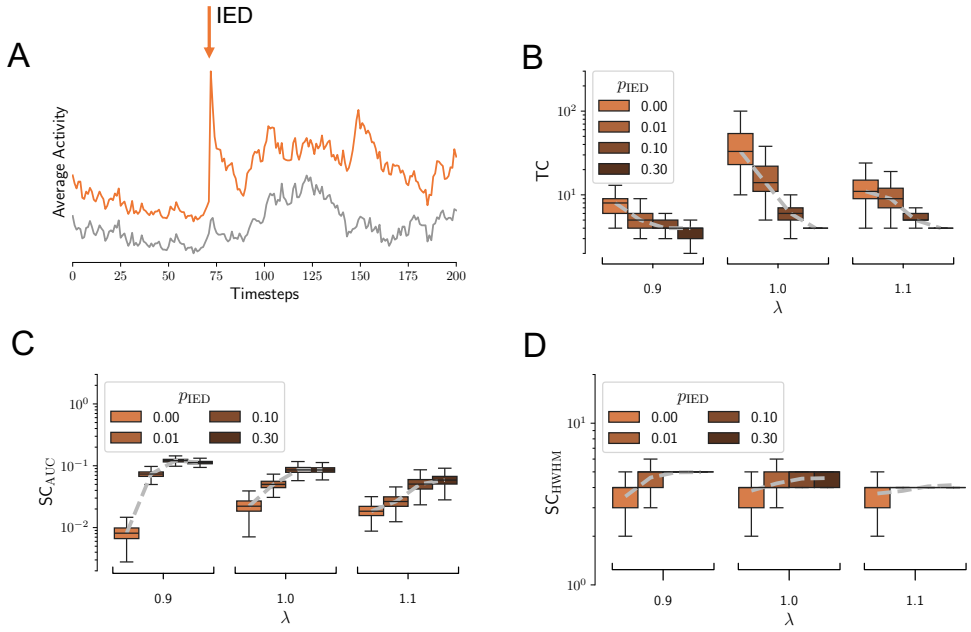

FIGURE 4.4: Interictal Epileptiform Discharges in the Model: **A** One trajectory with an IED (orange) and one without (gray) for a network initiated at critical connectivity. **B** As IEDs are temporally uncorrelated, TCs gradually decrease with increasing probability for IEDs, p_{IED}. **C** $\mathrm{SC_{AUC}}$ and **D** $\mathrm{SC_{HWHM}}$ increase with increasing p_{IED} due to the spatially localized activation of neurons through each IED.

than during the dynamics around the saturation boundary. Hence, SCs are increased for small p_{Off} (Fig. 4.3 C and D). With rising p_{Off}, even the transients get disrupted, leading to weaker correlations between distant sites and, thus, SCs eventually decrease (Fig. 4.3 C and D).

In summary, SWA disrupts the network dynamics in a temporally uncorrelated manner, which decreases TCs for critical networks. This aligns with the findings by Meisel, Klaus, et al., 2017, where off-periods simulating SWA were introduced in a similar model. However, introducing off-periods is a global pattern that can lead to an increase in SCs. If the off-periods become too frequent, the network dynamics are disrupted, and both SCs and TCs decrease compared to the unperturbed state.

4.1.2.2 Interictal Epileptiform Discharges

Second, IEDs are introduced as activations of local cohorts of neurons with probability p_{IED} at random places and times. In Fig. 4.4 A, a trajectory with (orange) and without (gray) an IED is shown for a system initiated with $\lambda = 1$. The IED can be observed as a large spike in the average activity.

These abnormal, uncorrelated events disrupt not only the information from a neuron's past but also from the past of its neighbors, which are most influential for the neuron's future. Consequently, TCs progressively decline with increasing probability for IEDs, irrespective of the dynamical regime (Fig. 4.4 B).

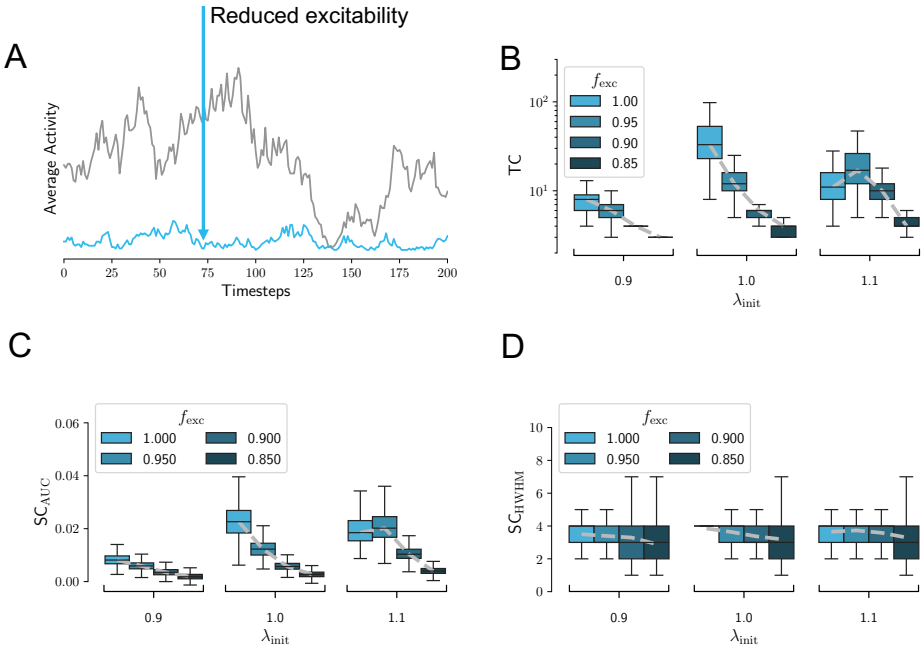

FIGURE 4.5: Antiseizure Medication in the Model: **A** Two trajectories for initially critical networks, one with by $f_{\text{exc}} = 0.9$ reduced excitatory connections (blue) and one unaltered (gray). **B** TCs tend to decrease with a stronger reduction of the excitatory connection strength, particularly for initially critical and subcritical systems ($\lambda_{\text{init}} \leq 1$). **C** SC_{AUC} and **D** SC_{HWHM} exhibit a similar trend as TCs, i.e., SCs become smaller with reduced excitatory connection strength.

However, the joint activation of local neuron cohorts introduces significant correlations between the neurons, leading to a general increase in SCs with increasing p_{IED} (Fig. 4.4 C & D). Thus, while the IEDs are uncorrelated in time, they are strongly localized spatially correlated patterns.

In summary, IEDs introduce localized, sudden increases in neural activity that disrupt temporal continuity, resulting in decreased TCs across all dynamical regimes. However, simultaneously, the synchronous activation of local neuron groups strengthens SCs.

4.1.2.3 Antiseizure Medication

Third, ASMs are introduced by altering the excitation-inhibition balance. Here, the focus is on the effect of reduced excitability, which can be associated with ion-channel blockers like Phenytoin or Carbamazepine (Sankar & Holmes, 2004). In the model this has been achieved by decreasing the outgoing connection strength of excitatory neurons by a factor f_{exc}. In Fig. 4.5 A, two trajectories are shown. Both are initially set with $\lambda_{\text{init}} = 1$, but for one of them (blue), the excitatory connection strength is decreased by a factor of $f_{\text{exc}} = 0.9$. It has been shown that increased inhibitory connection strength, as associated with GABAergic drugs, can lead to similar changes in the model dynamics (Meisel, 2020).

Generally, a smaller f_{exc} leads to a decrease in the effective connectivity, reducing activity propagation. Fluctuations remain smaller, and the external noise driving the system starts to outweigh the internal dynamics. Consequently, a system with initially critical or subcritical connectivity ($\lambda_{\text{init}} \leq 1$) behaves more subcritical, and TCs decline (Fig. 4.5 B). Similarly, the reduced connectivity between neurons makes them less correlated, causing SCs to decline (Fig. 4.5 C & D). Note that f_{exc} scales the effective connectivity, and if one recalculates λ after applying f_{exc}, it is also reduced (Fig. 4.6).

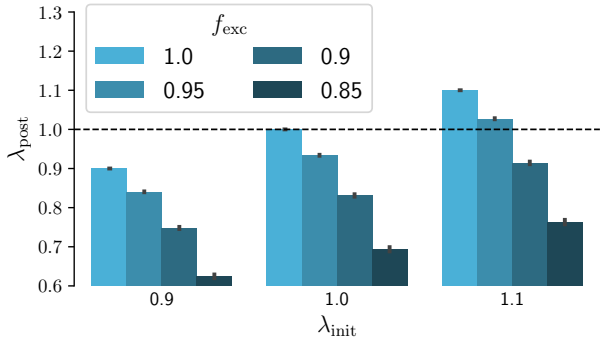

FIGURE 4.6: Network λ After Scaling With f_{exc}: Networks were initialized with λ_{init}. After scaling with the ASM effect, $f_{\text{exc}} < 1$, λ_{post} was reduced.

In the supercritical regime, a small reduction in effective connectivity can push the system closer to the critical point, leading to increased TCs and SCs for moderately small f_{exc} (Fig. 4.5 B - D). However, a stronger reduction of f_{exc} shifts the system beyond the critical point, causing both TCs and SCs to decline again (Fig. 4.5 B - D). This can be explained by f_{exc} scaling the effective connectivity and thus reducing λ (Fig. 4.6).

In summary, ASMs modeled as a reduction in excitatory connection strength generally lead to more subcritical behavior. This results in decreased TCs and SCs for systems at or below criticality. These findings for TCs align with the findings by Meisel, 2020, where the effects of ASMs were investigated in a similar model. In supercritical systems, a mild reduction in excitatory strength can paradoxically increase both measures by bringing the system closer to criticality before eventually causing decreases with further reductions.

4.2 Model Conclusion

This chapter extended on previous investigations and analyzed a model that allowed for the investigation of SCs and TCs around criticality and under the impact of perturbative mechanisms (SWA, IEDs, and ASMs).

The Connectivity Determines SCs and TCs

Similar to previous studies, we showed that the model exhibits a phase transition between ceasing and saturating activity when changing the overall connection strength (Larremore et al., 2014). Specifically, the critical point emerged as the largest absolute eigenvalue of the connectivity matrix approached $\lambda = 1$. At the critical point, both SCs and TCs were maximized, aligning with previous studies showing the maximization of other information theoretical properties at the critical point (Shew & Plenz, 2013), e.g., dynamical range (Shew et al., 2009), or information capacity (Shew et al., 2011). Varying the connection strength, SCs and TCs covaried similarly. This emphasizes the importance of the underlying network structure for the system's dynamics, SCs, TCs, and the proximity to the critical point. While here only the effect of the overall connection strength was investigated, it has been shown that factors like the degree correlation can impact the critical point, too (Larremore et al., 2011).

Impacts of Perturbative Mechanisms

While changing connectivity in the model is achieved straightforwardly, this is much more difficult in an experimental setting. To address this, we introduced three biologically inspired mechanisms that can alter the dynamics of cortical networks and showed how they impact SCs and TCs in the model. The specific results are summarized in Table 4.1. Generally, at the critical point, TCs were disrupted by all three perturbations: SWA, IEDs, and ASMs. While SCs followed this trend for SWA and ASMs, they showed an increase under higher IED pressure.

These results suggest that if SCs and TCs gradually increase, the system is pushed further towards criticality. While decreasing SCs and TCs are a sign of a drift away from criticality, it is not possible to argue if this happened toward supercritical or subcritical dynamics.

	Effect on TCs			Effect on SCs		
	$\lambda < 1$	$\lambda \approx 1$	$\lambda > 1$	$\lambda < 1$	$\lambda \approx 1$	$\lambda > 1$
Baseline SC & TCs	Low	Maximal	Low	Low	Maximal	Low
SWA	↘	↘	↗↘	↘	↘	↗↘
IEDs	↘	↘	↘	↗	↗	↗
ASM	↘	↘	↗↘	↘	↘	↗↘

TABLE 4.1: Effect of Perturbations on SCs and TCs: SCs and TCs change under perturbation across different dynamical regimes (subcritical: $\lambda \leq 1$, critical $\lambda \approx$, supercritial $\lambda \geq 1$). ↘ = decrease, ↗ = increase, ↗↘ increased followed by a decrease when effect is stronger.

Predictions for Human Cortical Data

This model provides a framework for understanding how various perturbations affect SCs, TCs, and criticality in human cortical dynamics. Together with the brain criticality hypothesis, it allows for the formulation of testable predictions. While the

following predictions are not exhaustive, they remain testable in the experimental boundaries of this study:

(a) SCs and TCs are interconnected.

(b) SWA typical for SWS disrupts SCs and TCs.

(c) TCs decline and SCs increase with increasing IED load.

(d) SCs and TCs decline with increased ASM load.

These predictions will be tested in the following Chapter 5 where human intracranial EEG recordings are combined with automatically extracted SWS and IED markers and ASM charts.

Chapter 5

Spatial and Temporal Correlations in Intracranial EEG

The previous chapter showed neuronal network model simulations, and analyzed how spatial correlations (SCs) and temporal correlations (TCs) varied under parameter changes and perturbations in these simulations. The model exhibited a critical point at which SCs and TCs became maximal, aligning with the brain criticality framework (Beggs, 2022a; Beggs & Plenz, 2003; Chialvo, 2004).

The criticality framework and model simulations in the previous chapter predicted SCs' and TCs' behavior for cortical network dynamics. This chapter aims to verify these predictions in human EEG data. Specifically, the model predicted that SCs and TCs co-vary and decline when subjected to antiseizure medication (ASM) or slow-wave activity (SWA). Under increased interictal epileptiform discharge (IED) rates, TCs decreased while SCs increased. While some previous research investigated such changes, e.g., the decline of TCs during SWS (Meisel, Klaus, et al., 2017) and ASM (Meisel, 2020), experimental evidence on the interconnection between SCs and TCs remains sparse. This may be attributed to several limitations in previous studies, like short recording duration, sparse spatial coverage, coarse temporal resolution, and small patient cohort size.

Addressing these limitations, this chapter analyzes multiday intracranial EEG (iEEG) recordings from 104 persons with drug-resistant epilepsy (PwDRE) undergoing pre-surgical evaluation from two independent datasets. The iEEG data has a high temporal and spatial resolution (up to 118 electrodes per patient). The length and sampling of the datasets allow for a nuanced analysis of SCs and TCs, their co-variation, and changes under perturbative mechanisms. The spatial placement of electrodes was clinically decided, leading to variation in the cortical coverage. While this introduced additional variance, it allowed for spatial analysis of cortical network dynamics. We address two additional questions arising from this:

1. Electrodes placed in different brain regions might exhibit distinct TC characteristics, potentially aligning with the functional hierarchy shown in non-human primates (Murray et al., 2014). To investigate this, TC variations will be analyzed in analogous human regions along the hierarchical hierarchy.

2. Electrodes are placed to cover the likely seizure onset zone (SOZ), which might not accurately represent typical cortical network dynamics. Within the brain criticality, the SOZ has even been hypothesized to be closer to the critical point (Meisel et al., 2012). We will compare TCs from SOZ electrodes against non-SOZ (nSOZ) electrodes to account for this.

This chapter is structured as follows:

1. Qualitative examination of SCs and TCs over multiple days and their co-variability (Section 5.1.1).
2. Investigation of TCs along the functional hierarchy (Section 5.1.2).
3. Changes of SCs and TCs corresponding to SWS, IEDs, and ASM (Section 5.1.3).
4. Nuanced comparison of perturbative mechanisms in SOZ versus nSOZ (Section 5.1.3.4).
5. Summary of findings and brief discussion (Section 5.2).

The main discussion in the context of brain criticality will be presented at the end of this thesis (Chapter 7). Some of these results have been previously published: Points: 1. - 3. in (Müller & Meisel, 2023) and points: 3. & 4. (Müller et al., 2024).

5.1 Results

Long-range SCs and TCs have been proposed to measure information processing (Jensen, 2021; Linkenkaer-Hansen et al., 2001; Meisel, Klaus, et al., 2017). However, previous investigations were mainly task-related and thus limited in duration. Consequently, the variance of SCs and TCs over time, their interdependence, and their relationship with external and internal mechanisms remains mostly unexplored. While for Dataset 1 (Section 3.4), no exact electrode positions were available, Dataset 2 (Section 3.4) had standard MNI coordinates for all intracranial electrodes, allowing the calculation of SCs. The feature extraction is illustrated in Fig. 5.1 A. For one example patient, the time course of SCs and TCs is shown for two days in Fig. 5.1 B and C. Both SCs and TCs varied over one day and between days. Most prominent was this for TCs, which exhibited larger fluctuation on the second day (Fig. 5.1 C) compared to generally lower values on the first day (Fig. 5.1 B).

5.1.1 Spatial and Temporal Correlations Co-Vary

The model from the previous chapter predicted maximal SCs and TCs at the critical point and a joint decline induced by the dynamics drifting away from the critical point.

Indeed, the variations of SCs and TCs over time were strongly correlated, i.e., an increase in SCs aligned with an increase in TCs and vice versa. This is shown

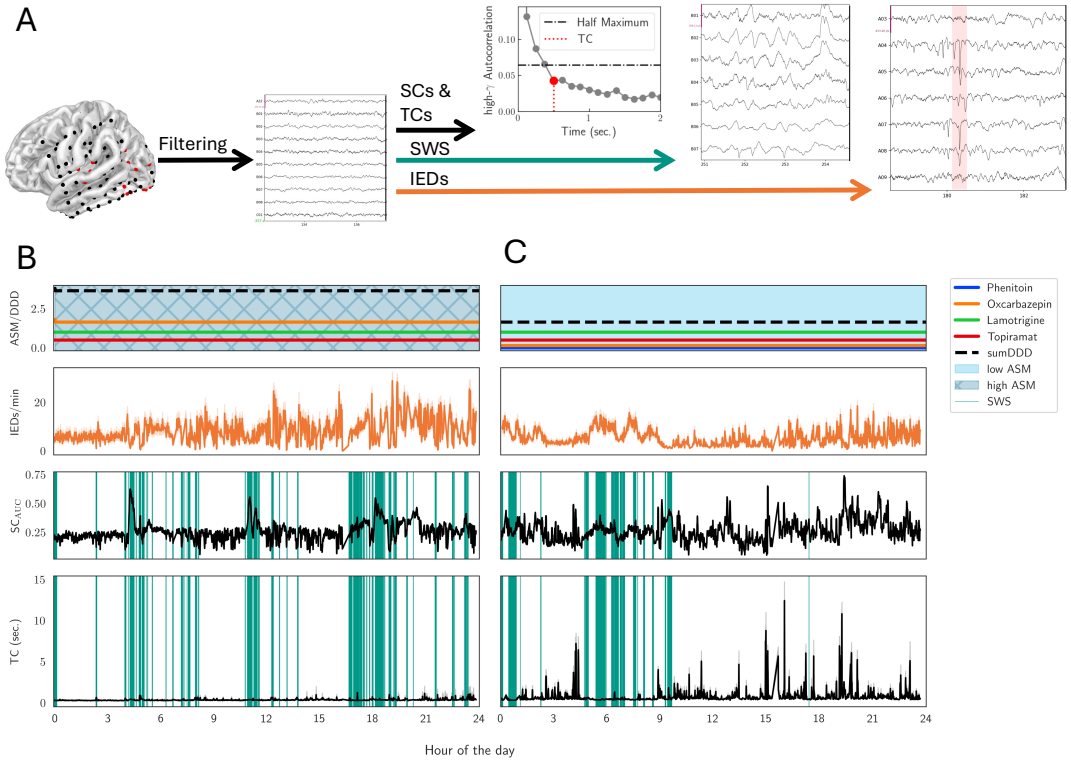

FIGURE 5.1: Processing Pipeline and Time Course: **A** Intracranial EEG recordings are filtered, and the features are extracted. SCs and TCs are extracted from the high-γ band of the signal only, whereas SWS and IED markers used the raw time series. **B** Day with the highest ASM load. From top to bottom: ASM loads, interictal epileptiform discharges (IEDs), SCs, and TCs. SWS episodes are marked with teal vertical lines. **C** Same for the day with the lowest ASM load.

for four randomly selected patients in Fig. 5.2. This correlation was quantified by calculating a Spearman rank correlation for each patient, which was a significantly positive correlation in 22 of 23 PwDRE from Dataset 2 (average Spearman rank correlation $\rho = 0.50 \pm 0.25$, Fisher's combined p-value below machine precision). Time-shuffling the high-γ band power series in each segment destroyed this co-variation (average Spearman rank correlation $\rho = 0.01 \pm 0.01$). This underlines the importance of the temporal and spatial coordination of the signal and shows that the mere power within the signal can not explain the results.

5.1.2 Temporal Correlations Follow a Hierarchical Gradient

Murray et al., 2014 demonstrated an organization of TCs across different cortical areas in non-human primates. They identified increasing TCs along the functional hierarchy in the visual pathway.

To investigate a similar ordering of TCs in humans, we evaluated five regions that functionally correspond to the non-human primate areas studied by Murray et al., 2014 (Table 3.2). These regions are depicted in Fig. 5.3 A and B, along with all electrodes from Dataset 2 mapped onto a standard cortical surface. This mapping demonstrates

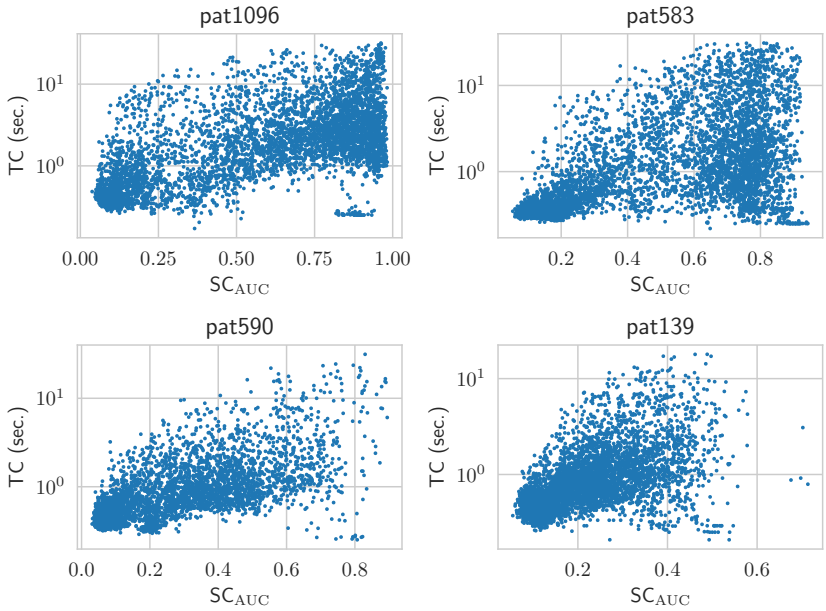

FIGURE 5.2: Co-Variation of Spatial and Temporal Correlation: SCs and TCs are shown for four randomly selected patients. All exhibited a significantly robust correlation between SCs and TCs.

wide cortical coverage across patients. However, clinical needs alone determined electrode placement, explaining the variation of which PwDRE had electrodes in each region (Fig. 5.3 C).

In Fig. 5.3 D, the TCs from these five areas are shown during the low ASM day and in nonSWS periods. With the hierarchy increasing from left (MT) to right (ACC), TCs also showed an increasing trend, thus extending Murray et al., 2014's results to human PwDRE. The average increase from area to area was (0.4 ± 0.2) sec./area, and statistically significantly different from zero on the population level ($p < 0.05$; Wilcoxon signed-rank test).

To validate these findings, we created surrogate TCs from time-shuffled data. These showed no such trend and were generally small (gray bars in Fig. 5.3 D).

The electrode coverage allowed for the assessment of TCs, but a finer-grained coverage would be necessary to explore SCs along the functional hierarchy.

5.1.3 Perturbations of SCs and TCs

The previous sections discussed the temporal and spatial patterns of SCs and TCs. In particular, the emergence of the temporal changes of SCs and TCs might be linked to other biological mechanisms. The model presented in Chapter 4 incorporated three such mechanisms: slow-wave activity (SWA), interictal epileptiform discharges (IEDs), and antiseizure medication (ASM). Further, the model simulations lead to precise predictions for the changes of SCs and TCs under these mechanisms. The following paragraphs will discuss these mechanisms and predictions one after the other.

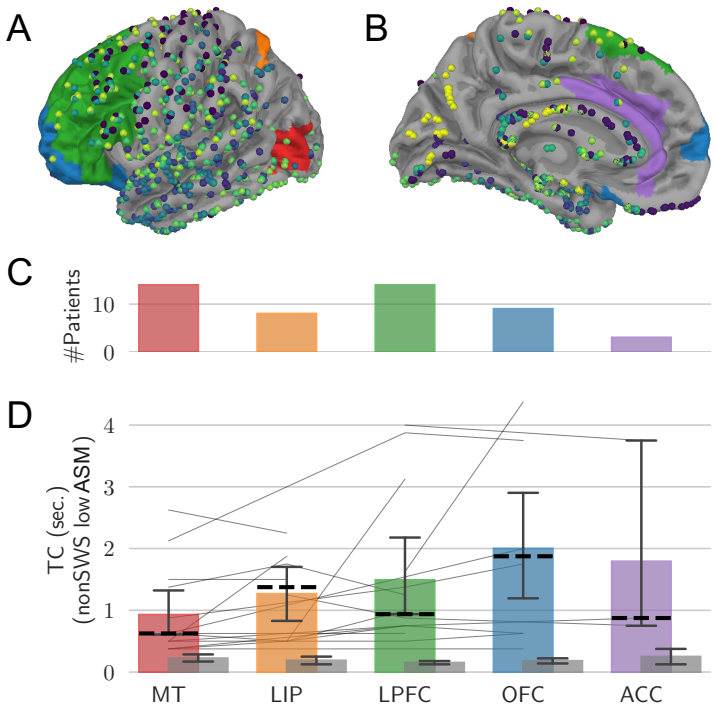

FIGURE 5.3: Temporal Correlations Along the Cortical Hierarchy: **A** Lateral and **B** Medial view of a template brain surface with electrodes of all PwDRE from Dataset 2. Cortical regions along the visual pathway similar to (Murray et al., 2014) are colored (Table 3.2). **C** Number of patients with electrodes in each region. **D** Mean TCs in the cortical region are ordered according to their functional hierarchy from left to right. Dashed lines show the median, and whiskers extend to the 95% confidence interval. Gray bars represent surrogate TCs from time-shuffled time series. The gray lines show individuals' data. MT: Medial temporal areas in visual cortex, LIP: Lateral intraparietal area in visual cortex, LPFC: Lateral prefrontal cortex, OFC: Orbitofrontal cortex ACC: Anterior cingulate cortex. Adapted from previously published results (Müller & Meisel, 2023) [CC BY 4.0].

5.1.3.1 Slow-Wave Sleep

To explore the impact SWA typical for slow-wave sleep (SWS) on SCs and TCs, SWS was first scored using a validated algorithm (Reed et al., 2017). Overall, the algorithm classified $(18 \pm 7)\%$ of the segments in Dataset 1 and $(19 \pm 6)\%$ in Dataset 2 as SWS. All patients could be analyzed here.

Then, we compared SCs and TCs during SWS to nonSWS across PwDREs. As predicted by the model simulations, SCs (Fig. 5.4 A) and TCs (Fig. 5.5 A & D) were significantly smaller during SWS. In Dataset 1, TCs decreased on average from (0.6 ± 0.2) seconds during nonSWS to an average of (0.4 ± 0.1) seconds during SWS ($p < 0.001$, Fig. 5.5 A). Similarly, in Dataset 2, TCs decreased on average from (0.9 ± 0.4) to (0.7 ± 0.4) seconds (nonSWS to SWS, $p < 0.05$, Fig. 5.5 D). Additionally, SCs in Dataset 2 decreased significantly from 0.30 ± 0.18 during nonSWS to 0.27 ± 0.17 during nonSWS ($p < 0.05$, Fig. 5.4 A).

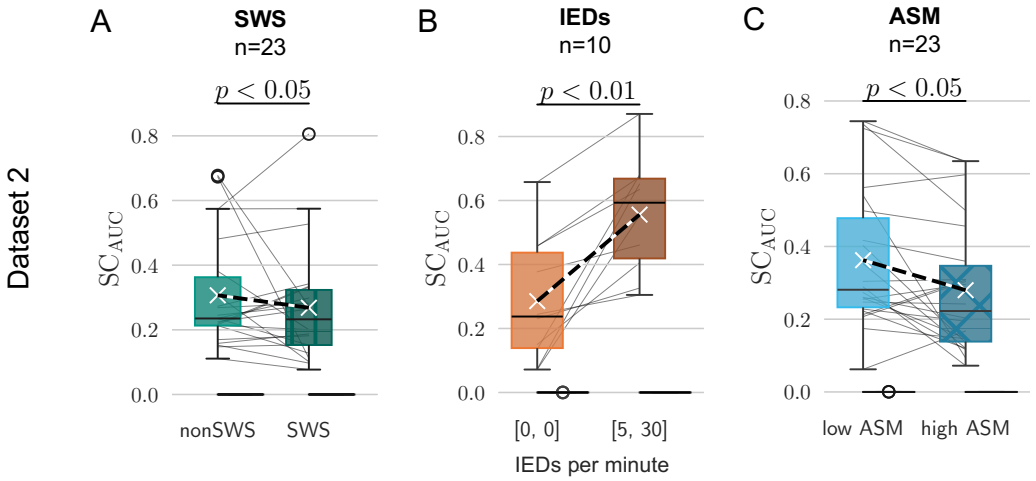

FIGURE 5.4: SCs Under Perturbations: **A** SCs decline in SWS compared to nonSWS. **B** SCs increase with more IEDs. IED count per minute is the average over all channels. **C** Increased ASM loads lead to decreased SCs. All results are from Dataset 2. Bars cover the middle quartiles and are split by the median (black horizontal line). Whiskers extend to 1.5 times the interquartile range. White crosses mark the mean. Single PwDRE results are shown as circles and are connected by thin lines. Surrogate SCs are shown as right-displaced gray bars and are close to zero. P-values are obtained through Wilcoxon-signed rank tests.

Surrogate SCs and TCs support these findings as they showed no trend between SWS and nonSWS (gray bars in Fig. 5.4 A and Fig. 5.5 A & D).

Thus, the consistent decrease of SCs and TCs in both datasets aligned with the model predictions (Section 4.2).

5.1.3.2 Interictal Epileptiform Discharges

To explore how IEDs influence SCs and TCs, a validated algorithm was used to measure IED frequency (Quon et al., 2022). The PwDRE in Dataset 1 experienced an average of (2.6 ± 2.4) IEDs per channel and minute, while the PwDRE in Dataset 2 had (3.1 ± 1.7) IEDs per channel and minute. The analysis already excluded SWS segments.

SCs and TCs were compared for segments with no IEDs to segments with 5 to 30 IEDs per minute. In Dataset 1, nine PwDRE were excluded as they did not have enough data points with sufficient IEDs for this comparison, i.e., less than 50 segments with 5 to 30 IEDs per minute. In Dataset 2, across channels, only ten patients reached this threshold, so SCs were only extracted for these. However, all PwDRE had at least one channel reaching more than 50 segments for both categories, allowing TCs estimation for all 23 PwDRE.

Across both datasets, TCs were shorter when IEDs were present (Fig. 5.5 B & E). In Dataset 1, the absence of IEDs was associated with longer TCs (0.6 ± 0.4) sec. compared to periods with IED counts between 5 and 30 per minute (0.5 ± 0.2) sec. ($p <$

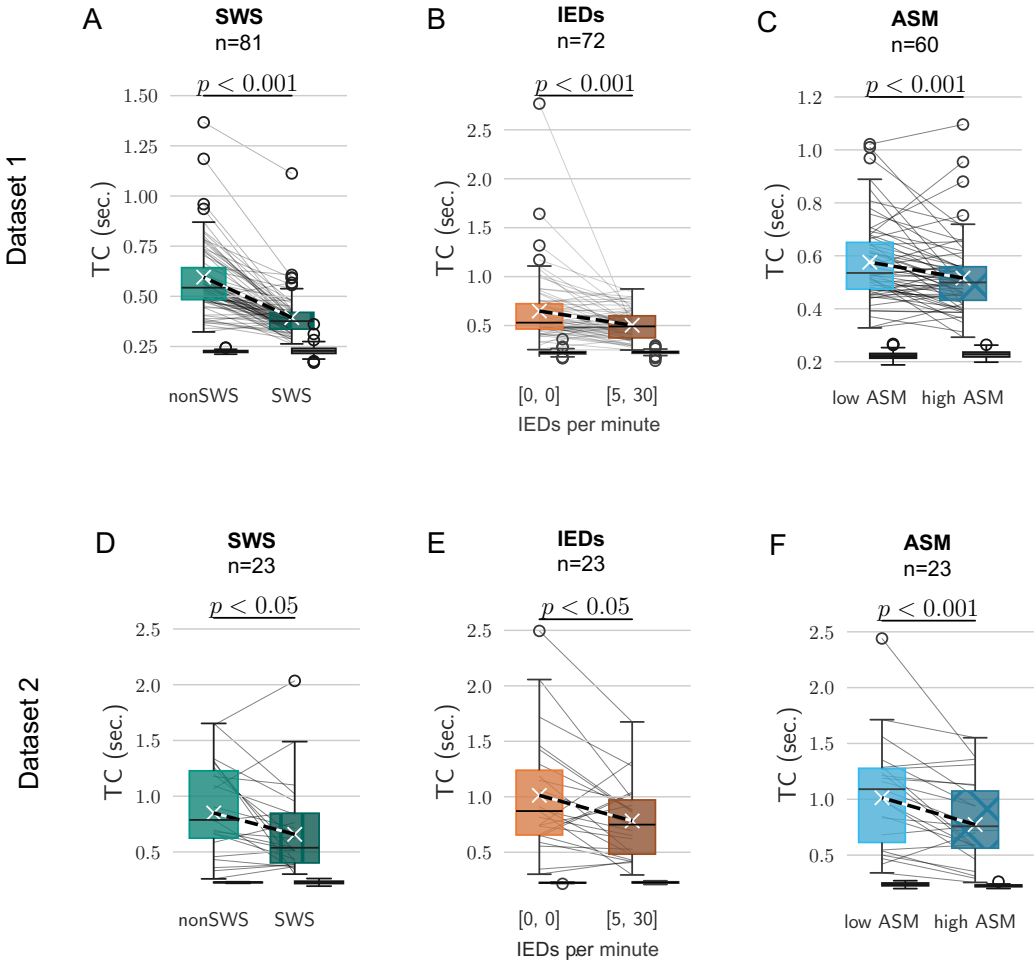

FIGURE 5.5: TCs Under Perturbations: TCs decline in SWS compared to nonSWS in **A** Dataset 1 and **D** Dataset 2. SCs decrease with more IEDs in **B** Dataset 1 and **E** Dataset 2. IED count per minute is the average over all channels. Increased ASM loads lead to decreased TCs in **C** Dataset 1 and **E** Dataset 2. Bars cover the middle quartiles and are split by the median (black horizontal line). Whiskers extend to 1.5 times the interquartile range. White crosses mark the mean. Single PwDRE results are shown as circles and are connected by thin lines. Surrogate TCs are shown as right-displaced gray bars and are close to their minimal value at 0.125. P-values are obtained through Wilcoxon-signed rank tests.

0.001, Fig. 5.5 B). Similarly, in Dataset 2, TCs were longer without IEDs (0.9±0.5) sec. versus during higher IED activity (0.7 ± 0.3) sec. ($p < 0.05$,Fig. 5.5 E). Furthermore, in Dataset 2, SCs could be evaluated for $n = 10$ PwDRE which had more than 50 segments with low and high IED load. They showed a significant increase from 0.3±0.2 for no IEDs to 0.6 ± 0.2 for higher IED counts ($p < 0.01$, Fig. 5.4 B).

Surrogate SCs and TCs showed no trend between different IED loads, suggesting that our findings did not arise by chance (gray bars in Fig. 5.4 B and Fig. 5.5 B & E).

Generally, the changes of SCs and TCs under increased IED load are consistent between datasets and align with the model predictions (Chapter 4).

5.1.3.3 Antiseizure Medication

The high ASM compared to the low ASM day in the example PwDRE showed already stronger fluctuations of SCs and TCs during the low ASM day (Fig. 5.1 B & C). To quantify the impact of antiseizure medication (ASM), we analyzed SCs and TCs on days with varying ASM dosages among 60 PwDRE from Dataset 1 and 23 PwDRE from Dataset 2 who underwent ASM tapering during monitoring. In Dataset 1, ASMs were reduced by an average of $(50 \pm 30)\%$, while in Dataset 2, the reduction averaged $(70 \pm 30)\%$ from high to low ASM days. The analysis already excluded SWS segments.

In both datasets, TCs were consistently larger during low ASM days compared to high ASM days (Dataset 1: $\mathrm{TC}_{\mathrm{lowASM}} = (0.6 \pm 0.2)$ sec. vs. $\mathrm{TC}_{\mathrm{highASM}} = (0.5 \pm 0.1)$ sec., $p < 0.001$, Fig. 5.5 C; Dataset 2: $\mathrm{TC}_{\mathrm{lowASM}} = (1.0 \pm 0.5)$ sec. vs. $\mathrm{TC}_{\mathrm{highASM}} = (0.8 \pm 0.4)$ sec., $p < 0.001$, Fig. 5.5 F). Further, the analysis of SCs in Dataset 2 revealed a significant reduction of SCs under increased ASM dosage ($\mathrm{SC}_{\mathrm{AUC,lowASM}} = 0.4 \pm 0.2$ vs. $\mathrm{SC}_{\mathrm{AUC,highASM}} = 0.3 \pm 0.2$, $p < 0.05$, Fig. 5.4 C).

These changes were not present in time-shuffled surrogate data (gray bars in Fig. 5.4 C and Fig. 5.5 C & F).

In conclusion, ASMs led to a robust decline of SCs and TCs, which aligns with the model predictions (Chapter 4) and previous studies (Meisel, 2020).

5.1.3.4 Seizure Onset Zone

Both datasets stemmed from PwDRE in the pre-surgical monitoring unit. Hence, clinical needs determined the electrode placement alone and coverage of the likely seizure onset zone (SOZ) was an essential factor. To verify that the TC results were not an artifact of the epileptic tissue, we performed a sub-analysis by splitting the electrodes into SOZ and their complement the nSOZ. Furthermore, as IED counts can vary between SOZ and nSOZ, only segments without IEDs were included, naturally excluding the case when IED count was of interest for the analysis.

The effect that SWS disrupted TCs was observable in both the SOZ and the nSOZ for Dataset 1 ($p < 0.001$, Fig. 5.6 A). In Dataset 2, the SWS disrupted TCs trend was also observable in SOZ and nSOZ. However, it was only significant in the nSOZ ($p < 0.05$, Fig. 5.6 D).

To provide a detailed analysis of the impact of IEDs on TCs, TCs from nonSWS segments were grouped into four categories based on their IED rate (Fig. 5.6 B and E). The rate of TC change was then quantified using a linear mixed effects model. For Dataset 1, the mixed effects model had both negative linear (coefficient: -0.13 [-0.20,-0.07], $t = -3.9$) and quadratic coefficients (coefficient: -0.069 [-0.136,-0.02], $t = -2.0$). This indicates that while TCs generally decline with more IEDs, this decline slows as IEDs become more frequent (Fig. 5.6 B). Furthermore, the mixed effects model showed smaller TCs in the nSOZ compared to the SOZ if one corrects for the IEDs (coefficient: -0.052 [-0.997, -0.02], $t = -2.1$). The results for Dataset 2 were less robust. Here, only the linear decrease of TCs with more frequent IEDs remained robust (coefficient:

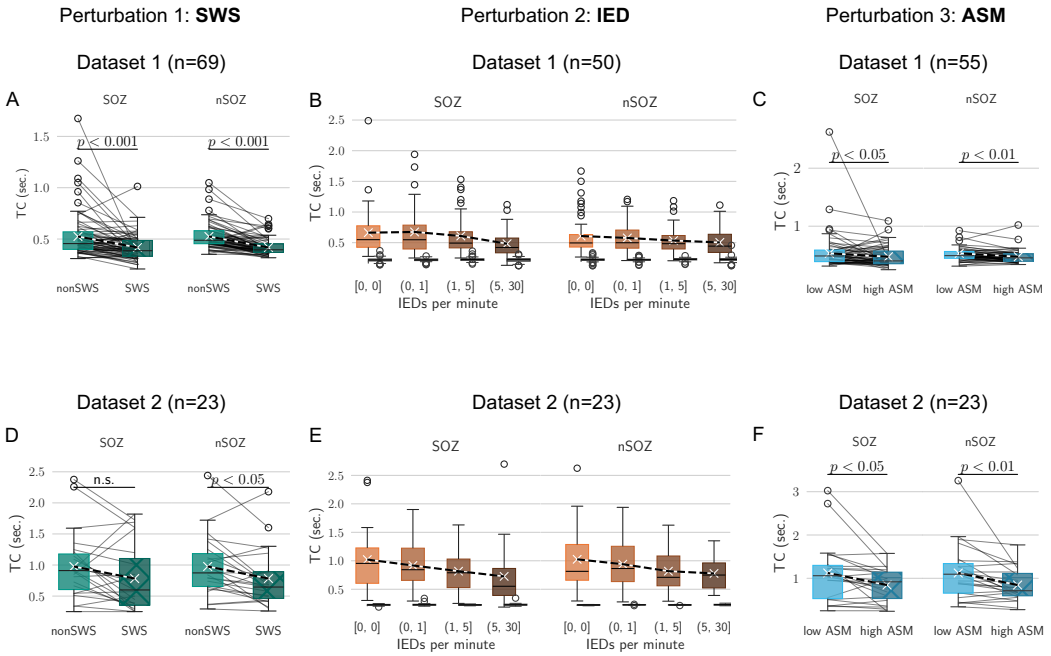

FIGURE 5.6: TCs in SOZ and nSOZ: **A** TCs decline under SWS in both the SOZ and the nSOZ for both Dataset 1 and **D** Dataset 2. **B** More frequent IEDs lead to a gradual decline of TCs irrespective of SOZ or nSOZ in both Dataset 1 and **E** Dataset 2. **C** Higher ASM loads are associated with lower TCs in Dataset 1 and **F** Dataset 2. Bars cover the middle quartiles while whiskers extend to 1.5 times the interquartile range. White crosses mark the mean. Single PwDRE results are shown as circles and are connected by thin lines. P-values are obtained through Wilcoxon-signed rank tests. Re-plotted from (Müller et al., 2024) [CC-BY-NC-ND 4.0].

-0.24 [-0.35 to -0.13], $t = -4.1$, Fig. 5.6 E). The combined results from both datasets suggest a general reduction of TCs through IEDs. The predictions from the linear mixed effects model illustrate this finding (Fig. 5.7).

Lastly, the reduction of TCs under higher ASM load remained robust in both SOZ and nSOZ for both datasets (Fig. 5.6 C and F). However, no difference between SOZ and nSOZ was observed when investigating the effect of ASM, even after correcting for IEDs and SWS.

5.2 Summary of SCs and TCs in Human iEEG

This chapter systematically explored spatial and temporal correlations (SCs and TCs) within the human cortex. The primary aim was to test the predictions about SCs and TCs derived from the model in human cortical dynamics (Chapter 4, prediction (a)-(d)). Therefore, two independent datasets from PwDRE in pre-surgical monitoring were studied. For each PwDRE in the cohort, multiple days of intracranial EEG recordings were analyzed concerning their variations of SCs and TCs. Notably, all predictions of the model could be verified, i.e., (a) SCs and TCs co-varied, (b) SWS

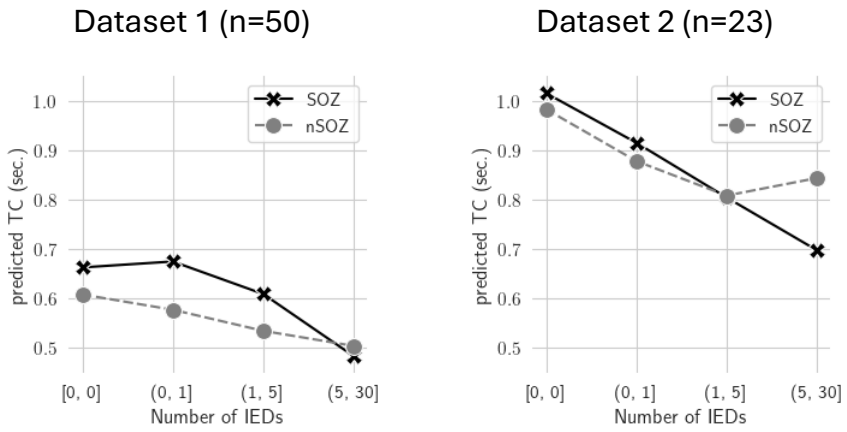

FIGURE 5.7: Linear Mixed Effects Model for TCs Under IEDs: **A** Prediction of the linear mixed effects model for TCs as formulated in Eq. (3.3) in Dataset 1 and **B** Dataset 2. Reprinted from (Müller et al., 2024).

disrupted SCs and TCs, (c) IEDs increased SCs but decreased TCs, and (d) ASMs led to the decline of SCs and TCs. Importantly, these findings were similar inside and outside the SOZ. Furthermore, TCs were not spatially homogenous but showed a posterior to frontal gradient that aligned with the functional hierarchy of the cortex.

The following contextualizes these results, and a joint discussion of all results of this thesis is provided in Chapter 7.

Co-variation of SCs and TCs

The variation of SCs and TCs over time was studied across multiple days. This revealed a strong co-variation of SCs and TCs, i.e., when SCs increased, TCs tended to increase too, and vice versa.

This analysis did not account for perturbative effects like SWS, IEDs, or ASMs. SWS and ASM exerted the same effect on SCs and TCs, i.e., reduction of SCs and TCs under SWS and higher ASM load. However, IEDs had opposite effects on SCs and TCs, i.e., more IEDs lead to increased SCs but decreased TCs. While ASMs and SWS add positive correlation between SCs and TCs, IEDs add negative correlation. Thus, accounting for the pathological IEDs would lead to even stronger correlation between SCs and TCs.

The model simulations predicted such a behavior (prediction (a), Section 4.2) for systems that vary in their proximity to a critical point. Generally, when the system is further away from the critical point, it exhibits lower SCs and TCs, while when it is closer to the critical point, it shows extended SCs and TCs. Thus, the model and experimental results suggest that cortical network dynamics might vary in their proximity to criticality over time.

TCs Increase Along the Functional Hierarchy

TCs were mapped along the visual pathway, specifically along the five regions corresponding to the regions investigated in (Murray et al., 2014). Extending the results from Murray et al., 2014, TCs in the human cortex increased along the functional hierarchy.

The medial temporal area in the visual cortex exhibited the lowest TCs and was also the lowest in the functional hierarchy. From there, TCs showed a trend of progressive increments that aligned with their hierarchical order. This could be interpreted as regions low in the hierarchy needing to adapt to quickly changing stimuli and to "forget" about the previous stimuli (Murray et al., 2014). Thus, short TCs are more beneficial in this scenario as less memory over time is preserved. However, regions higher in the hierarchy must process multiple inputs and more complex information integrations, requiring extended memory over the different inputs, marked by long TCs (Murray et al., 2014).

SWS Disrupts SCs and TCs

SCs and TCs were significantly shorter during SWS, as also predicted by the model simulations (prediction (b), Section 4.2). These results extend previous TCs investigations in rats (Meisel, Bailey, et al., 2017; Meisel, Klaus, et al., 2017; Xu et al., 2024). Intermittent pauses of neuronal firing are suggested to explain this decline of TCs during SWS (Meisel, Klaus, et al., 2017). This interruption of the neuron firing could disrupt information transmission between neurons, marked by short SCs and TCs. This aligns with theories arguing that during sleep, the brain's information integration abilities become less effective (Tononi, 2008). Similarly, SWA seen in sleep-deprived individuals showed similar effects on TCs (Meisel, Bailey, et al., 2017) and was linked to the deterioration of cognitive performance if timed precisely to the cognitive testing (Alhola & Polo-Kantola, 2007).

IEDs Increase SCs but Decrease TCs

Interictal epileptiform discharges (IEDs), an abnormal pattern found in PwDRE's cortical dynamics, were shown to impact SCs and TCs in distinct ways. While increasing loads of IEDs progressively disrupted TCs, they did increase the strength of SCs. The model simulations precisely predicted both of these trends (prediction (c), Section 4.2). In the temporal plain, IEDs disrupt the flow of information by overwriting the current signal with the IEDs. While SCs were increased, this may arise as IEDs are spatially coordinated activation-patterns, increasing SCs but not necessarily carrying information about previous activities. This interpretation could explain phenomena like "transient cognitive impairment", i.e., the observation of impaired cognitive performance when IEDs are present during the cognitive testing (Kleen et al., 2013; Lam et al., 2017).

ASMs Reduce SCs and TCs

SCs, and TCs declined during days of increased ASM dosage as predicted by the model simulations (prediction (d), Section 4.2). These results align with previous findings of decreased TCs during increased ASM loads (Meisel, 2020). The disruption of SCs and TCs could be explained by ASMs changing the effective connectivity by affecting the excitation/inhibition balance (Lang et al., 2013; Ossemann et al., 2016), which has been proposed as necessary for establishing long-range correlation (Poil et al., 2011). Furthermore, the disruption of SCs and TCs by ASMs could explain the adverse cognitive side effects of many of these ASMs (Eddy et al., 2011).

The Potential for Longer TCs in the SOZ

The data stems from PwDREs, and electrodes were placed to cover the likely seizure onset zone (SOZ). We analyzed all perturbative effects in the SOZ and nSOZ separately to investigate the impact that the epileptic tissue could have.

All results of TC variations were observed similiarly in the SOZ and nSOZ. Accounting for IEDs revealed a trend that the SOZ might exhibit longer TCs than the nSOZ. Long TCs are markers for criticality and are also markers for the proximity to the boundary of instability of the system. Thus, long TCs in the SOZ could indicate that the SOZ is closer to a phase transition towards a seizure, associated with supercritical dynamics (Meisel & Kuehn, 2012; Meisel et al., 2012). SCs could not be analzed on a channel basis.

Limitations

While the comparison for IEDs and SWS happened on the same day, the comparison for ASM was across multiple days. These days were a different duration away from the electrode implantation surgery, and mostly, the high ASM day was closer to the surgery. The proximity to surgery could confound the ASM results. However, a subanalysis of patients with low ASM days closer to surgery could not reveal such an effect as previously reported in (Müller & Meisel, 2023).

Dataset 2 recorded only 5 minutes per hour. However, segments over multiple days and from 81 patients were included, making this a relatively large sample set compared to similar datasets, e.g., Dataset 1. Moreover, results are similar between the continuously sampled Dataset 1 and Dataset 2.

Due to the large sample size, expert annotation of IEDs was not feasible. Instead, a state-of-the-art algorithm was employed for IED detection (Quon et al., 2022). While the algorithm might still misclassify individual IEDs, the general count per minute estimation was less prone to timing errors of individual IEDs.

Standardized polysomnographic vigilance assessment was impossible in the datasets as neither EMG nor scalp EEG recordings were continuously available. Therefore, an automated classification scheme to identify SWS was utilized, which, however, was less accurate than expert annotation and did not resolve the other sleep stages (Reed

et al., 2017). Future research could address this issue by using other algorithms, e.g., (von Ellenrieder et al., 2022)

Chapter Conclusion

These results showed that SCs and TCs are intimately linked and are predictably perturbed by mechanisms also known to affect cognition. Further, we found that TCs increase along the functional hierarchy underlining their importance for complex computation. However, a direct link between TCs cognitive performance remains elusive. The next chapter will address this question and investigate the correlation of the cortical structure and TCs to cognitive impairment.

Chapter 6

Structure, Dynamics, and Cognition

The previous chapter investigated SCs and TCs in human intracranial EEG dynamics. Interestingly, TCs were the longest in regions high in the functional hierarchy, supporting that long TCs could be beneficial for complex information processing. Furthermore, SCs and TCs changed predictably under mechanisms that also adversely affect cognition, i.e., SWA (Alhola & Polo-Kantola, 2007), IEDs (Kleen et al., 2013; Lam et al., 2017), and ASM load (Eddy et al., 2011).

These results align with previous research proposing a connection of TCs and even more general brain criticality to cognitive performance (Jensen, 2021; Linkenkaer-Hansen et al., 2001; Shew & Plenz, 2013). However, previous research on the direct experimental link between brain criticality measures like TCs and cognitive performance was mostly limited to short recordings and single cognitive tasks (Kardan et al., 2023; Mahjoory et al., 2019). Thus, a broader connection between cognitive performance and brain criticality measures is still missing.

To bridge this gap, this chapter will consist of two parts, which compare structural changes and TCs to a broad range of cognitive tests.

The first part is labeled "Structure & Cognition". It investigates structural MRI data to link cortical thickness changes in PwDRE with cognitive impairment. The PwDRE were categorized into impairment severity groups based on a new taxonomy, i.e., the International Classification of Cognitive Disorders in Epilepsy (IC-CoDE) McDonald et al., 2023. This approach unifies many cognitive tests, allows for better comparison between different centers and languages, and provides a more general assessment of cognitive impairment apart from single tests (McDonald et al., 2023).

The goal of this study was to investigate which regions in the brain were associated with cognitive impairment. Furthermore, the study then aimed to use these regions to evaluate the risks for increasing impairment after epilepsy surgery. This part follows the analysis previously reported in (Miron et al., 2024).

The second part, labeled "Dynamics & Cognition", then investigates the link of TCs. Here, PwDRE with and without impairment in four cognitive domains will be compared with respect to their TCs. Both the dataset, and the TCs evaluation methods have been already used in Chapter 5. In general, shorter TCs could be a

sign of a deviation from brain criticality which consequently could lead to deteriorated cognitive performance. These results were previously reported in (Müller et al., 2024). To support that our findings are not found by chance or can be explained by simpler measures, for instance α-band power variations, we show a wide range of other measures as controls, e.g, ASM load, IED frequency, standard EEG band powers.

6.1 Results

6.1.1 Study 1: Structure and Cognition

6.1.1.1 Cognitive Phenotyping

In order to test how cortical thickness changes as a function of cognitive impairment, PwDRE are first clustered into three cognitive phenotypes following the IC-CoDE criteria (Fig. 3.6) (McDonald et al., 2023). Out of 124 PwDRE, 66 (53.2%) were multi-domain impaired (MDI), 37 (29.8%) were focal impaired (FI), and 21 (16.9%) were minimal impaired (MI). The MDI group showed the lowest cognitive scores across all domains, while the MI group showed the highest scores (Fig. 6.1). The MI group's test scores spread around the norm (50. percentile rank). While there was no difference in age and sex between the three groups, the MDI cohort showed a significantly lower education level than the other cohorts ($p < 0.01$ chi-squared test, Table 3.3).

6.1.1.2 Cortical Thickness Changes in Cognitive Phenotypes

Each group was evaluated against age- and sex-matched healthy controls to investigate the cortical thickness changes across cognitive phenotypes. The full results for the ANOVA-based analysis can be found in Supplement Table 1 of our previous publication (Miron et al., 2024).

Fig. 6.2 shows the ROIs for each cognitive phenotype significantly different from the healthy controls after conservative Bonferroni correction, comparison to the surrogate p-value distribution, and exclusion of ROIs closely connected to the MRI scanner variable. Supplement Table 2 of our previous publication (Miron et al., 2024) reported the complete regions list. In general, the more severely impaired cognitive phenotypes also exhibited the most cortical regions with changes in thickness compared to healthy controls.

The MDI group showed the most prominent cortical changes with 28 significantly different ROIs. Affected regions were mainly in the bilateral anterior cingulate and medial prefrontal cortex (7 ROIs) and bilateral early auditory cortex (4 ROIs).

The FI group had the second-most changed ROIs, with 12 affected ROIs. These regions were primarily located in the bilateral anterior cingulate and medial prefrontal cortex (3 ROIs). Furthermore, 7 of the affected ROIs in the FI group were also affected in the MDI group.

The MI group had the least affected regions, with only 3 ROIs. These ROIs were in the bilateral early auditory (2 ROIs) and left primary visual left (1 ROI) cortical

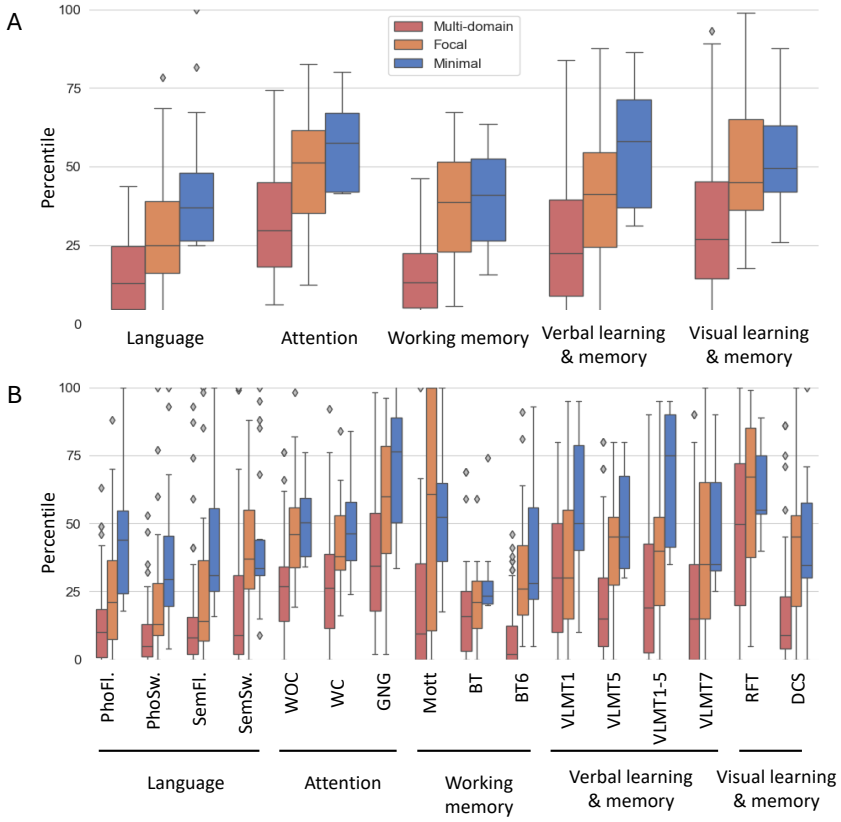

FIGURE 6.1: Cognitive Scores per Phenotype: **A** Domain average cognitive score for each cognitive phenotype. **B** Test scores split by cognitive phenotype. Boxes show median and interquartile range. Whiskers extend to 1.5 times the interquartile range. Diamonds denote datapoints outside of this range. PhoFl. = phonetic word fluency; PhoSw. = phonetic category switching; SemFl. = semantic word fluency; SemSw. = semantic category switching; WOC = TAP Alertness subtest without auditory warning cue; TAP = Testbatterie für Aufmerksamkeitsprüfung; WC = TAP Alertness subtest with auditory warning cue; GNG = TAP Go/No-Go subtest; Mott = Mottier test; BT(6) = Block Tapping; VLMT = Verbaler Lern- und Merkfähigkeitstest; RFT = Recurring Figures Test; DCS = Diagnosticum für Cerebralschädigung test. Adapted from (Miron et al., 2024) [CC BY-NC 4.0].

regions. The left early auditory ROI was also affected in the MDI group.

Generally, all cortical thicknesses were lower in the epilepsy cohort compared to the healthy controls, except the left somatosensory and motor cortex in the FI group (Fig. 6.3). Of the clinical variables, only age was associated with 7 of the above ROIs (see Supplement Table 2 of our previous publication (Miron et al., 2024)).

6.1.1.3 Post-Surgical Outcome Prediction

A sub-group of 69 patients underwent epilepsy surgery and repeated cognitive evaluation after one year (patient characteristics in Table 3.4). For this sub-group, an analysis of cognitive decline after surgery was possible, which could help to evaluate

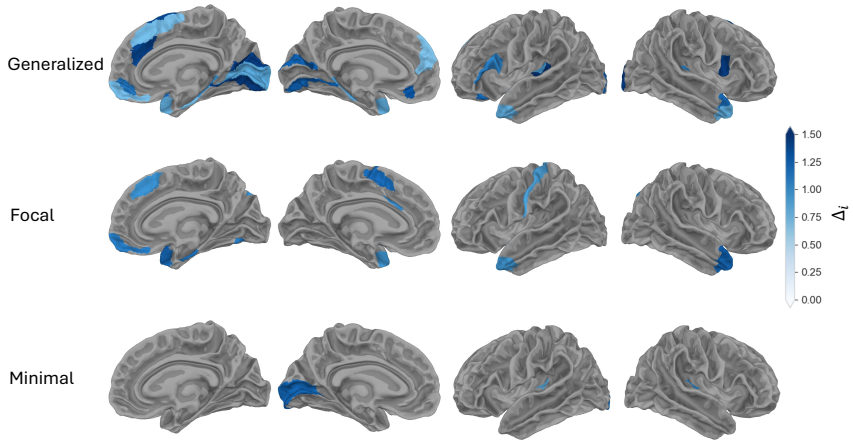

FIGURE 6.2: Affected ROIs in Cognitive Phenotypes: From healthy controls robustly changed cortical thicknesses for each cognitive phenotype. Δ_i is defined in Eq. (3.4). Adapted from (Miron et al., 2024) [CC BY-NC 4.0].

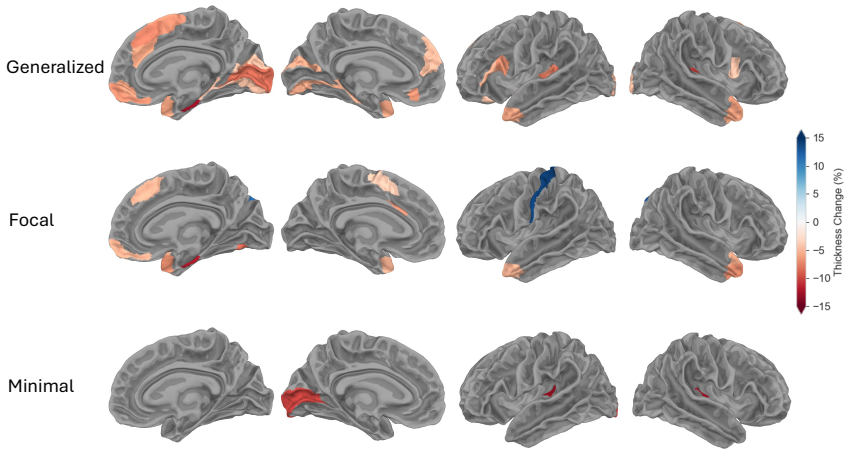

FIGURE 6.3: ROI Thickness Changes in Cognitive Phenotypes: Percentage change of ROI thickness with respect to healthy controls for each cognitive phenotype and the robustly changed ROIs (Fig. 6.2). Reprinted from Supplement Material of (Miron et al., 2024) [CC BY-NC 4.0].

the risks of epilepsy surgery better. A domain was post-surgically worse if the average score had decreased by five percentile ranks. Otherwise, it was labeled stable. The analysis excluded the attention domain because post-surgical testing was not sufficiently available.

The cognitive phenotype was not directly associated with the worsening. To test if the cortical changes in the specific ROIs provide information about cognitive outcome, logistic regression models were fit using the most robust ROIs as input features. In particular, all ROIs with $\Delta_i < 1$ were included resulting in $n = 13$ ROIs (Table 6.1). Data from all cognitive phenotypes had to be joined; otherwise, the sample size would have been too small.

First, an exploratory logistic regression model was fit to the whole dataset (Fig. 6.4). Input features were the thicknesses in the 13 above-identified ROIs and age. Age was

Name	Description	Side	Lobe	Group	Δ_i
l9m	Anterior cingulate and medial prefrontal	Left	Frontal	MDI	0.72
l1	Somatosensory and motor	Left	Parietal	FI	0.92
lTA2	Auditory association	Left	Temporal	FI	0.99
lA1	Early auditory	Left	Temporal	MDI	0.92
lTGd	Lateral temporal	Left	Temporal	FI	0.97
lPreS	Medial temporal	Left	Temporal	MDI	0.89
r10v	Anterior cingulate and medial prefrontal	Right	Frontal	MDI	0.74
r8BM	Anterior cingulate and medial prefrontal	Right	Frontal	FI	0.75
rSCEF	Paracentral lobular and mid cingulate	Right	Frontal	MDI	0.73
rV1	Primary visual	Right	Occipital	MDI	0.86
rTGd	Lateral temporal	Right	Temporal	MDI	0.82
rEC	Medial temporal	Right	Temporal	MDI	0.74
rPreS	Medial temporal	Right	Temporal	MDI	0.98

TABLE 6.1: ROIs with $\Delta_i < 1$: ROIs with $\Delta_i < 1$ for all cognitive phenotypes.

included as it showed associations with some of these ROIs itself. The target was the cognitive worsening in the domains. The models revealed a significant connection between l9m, rSCEF, rV1, and l1 and verbal learning and memory worsening (Fig. 6.4 A). Strong associations were also found for lA1 and l1 with visual learning and memory worsening (Fig. 6.4 B), and for r10v and rSCEF with language worsening (Fig. 6.4 C). No region was associated with working memory worsening (Fig. 6.4 D).

While this analysis described how ROI thicknesses were associated with cognitive worsening, it is not suitable to claim the predictive power of these ROIs concerning post-surgical outcome predictions. Therefore, logistic regression models were tested in a 5-fold repeated cross-validation scheme to address this issue (Fig. 6.5). For predicting post-surgical verbal worsening and learning, they achieved an ROC-AUC of 0.70 ± 0.15 (mean$\pm$ standard deviation) and an accuracy of 0.65 ± 0.13 (Fig. 6.5 A). This performance was significantly better than chance and outperformed the model based only on the clinical variables (ROC-AUC 0.66 ± 0.14). Combining ROI features and clinical variables further boosted the performance to ROC-AUC 0.75 ± 0.14 and accuracy 0.69 ± 0.12 (Fig. 6.5 A). This showed that the ROIs provided additional information to clinical information alone.

For the other domains, models built with ROI features only reached ROC-AUCs close to the chance level (Fig. 6.5 B - D). Furthermore, they performed worse than the models based on clinical variables alone. Thus, the ROI thicknesses provided no additional information to the post-surgical outcome prediction for visual learning and memory, language, and working memory.

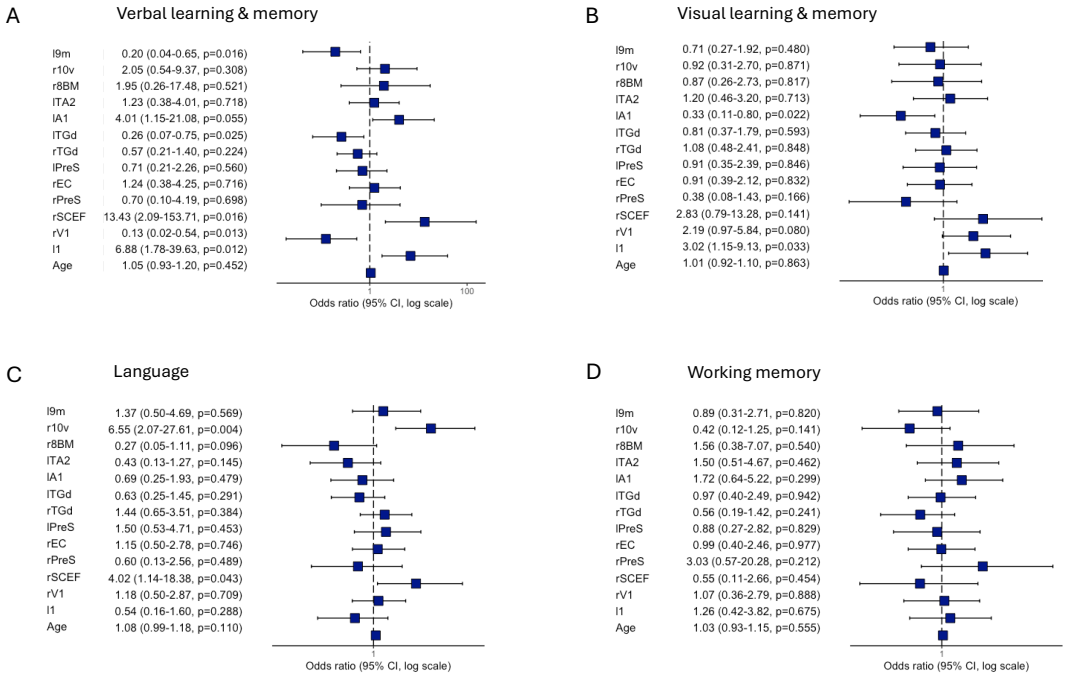

FIGURE 6.4: Connections Between ROI Thicknesses and Domain Worsening: The odds ratios of descriptive logistic regression models show associations between the strongest ROIs connected to cognitive phenotypes. ROI names are defined in Table 6.1. Odds ratios are listed with their 95% confidence interval and the corresponding p-value. **A** Verbal learning and memory domain, **B** visual learning and memory domain, **C** language domain, and **D** working memory domain. Adapted from (Miron et al., 2024) [CC BY-NC 4.0].

6.1.2 Study 2: Dynamics and Cognition

While Study 1 investigated the structural changes linked to cognitive worsening, the aim of Study 2 was to investigate the correlations between cortical dynamics, particularly TCs, and cognitive performance. Therefore, Dataset 1 from Chapter 5 was utilized again. For the 81 PwDRE, 14 cognitive tests spanning four domains were available. Cognitive phenotyping was not performed as the data had only four cognitive domains, i.e., one fewer than Study 1 and the IC-CoDE publication (McDonald et al., 2023).

In Chapter 5, TCs have been introduced to evaluate cortical dynamics and their information maintenance. From the investigations in Chapter 5, we have learned that TCs change through many factors, e.g., SWS or ASMs. Furthermore, the clinical needs decided about the length of the pre-surgical monitoring, ASM loads, and electrode positions. In order to minimize the effect of different recording lengths and ASM changes, only three distinct days were analyzed: The first, last, and lowest ASM load days. Further, only nonSWS episodes were analyzed to account for the disruptive effect of SWS on TCs. Additionally, sub-analyses for different hemispheres and lobes were performed to reduce the effect of variability in the electrode placement. Lastly, all SOZ electrodes were excluded, which reduced the effect of IEDs and SOZ. In total,

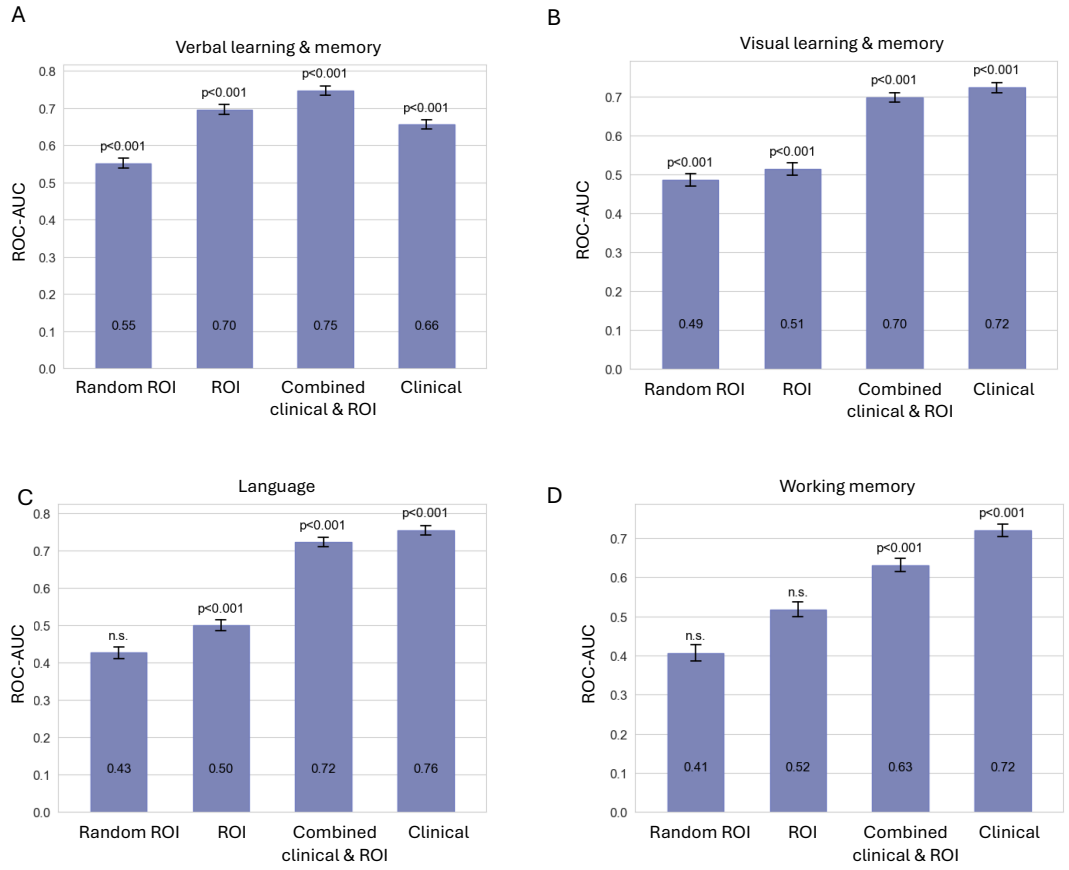

FIGURE 6.5: Prediction of Cognitive Worsening After Epilepsy Surgery: Average area under the receiver operating curves (ROC-AUC) for logistic regression models predicting post-surgical cognitive domain worsening from 5-fold 100 repeated cross-validation. Whiskers extend to the 95% confidence interval. Reported p-values are comparisons against random classifiers where the predictions are randomly assigned with the same prevalence as the actual results. Random ROI are models from 13 randomly chosen ROIs. ROI are models with the 13 most robust ROIs from the ANOVA analysis. **A** Verbal learning and memory domain, **B** visual learning and memory domain, **C** language domain, and **D** working memory domain. ROI = Region of interest. Adapted from (Miron et al., 2024) [CC BY-NC 4.0].

108 sub-analyses were performed (three days, two lobes plus all, two hemispheres plus both, and four cognitive domains). Of these, six did not reach the minimum requirement of $n \geq 5$ per group, which was necessary to achieve statistical significance for the Brunner-Munzel test. Hence, 102 comparisons were performed for all measures except SWS and ASM. SWS and ASM were cortex-wide measures, resulting in twelve comparisons (three days and four domains).

The results for all measures and sub-analyses are presented in Fig. 6.6 A. Notably, 19 of the comparisons for TCs reached significance before multiple comparison correction ($p < 0.05$). Of these, 12 remained significant after multiple comparisons correction with the Benjamini-Hochberg method at an $\alpha = 0.05$ (circles with triangles in Fig. 6.6 A). The strongest associations between cognitive impairment and TCs

were found in the attention and language domain, particularly during the first full day of recording. These associations showed that PwDRE with impaired language or attention had shorter TCs as the effect size was above 0.5. In other words, it was more likely that if one randomly drew an impaired and a not impaired PwDRE, the impaired would likely have lower TCs (blue shaded in Fig. 6.6 A). This result is in line with the prediction of long TCs and optimal computation in the vicinity of brain criticality. For the working memory domain, shorter TCs in the temporal lobe electrodes were also aligned with impaired working memory during the first day. However, the right-sided and, in particular, the temporal lobe electrodes showed longer TCs during the last day of the recording in the working memory impaired PwDRE. Thus, further research is needed to disentangle the complex interplay of TCs with working memory.

No test for the other iEEG features was significant after multiple comparison corrections (Fig. 6.6 A). Notably, for neither surrogate TCs nor high-γ power, significant associations with cognitive impairment were found, suggesting that the temporal alignment of the data is crucial. Neither were known lesions associated with cognitive impairment. Only for SWS, one sub-analysis for the last day in the working memory domain was significant after multiple comparison correction. However, for SWS only 12 comparisons were performed. To further evaluate if the results could arise by chance, the distribution of p-values was compared to a uniform distribution (Fig. 6.6 B). The uniform distribution could be expected if the null hypothesis that impaired and not impaired groups come from the same distribution was true. This analysis showed that only the p-value distribution for TCs was significantly different from the uniform distribution ($p < 0.01$ Kolmogorov-Smirnov test). Notably, the distribution for SWS remained insignificant in this test.

6.2 Chapter Summary

We observed that both cortical structure and dynamics were related to cognitive impairment. Analyzing structural MRI data from PwDRE showed that more severely cognitively impaired PwDRE also had more cortical thickness changes. Analyzing TCs in iEEG showed that shorter TCs were associated with cognitive impairment, particularly in the language and attention domain. Together, these results suggest that structure and dynamics are essential for cognition and that some structures and dynamics might be more optimal than others, e.g., the structure of healthy individuals and dynamics with maximal TCs. The following sections will contextualize the studies, and the next chapter will discuss all results in context with brain criticality.

Structure and Cognition

Study 1 focussed on the link between structural MRI changes and cognitive impairment severity in PwDRE. It was the first application of cognitive phenotyping in a German-speaking TLE cohort using the International Classification of Cognitive Disorders in Epilepsy (IC-CoDE) criteria (McDonald et al., 2023). Previous studies have

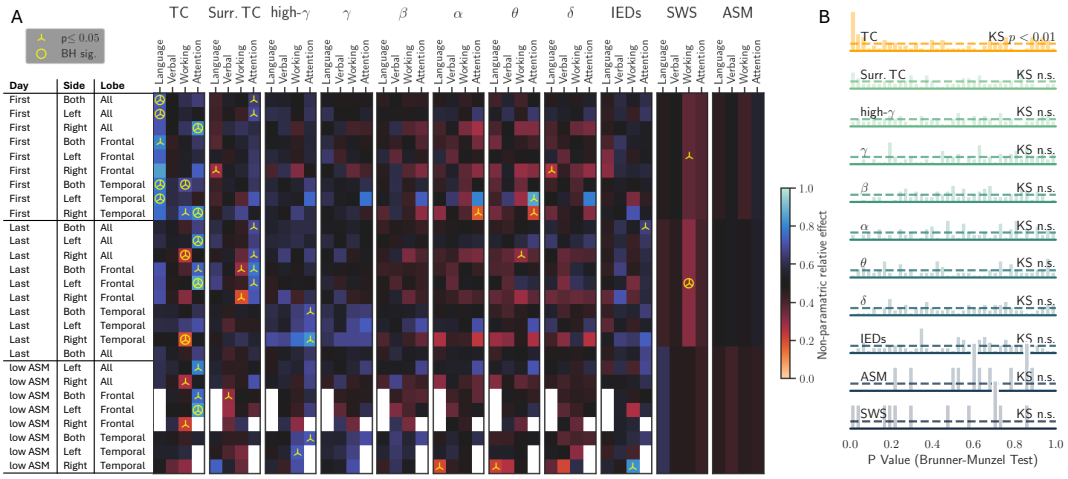

FIGURE 6.6: Cognitive Impairment and iEEG Measures: **A** Non-parametric effect sizes are shown for up to 102 comparisons per measure. Values larger than 0.5 (blue) mean that it is more likely for PwDRE with cognitive impairment to have shorter TCs compared to people without impairment and vice versa for values smaller than 0.5 (red). Uncorrected significant associations are marked with yellow triangles, and Benjamini-Hochberg (BH) corrected significant associations with additional yellow circles. Multiple comparison correction was performed separately for each measure. **B** The distributions of p-values are compared to uniform distributions (dashed lines) with Kolmogorov-Smirnov (KS) tests. Reprinted after (Müller et al., 2024) [CC-BY-NC-ND 4.0].

established the approach in a large American, English-speaking cohort (McDonald et al., 2023) and an American, Spanish-speaking cohort (Reyes et al., 2023). In our cohort, 53.2% showed MDI, followed by 29.8% FI, and finally 16.9% MI. The percentage of MDI patients was higher compared to previous studies (B. P. Hermann et al., 2021). Potentially, this could be attributed to the entire cohort consisting of PwDRE with long average epilepsy duration (18 ± 13 years). However, PwDRE were investigated because one of the aims of Study 1 was to specifically identify MRI patterns that could help in the surgical risk assessment.

Comparing cortical thicknesses for each cognitive phenotype (MI, FI, MDI) to age- and sex-matched healthy controls revealed that more severely impaired PwDRE had more affected ROIs. Specifically, 3 ROIs were affected for MI, 12 for FI, and 28 for MDI. This aligns with previous studies showing that MDI compared to MI had more diffusion and functional MIR abnormalities (Kaestner et al., 2019; Reyes et al., 2019; Rodríguez-Cruces et al., 2018) and more prominent changes in functional network measures (Garcia-Ramos et al., 2022; Larivière et al., 2020). Of the few studies that also investigated cortical thickness corresponding to cognitive phenotype, two showed only small associations between phenotype and cortical thickness (Dabbs et al., 2009; B. Hermann et al., 2020). However, these studies investigated patients with relatively benign TLE, and a third study with more severe epilepsy showed results closer to ours (Kaestner et al., 2019). This emphasizes the need to differentiate cohorts based

on the severity of the disease and suggests that there might be structural differences between PwDRE and responsive PwE.

In total, 43 regions (18 temporal and 25 extratemporal) across phenotypes showed significant differences from healthy controls despite Bonferroni correction. Some ROIs were found for multiple phenotypes; for example, FI and MDI had seven overlapping ROIs. For instance, the FI and MDI groups showed reduced cortical thickness in the lateral and medial temporal regions. These ROIs are known to be related to cognitive functions, including memory, learning, and language (Bell et al., 2011). The most widespread bilateral differences to healthy controls were identified in the anterior cingulate and medial prefrontal cortical regions (7 in MDI and 3 in FI). This finding aligns with previous studies in TLE identifying associations of these ROIs with impaired memory, cognitive slowing, and attention (Bell et al., 2011; Hwang et al., 2019; Keller et al., 2009).

To test if these findings could have direct clinical use, cortical thickness changes were used to predict the risk of cognitive worsening after epilepsy surgery. Therefore, logistic regression models were trained with the cortical thicknesses from the 13 ROIs most robustly associated with the phenotypes. Notably, for the verbal learning and memory domain, these thicknesses were better at predicting cognitive worsening than clinical features (ROC-AUC 0.70 ± 0.15 and 0.66 ± 0.14, respectively). Combining clinical features and ROI thicknesses further improved the performance to a ROC-AUC of 0.74 ± 0.14. This underscored that cortical thicknesses in these ROIs contain more information than clinical information alone. Previous studies identified correlations between cognitive phenotypes and imaging abnormalities but did not apply their findings to surgery risk assessment (Bell et al., 2011; Hwang et al., 2019; Pardoe et al., 2017). One study used MRI measures to predict post-surgical outcome but required four imaging measures compared to only one needed in our study (Lee et al., 2022).

Limitations

This work has several limitations. The structural data analysis relied on healthy age- and sex-matched controls from an external source, which may not perfectly represent the characteristics of the PwDRE in this study. For instance, education levels could not be matched due to differences in educational systems between countries. However, the effect of education on cortical thickness is not well-established in PwE and is relatively small in healthy individuals (Steffener, 2021).

Moreover, the MRI protocols of healthy controls differed from those for the PwDRE. However, we took several precautions to mitigate this effect. First, the MRI scanner and, thus, the protocol were included as additional variables in the ANOVA model to account for protocol differences. ROIs closely connected to this variable were excluded. Second, the ANOVA was repeated for permuted ROI labels in each patient. This could have revealed systematic differences and provided further validation against chance. Third, the MI group and controls were similar, which suggests

comparability despite the different MRI protocols.

The definition of cognitive worsening in this study deviates from standard clinical definitions. However, other definitions for cognitive worsening based on test-retest-reliability and population standard deviations showed similar results as shown in the Supplement to our publication (Miron et al., 2024).

Last, the post-surgical cognitive evaluation was limited to a single testing session one year after surgery. However, previous research has shown that cognitive results remain relatively stable after one year (Helmstaedter et al., 2018).

The content of Study 1 followed our previously reported results in (Miron et al., 2024).

Dynamics and Cognition

The focus of Study 2 was to understand the link between cortical network dynamics and cognitive function. The analysis included TCs as established in Chapter 5 and other more standard EEG measures, e.g., α-power. Notably, only TCs showed a widespread association with cognitive impairment. In particular, TCs were shorter for PwDRE with language and attention impairment.

The results for attention align with a previous study which reported that longer TCs correlated with shorter response times in a visual oddball task, requiring sustained attention (Irrmischer et al., 2018). Similarly, another study showed that longer TCs enable higher cognitive flexibility (Simola et al., 2017). TCs correlating robustly with language impairment could be explained by electrode locations. Electrodes were preferentially sampled in left lateral temporal and frontal brain regions. These regions have an established association to the function of language networks. Furthermore, TCs during the first recording day correlated strongest with cognitive impairments. On this day, the PwDRE's ASM levels were mainly at their therapeutic levels, likely aligning with the levels during the cognitive testing.

Moreover, TCs in the right hemisphere during the last day were longer for PwDRE with memory impairment compared to PwDRE without impairments. While this might seem counterintuitive as long TCs are thought to be beneficial for information processing, it aligns with findings that working memory tasks require short and long TCs (Wasmuht et al., 2018). Regions with short TCs in these tasks could be associated with the fast encoding of stimuli, and regions with long TCs might need to carry information over a delay period (Wasmuht et al., 2018). As exact electrode placement was unknown, it is impossible to rule out that regions required for fast encoding were sampled.

None of the other EEG features showed a statistically robust correlation. Notably, even the high-γ power did not show a correlation to cognitive impairment, even though it was the basis for TCs calculation. Only the SWS count during the last recording day was higher in the PwDRE with memory impairment. However, a second analysis of the p-value distribution against a uniform distribution was not significant for SWS

in contrast to the distribution for TCs. This underscores that TCs could be a valuable marker for cognitive impairment.

Limitations

While cognitive testing was done according to clinical standards, it was performed before the intracranial EEG recordings. This temporal mismatch and potential changes in ASM loads and sleep patterns could be a cofounder in the analysis. Several steps were taken to address this. First, averaging cognitive tests into domain scores reduced the variability from single tests. Second, surrogate TCs from time-shuffled high-γ-power time series showed no correlations to cognitive impairment. Third, IEDs, ASM levels, and IED counts were included as additional control measures. In particular, the fact that neither IEDs nor ASM were associated with cognitive impairment showed that the results can not be explained by disease severity or treatment path. Fourth, all statistical testing was corrected for multiple comparisons, and the p-value distribution was compared to the chance level.

The content of Study 2 followed our previously reported results in (Müller et al., 2024).

Chapter Conclusion

This chapter analyzed how cortical thickness changes and TCs correlated with cognitive impairment. Notably, the stronger the cognitive impairment was, the more ROIs were affected. Furthermore, shorter TCs were associated with cognitive impairment, particularly in the language and attention domain. The next chapter will discuss the results of this thesis in context with each other and the brain criticality framework.

Chapter 7

Discussion

In this thesis, we have investigated the connection between cortical structure, cortical dynamics, and cognitive function. Therefore, we analyzed a neuronal network model, intracranial EEG data, and MRI images from PwDRE. Tuning the network structure of the model to criticality led to maximal spatial and temporal correlations (SCs and TCs, Chapter 4). Both in the model simulations and iEEG recordings, SCs and TCs were found to be interconnected and distinctively shaped by slow-wave activity (SWA), interictal epileptic discharges (IEDs), and antiseizure medication (ASM) (Chapters 4 and 5). Ultimately, we showed that cognitive impairment correlated with short TCs and increasing numbers of MRI-extracted cortical thickness abnormalities (Chapter 6). Brain criticality could be a unifying framework for interpreting these results, which will be discussed in the following (Fig. 7.1).

Balanced Networks Exhibit Critical Dynamics

For the model in this thesis, we identified a phase transition between vanishing (subcritical) and exploding (supercritical) activity, similar to the model's foundational predecessors (Haldeman & Beggs, 2005; Larremore et al., 2011, 2014; Meisel, 2020) (Chapter 4). Critical dynamics emerged when the largest absolute eigenvalue of the connectivity matrix approached $\lambda = 1$, aligning with previous results for a similar degree-uncorrelated network model (Larremore et al., 2011). SCs and TCs reached their maximum for this critical network structure. In contrast, for very weakly connected networks, i.e., $\lambda \ll 1$, the network activity was driven mainly by the background noise, and SCs and TCs remained short. Strongly connected networks, i.e., $\lambda \gg 1$, led to dense dynamics and short SCs and TCs.

Similar to our model, earlier research showed that the correlation length maximizes at the critical point (Langton, 1990). Hence, long SCs and TCs have been proposed as measures for information integration and as hallmarks for criticality (Cavagna et al., 2010; Goldenfeld, 1992; Jensen, 2021; Linkenkaer-Hansen et al., 2001; Meisel et al., 2015). Additionally, researchers have found that many other information theoretical measures were optimized at the critical point, e.g., dynamical range (Gautam et al., 2015; Kinouchi & Copelli, 2006; Larremore et al., 2011; Shew et al., 2009), information capacity and transmission (Langton, 1990; Shew et al., 2011), or phase variability (Yang et al., 2012). Following these theoretical arguments, cortical networks have

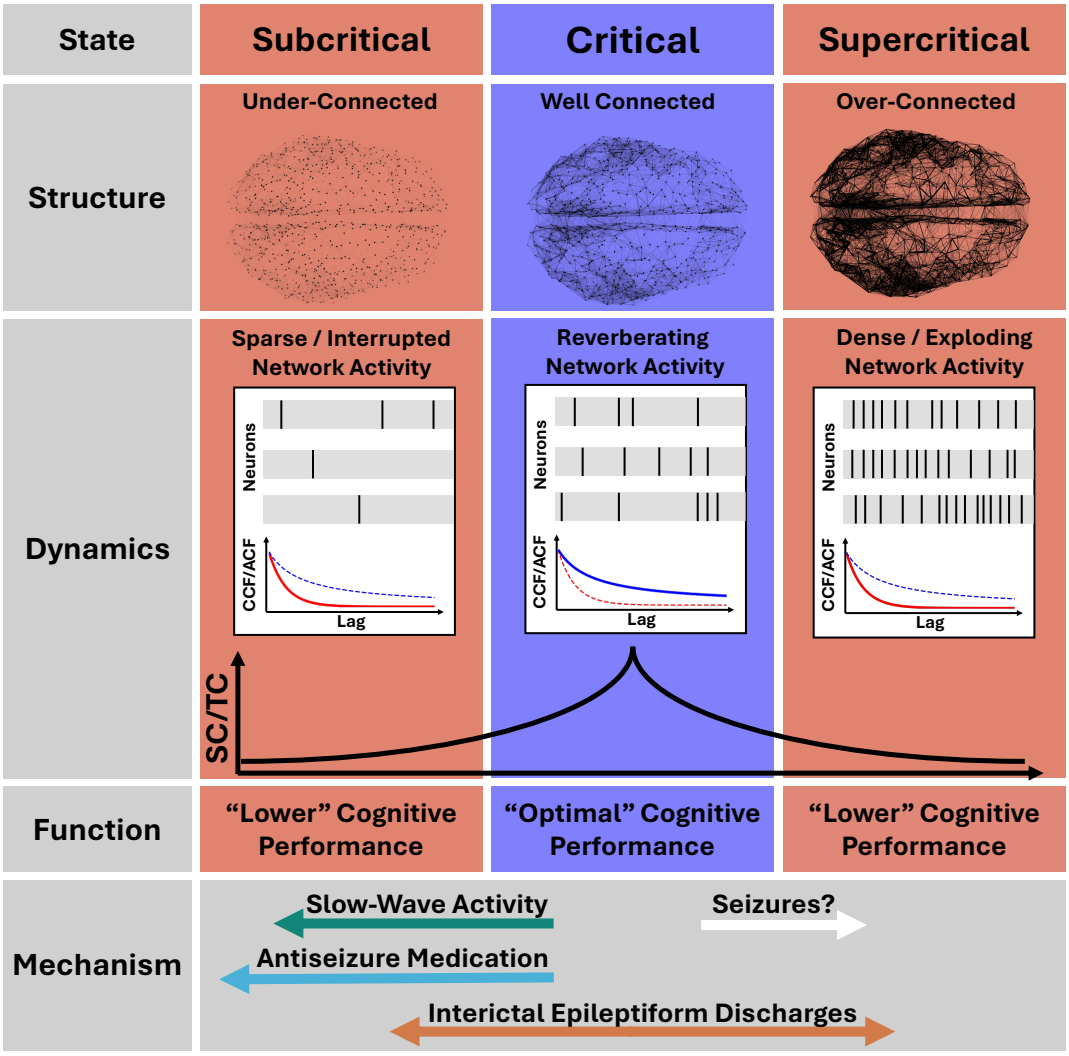

FIGURE 7.1: Brain Criticality Unifies Structure, Dynamics, and Function: The subcritical (left), critical (middle), and supercritical (right) regimes are supported by different network structures and show distinct dynamics. Spatial and temporal correlations (SCs and TCs) characterize information maintenance, are extracted from the cross-correlation and auto-correlation function (CCF and ACF), and peak in the critical regime. Hence, the critical regime allows for optimal function. Various mechanisms can perturb the dynamics and change the system's regime. Reprinted from (Müller et al., 2024) [CC-BY-NC-ND 4.0].

been hypothesized to achieve optimal information processing by tuning to a critical point (Fig. 7.1).

Variation of SCs and TCs

Despite many theoretical arguments linking criticality to cognition (Beggs & Plenz, 2003; Chialvo, 2004; Gautam et al., 2015; Kinouchi & Copelli, 2006; Larremore et al., 2011, 2014; Meisel & Gross, 2009; Ribeiro et al., 2010; Shew et al., 2009; Shew & Plenz, 2013; Shew et al., 2015; Tagliazucchi et al., 2012), experimental evidence in

humans remained limited. Constraining factors include limited temporal duration and resolution, coarse spatial coverage, and assessment of only single cognitive tests.

To address these limitations, we investigated SCs and TCs in multi-day intracranial EEG data from two independent datasets (Dataset 1: 81 PwDRE and Dataset 2: 23 PwDRE, Chapter 5).

SCs and TCs Co-Vary

Dataset 2 in this thesis listed exact electrode positions, which allowed for the investigation of SCs in addition to TCs. SCs and TCs co-varried during the recording duration, i.e., high SCs were associated with long TCs and vice versa.

These co-variations could be explained by the system's proximity to criticality changing over time. Our model simulations showed that systems closer to criticality had longer SCs and TCs. In humans, stimuli and inputs could cause changes of the cortical networks' proximity to criticality. For instance, systems have been shown to tune closer to criticality when presented with structured inputs (Habibollahi et al., 2023) or while performing tasks (Gao et al., 2020). Furthermore, Kashyap et al., 2024 showed that many criticality-related measures, including SCs and TCs, vary as a function of the circadian cycle. The perturbative mechanisms discussed in the following could also add to this co-variability of SCs and TCs.

Slow-Wave Activity Disrupts SCs and TCs

We introduced SWA in the model as neuronal off-periods following previous research (Meisel, Klaus, et al., 2017). These off-periods disrupted SCs and TCs. Similarly, SCs and TCs in human iEEG declined during slow-wave sleep (SWS), a sleep stage associated with SWA (mechanisms in Fig. 7.1).

Disrupted SCs and TCs during SWS align with theories suggesting that during sleep, the effectiveness of the brain's information integration abilities across cortical areas and time declines (Tononi, 2008). Additionally, decreased SCs and TCs during SWS suggest that the system might be further away from the critical point. For instance, SWA has been associated with drift away from criticality in sleeping rats (Meisel, Klaus, et al., 2017). Removing SWA segments from sleep data led to the recovery of critical dynamics similar to wake (Meisel, Klaus, et al., 2017).

Furthermore, previous studies demonstrated that intermittent local SWA during extended wakefulness might lead to dynamics further away from criticality (Meisel, Bailey, et al., 2017; Meisel, Klaus, et al., 2017) and impaired cognition (Alhola & Polo-Kantola, 2007). This aligns with findings associating attention lapses with coocurring SWA (Andrillon et al., 2021). Although cortical networks dynamics are potentially farther away from criticality while SWA is present, evidence was shown that overall, SWS might be essential to reestablish critical dynamics (Meisel, Klaus, et al., 2017; Xu et al., 2024).

In the context of epilepsy, these findings take on an additional dimension. Epilepsy

disturbs sleep by influencing sleep structure, architecture, continuity, and oscillations (Sudbrack-Oliveira et al., 2019). Thus, PwE are more prone to sleep disturbances, potentially contributing to cognitive impairments.

Interictal Epileptiform Discharges Decrease TCs and Increase SCs

IEDs are a typical EEG pattern in epilepsy. Their introduction in the model as synchronous activation of local neuron populations decreased TCs and increased SCs. The analysis of SCs and TCs in iEEG from PwDRE closely matched the model. While SCs were higher with more IEDs, TCs decreased progressively with more IEDs (mechanisms in Fig. 7.1).

In the model, IEDs occurred randomly and disrupted the background activity. Consequently, they masked the ongoing activity and, thus, the correlation within it, explaining the shorter TCs. In contrast, the distinct IED pattern occurs in many neurons and channels simultaneously, which could explain the high SCs under IEDs.

Therefore, drawing conclusions on SCs is difficult due to the synchrony of neurons induced by IEDs. In contrast, TCs suffer less from caveats; thus, reduced TCs could suggest disrupted information flow over time and potentially a drift away from critical dynamics. While the decreased TCs might suggest a drift away from criticality with increased IEDs, the exact direction of this deviation—whether towards sub- or supercritical dynamics—remains an open question. However, one prior study suggested that IEDs are supercritical phenomena (Arviv et al., 2016).

The disruption of TCs could also explain the "transient cognitive impairment" phenomenon, which describes impaired cognitive performance due to concurrent epileptic activity during cognitive testing (Kleen & Kirsch, 2017; Kleen et al., 2013), or cognitive deficits associated with IED-like activity in Alzheimer's disease (Ciliento et al., 2023; Devulder et al., 2024; Lam et al., 2017)."

Antiseizure Medication Shortens SCs and TCs

As the data stemmed from PwDRE undergoing presurgical monitoring, ASMs were routinely tapered down to provoke seizures. The ASM tapering provided a unique opportunity to examine how an external perturbation can affect cortical dynamics and markers of criticality, i.e., SCs and TCs.

ASMs led to declining SCs and TCs in iEEG data from PwDRE, extending previous research on ASM effects on TCs (Meisel, 2020). These results closely matched the observations in the network model, where the effect of ASM was modeled by reducing the strength of excitatory connections between neurons and thus changing the excitation-inhibition (E/I) balance (mechanisms in Fig. 7.1).

Changes in the E/I balance are commonly attributed to ASM action in cortical dynamics (Lang et al., 2013; Ossemann et al., 2016; Premoli et al., 2017; Ziemann et al., 1996). For example, some ASMs change the E/I balance by blocking ion channels and thus reduce the efficacy of excitatory connection (Sankar & Holmes, 2004). The

E/I balance has also been proven as a control parameter for the proximity to criticality (Poil et al., 2012).

Hence, ASMs changing the E/I balance and effective connectivity might shift cortical network dynamics away from the critical point. This could lead to a decline of SCs and TCs, which might explain the adverse effect of ASMs on cognition in PwE (Eddy et al., 2011). In particular, ASMs inducing a shift away from criticality might unify the effects of over 20 different ASMs with various mechanisms of action on cognition (Kwan et al., 2001).

TCs Varies Similar in the SOZ and nSOZ

The analysis excluded seizures but did not generally exclude electrodes that participated in seizures. We conducted a separate analysis of the seizure onset zone (SOZ) and the non-seizure onset zone (nSOZ) to test how the epileptogenic tissue impacted the results.

TCs changed similarly in the SOZ and nSOZ under SWS, IEDs, and ASMs. This suggested that the effects of SWS, IEDs, and ASMs on TCs were not just a consequence of seizure-generating tissue but occur cortex-wide. An analysis accounting for IEDs revealed a trend for shorter TCs in the nSOZ than in the SOZ (Dataset 1).

The trend of longer TCs in the SOZ supports the hypothesis that the SOZ might be closer to criticality and thus more likely to shift into the supercritical regime, a process linked to seizure initiation (Maturana et al., 2020; Meisel & Kuehn, 2012; Meisel et al., 2012). This observation could also explain the success of the *neural fragility index* as a marker for the SOZ, as the index assesses the instability associated with the SOZ (A. Li et al., 2021).

TCs Increase along the Functional Hierarchy

To further investigate how TCs change depending on the electrode location, we analyzed TCs in five regions along the visual pathway. TCs increased with the functional hierarchy of these regions, with short TCs early in the functional hierarchy and long TCs high in the hierarchy.

This showed the hierarchical gradient of TCs known from non-human primates (Honey et al., 2012; Murray et al., 2014; Wasmuht et al., 2018) (Section 2.2.1), human fMRI (Raut et al., 2020) and MEG (Golesorkhi, Gomez-Pilar, Tumati, et al., 2021; Sorrentino et al., 2023) for the first time in iEEG.

Specifically, regions high in the functional hierarchy might leverage long TCs to integrate information over time and from different sources (Murray et al., 2014). In contrast, regions early in the hierarchy might benefit from short TCs to adapt quickly to variable stimuli and reduce interference with previous stimuli (Murray et al., 2014). The increase of TCs along the functional hierarchy could indicate that these regions are closer to criticality, making regions high in the functional hierarchy more flexible and adjusted for complex computation.

Short TCs Predict Cognitive Impairment

Ultimately, to test if TCs directly correlate with cognitive performance, we analyzed iEEG data from 81 PwDRE for which cognitive testing was available (Section 6.1.2). Under the brain criticality hypothesis, short TCs could lead to a deterioration of cognitive performance.

Indeed, language and attention impairmed PwDRE showed shorter TCs than their non-impaired counterparts. In contrast, none of the control measures, including high-γ band power and surrogate TCs, were connected to cognitive impairment. Notably, neither lesion, IED rate, nor ASM load were related to cognitive impairment. This suggests that epileptic activity and disease severity are only minor factors. For example, while IEDs disrupted TCs, they were only one factor of many affecting TCs and, thus, cognitive function.

As clinical needs decided about the electrode location, sampling was preferentially in the left hemispheric lateral temporal and frontal brain region due to the large portion of temporal and frontal lobe epilepsy in the cohort. These regions are integral to language processing networks, which may have contributed to the observed relationship of short TCs for language impairmed PwDRE.

Regarding the attention domain, previous research reported similar results. For instance, one study observed that extended TCs, even in scalp EEG, corresponded with shorter response times in a visual oddball task, indicating enhanced attentional performance (Irrmischer et al., 2018). Similarly, another investigation linked prolonged TCs to increased cognitive flexibility (Simola et al., 2017).

Other criticality measures have been explored in the context of various cognitive states. Research has suggested that during rest periods, cortical network dynamics tends towards a critical state, potentially optimizing its receptivity to external and internal stimuli (Fagerholm et al., 2015; Hahn et al., 2017). Furthermore, the concept of criticality has been extended to investigations of more general alterations in consciousness. Studies examining the effects of anesthesia and sleep have provided insights into how criticality may be linked to different levels of awareness (Maschke et al., 2024; Priesemann et al., 2013).

Alternative Perspectives on SCs and TCs

While the previous sections interpreted the SCs and TCs changes within the brain criticality framework, other explanations are possible.

The interpretation within the criticality framework suggested that perturbative mechanisms push the system further from the critical point. Thus, the interpretation talked about relative changes and did not need to claim that cortical dynamics are exactly at criticality. Some researchers have argued that cortical dynamics are slightly subcritical (Wilting & Priesemann, 2019; Wilting et al., 2018). There, cortical network dynamics would be able to retain computational flexibility while also keeping a safety margin to supercritical dynamics and, thus, instability. This perspective could align

with the finding that the SOZ had a trend for longer TCs, thus positioning it closer to this instability boundary. However, the general claim that longer TCs benefit information processing remains untouched by this slightly different hypothesis about the cortical state.

Another perspective suggests that cortical network dynamics are always at criticality, albeit with distinct characteristics and scaling exponents. For instance, regions with different TCs would all be critical but have different critical exponents and scaling functions for auto- and cross-correlation coefficients. Similarly, the perturbative mechanisms, which led to the variation of SCs and TCs, could induce drifts on a critical hyperplane rather than a shift away from criticality. Such a drift on a critical surface was shown to be plausible in a recent model (Sormunen et al., 2023). Further, it could be interpreted in the context of quasi-criticality, which argues that cortical dynamics are in a broader regime with critical scaling, for example, a Griffiths phase (Fuscà et al., 2023; Muñoz et al., 2010). Further research is necessary to evaluate whether the results in this thesis are better explained by drifts on a critical manifold or deviations from it. However, the interpretation of SCs and TCs about cognition remains similar in both cases, i.e., long TCs are beneficial for complex computation. Specifically, the results showed that longer TCs correlated with intact cognition and shorter TCs with impaired cognition. Hence, long TCs and SCs could be interpreted as an additional constraint for the critical manifold to achieve optimal cognitive performance.

A completely different explanation could be that non-critical processes lead to changes in SCs and TCs. For example, external drives, inducing non-stationary in the time series, could artificially lengthen the correlations. Smaller and larger external drives would then explain the variation of SCs and TCs. While this is a valid critique if only short segments are analyzed, this scenario seems unlikely for this thesis's results as multiple days were analyzed. The external drives would have to change in a coordinated way over days, hours, and minutes to explain the effects of ASMs, SWS, and IEDs, respectively.

Summary: SCs and TCs

In summary, we investigated SCs and TCs, markers for information maintenance, using model simulations and iEEG from PwDRE. In the model, SCs and TCs were maximal at criticality. Mechanisms related to cognition, SWS, IEDs, and ASMs perturbed the dynamics and shaped SCs and TCs. In the model and iEEG data, all mechanisms reduced SCs and TCs except IEDs, which increased SCs. Ultimately, short TCs correlated with language and attention impairment in PwDRE.

These results show that different factors can influence SCs and TCs, potentially impacting the cortical network's proximity to criticality (Fig. 7.1). Notably, by investigating perturbations of SCs, TCs, and thus criticality, a common critique in brain criticality research was addressed, namely that often only point estimates are used to characterize the brain's proximity to criticality (Beggs, 2022b; Mariani et al., 2022).

In conclusion, our results support brain criticality, measured through SCs and TCs, as a unifying framework to explain cognitive impairments in epilepsy and potentially other neurological disorders.

Cortical Thickness Changes with Cognitive Impairment

To also investigate how cortical structure changes could impact cognitive impairment, we investigated 16 cognitive measures and gray matter thicknesses in 360 regions of interest (ROI). First, the PwDRE were assigned cognitive impairment phenotypes using the IC-CoDE criteria (McDonald et al., 2023). This approach, applied in a German-speaking cohort for the first time, was designed to improve the comparability of cognitive impairment between different language, cultural, and cognitive test settings. With 53% MDI, 30% FI, and 17% MI, results were comparable to distributions in non-Germam speaking cohorts (B. Hermann et al., 2020; Reyes et al., 2023).

Notably, the groups with more severe cognitive impairment had more cortical thickness abnormalities (MDI: 28 ROIs, FI: 12 ROIs, MI: 3 ROIs). While only few studies have identified similar trends in PwDRE (Dabbs et al., 2009; B. Hermann et al., 2020), in other cohorts, MDI PwE compared to MI showed more diffusion and functional MRI abnormalities (Kaestner et al., 2019; Reyes et al., 2019; Rodríguez-Cruces et al., 2018) and changes in functional network measures (Garcia-Ramos et al., 2022; Larivière et al., 2020).

The brain criticality hypothesis could explain the decreased cognitive performance associated with more cortical thickness abnormalities. Our model simulations showed that a balanced network structure is necessary for critical dynamics to emerge. Deviations from the critical structure hindering the emergence of critical dynamics could negatively impact cognitive performance. Although this connection is theoretically plausible, our data and analysis do not allow for a conclusion. Hence, further research is needed to investigate the relationship between structural changes and critical dynamics.

7.1 General Limitations

This thesis has some general limitations besides the study-specific limitations (see Chapters 5 and 6).

First, all data stemmed from persons with drug-resistant epilepsy, which could hinder the transferability of the results to a healthy population. However, iEEG recordings of healthy individuals do not exist because electrode implantation is a risky procedure that is only a last resort in severe neurological diseases like epilepsy. Nonetheless, future research might be able to confirm these results in less invasive measures like MEG.

Second, seizure foci and disease etiology are patient-specific. For instance, most patients had temporal lobe epilepsy, but some had seizure foci in other brain areas, like the frontal lobe. Generally, this led to variability in the cohort, for example, the

cortical coverage of the iEEG. Future studies could address this by investigating more specific cohorts and increasing the cohort size to analyze how heterogeneities in the disease affect SCs and TCs.

Third, the data stemmed from German-speaking individuals. While cognitive phenotyping and domain average scores were used as general cognitive evaluations, future research should test our results in other cohorts.

Fourth, despite the iEEG already including multiple days, we could not account for longer-term fluctuations that might impact cortical dynamics. For example, previous studies used implanted devices to identify cycles spanning weeks to month for IEDs, auto-correlation decay rates, and variance in implanted devices (Karoly et al., 2016; Maturana et al., 2020). To resolve this, SCs and TCs should be analyzed in longer time series, for instance, in data from implanted devices.

7.2 Outlook

This thesis aimed to help understand the connection between structural changes, SCs, TCs, and cognition and interpreted the results within the brain criticality framework. Despite being extensive, our analysis leaves many questions open and points to new directions for future research. While some open questions have been discussed within the limitations sections, some future directions are presented below.

Alignment of Structural with Dynamical Measures

A natural extension of this work would be to align the structural changes in the cortex with the dynamical variations, i.e., SCs and TCs, and potentially even cognitive function. On the one hand, this could experimentally confirm the theoretically predicted link between structure and dynamics. On the other hand, if strong correlations to cognitive testing are found, the cognitive results could indicate abnormalities in the cortex and its dynamics. Such insights might help identify lesions or epileptogenic tissue without requiring invasive or specialized measurements, like MRI or iEEG.

Delineate Effects of Different ASMs

This thesis investigated the general effect of ASMs on SCs and TCs. Therefore, different ASMs were aggregated based on their recommended levels. However, the action mechanisms between ASMs differ; thus, their effect on cortical dynamics could differ too. Future research in larger datasets could help to delineate the different ASMs based on their impact on SCs, TCs, and cognition. Specifically, if ASM effects were spatially heterogeneous, this might help identify the best choice of ASM for specific seizure foci.

Prediction of Surgery Success and Risk

In this thesis, we have shown that cortical thickness changes can predict cognitive worsening after epilepsy surgery. Furthermore, our previous work showed that markers for dynamics in the foramen ovale EEG could predict seizure freedom after surgery (Miron et al., 2023). Similarly, SCs and TCs could help to predict seizure freedom and cognitive risks after epilepsy surgery. If they provide predictive value, this could directly impact clinical decision-making by identifying suitable candidates for epilepsy surgery. Moreover, it might help patients better understand the risks and benefits of the treatment options and thus aid them in their decision-making.

Prediction of Seizure Risk

The analyses in this thesis excluded epileptic seizures and focused on the interictal EEG. However, epileptic seizures have been hypothesized to be related to the instability close to phase transition and potentially emerging supercritical dynamics (A. Li et al., 2021; Maturana et al., 2020; Meisel & Kuehn, 2012; Meisel et al., 2012). The insights about SCs and TCs could add to this line of research to find markers for such a phase transition toward a seizure state.

7.3 Concluding Remarks

This thesis explored the interplay between structural changes, network dynamics, and cognitive function in PwDRE. Therefore, we utilized computational modeling and analyzed intracranial EEG and MRI data. We found that in iEEG dynamics, SCs, and TCs, markers for information integration, co-varied and were distinctively perturbed by slow-wave activity, interictal epileptiform discharges, and antiseizure medication, as predicted by our model simulations. Further, TCs followed a hierarchical gradient, with the longest TCs in high cortical regions, i.e., regions associated with complex functions like decision-making. Ultimately, we found that shorter TCs and gray matter thickness abnormalities were associated with cognitive impairment.

These results align with the predictions of the brain criticality hypothesis, which states that the human brain's structure is poised close to a phase transition. This proximity to criticality then maximizes SCs and TCs and, consequently, optimizes information processing. The perturbative mechanisms, i.e., SWA, IEDs, and ASM, which have been proven to affect cognitive function, changed SCs and TCs. This change could indicate a drift away from the critical point and thus explain reduced cognitive performances. In general, our findings support criticality as the set point for optimal network function and cognition (Fig. 7.1).

Measuring deviations from criticality could allow future researchers and clinicians to better understand cognitive impairment and neurological disorders such as epilepsy. Thus, markers for proximity to criticality, like SCs and TCs, might become helpful in identifying, personalizing, and evaluating the risks of treatment options.

Bibliography

Aldenkamp, A. P., & Arends, J. (2004). Effects of epileptiform EEG discharges on cognitive function: Is the concept of "transient cognitive impairment" still valid? *Epilepsy & Behavior*, *5*, 25–34. https://doi.org/10.1016/j.yebeh.2003.11.005

Aldenkamp, A. P., & Baker, G. (2001). A systematic review of the effects of lamotrigine on cognitive function and quality of life. *Epilepsy & Behavior*, *2*(2), 85–91. https://doi.org/10.1006/ebeh.2001.0168

Alhola, P., & Polo-Kantola, P. (2007). Sleep deprivation: Impact on cognitive performance. *Neuropsychiatric Disease and Treatment*, *3*(5), 553–567.

Andrillon, T., Burns, A., Mackay, T., Windt, J., & Tsuchiya, N. (2021). Predicting lapses of attention with sleep-like slow waves. *Nature Communications*, *12*(1), 3657. https://doi.org/10.1038/s41467-021-23890-7

Arviv, O., Medvedovsky, M., Sheintuch, L., Goldstein, A., & Shriki, O. (2016). Deviations from critical dynamics in interictal epileptiform activity. *The Journal of Neuroscience*, *36*(48), 12276–12292. https://doi.org/10.1523/JNEUROSCI.0809-16.2016

Asadi-Pooya, A. A., Brigo, F., Lattanzi, S., & Blumcke, I. (2023). Adult epilepsy. *The Lancet*, *402*(10399), 412–424. https://doi.org/10.1016/S0140-6736(23)01048-6

Asadi-Pooya, A. A., Brigo, F., Trinka, E., Lattanzi, S., Karakis, I., Kishk, N. A., Valente, K. D., Jusupova, A., Turuspekova, S. T., Daza-Restrepo, A., Contreras, G., Kutlubaev, M. A., Guekht, A., Rahimi-Jaberi, A., Aljandeel, G., Calle-Lopez, Y., Alsaadi, T., Ashkanani, A., Ranganathan, L. N., ... Mwendaweli, N. (2022). Physicians' beliefs about brain surgery for drug-resistant epilepsy: A global survey. *Seizure: European Journal of Epilepsy*, *103*, 18–22. https://doi.org/10.1016/j.seizure.2022.10.012

Aschenbrenner, S., Tucha, O., & Lange, K. W. (2000). *Regensburger wortflüssigkeits-test: RWT*. Hogrefe, Verlag für Psychologie.

Bak, P., Tang, C., & Wiesenfeld, K. (1988). Self-organized criticality. *Physical Review A*, *38*(1), 364–374. https://doi.org/10.1103/PhysRevA.38.364

Bartolomei, F., Chauvel, P., & Wendling, F. (2008). Epileptogenicity of brain structures in human temporal lobe epilepsy: A quantified study from intracerebral EEG. *Brain*, *131*(7), 1818–1830. https://doi.org/10.1093/brain/awn111

Bassett, D. S., & Sporns, O. (2017). Network neuroscience. *Nature Neuroscience*, *20*(3), 353–364. https://doi.org/10.1038/nn.4502

Baxendale, S., & Thompson, P. (2020). The association of cognitive phenotypes with postoperative outcomes after epilepsy surgery in patients with temporal lobe

epilepsy. *Epilepsy & Behavior*, *112*, 107386. https://doi.org/10.1016/j.yebeh.2020.107386

Beggs, J. M., & Plenz, D. (2004). Neuronal avalanches are diverse and precise activity patterns that are stable for many hours in cortical slice cultures. *Journal of Neuroscience*, *24*(22), 5216–5229. https://doi.org/10.1523/JNEUROSCI.0540-04.2004

Beggs, J. M. (2022a, August 30). *The cortex and the critical point: Understanding the power of emergence*. The MIT Press. https://doi.org/10.7551/mitpress/13588.001.0001

Beggs, J. M. (2022b). Addressing skepticism of the critical brain hypothesis. *Frontiers in Computational Neuroscience*, *16*, 703865. https://doi.org/10.3389/fncom.2022.703865

Beggs, J. M., & Plenz, D. (2003). Neuronal avalanches in neocortical circuits. *The Journal of Neuroscience*, *23*(35), 11167–11177. https://doi.org/10.1523/JNEUROSCI.23-35-11167.2003

Beggs, J. M., & Timme, N. (2012). Being critical of criticality in the brain. *Frontiers in Physiology*, *3*. https://doi.org/10.3389/fphys.2012.00163

Bell, B., Lin, J. J., Seidenberg, M., & Hermann, B. (2011). The neurobiology of cognitive disorders in temporal lobe epilepsy. *Nature Reviews Neurology*, *7*(3), 154–164. https://doi.org/10.1038/nrneurol.2011.3

Berthouze, L., James, L. M., & Farmer, S. F. (2010). Human EEG shows long-range temporal correlations of oscillation amplitude in theta, alpha and beta bands across a wide age range. *Clinical Neurophysiology*, *121*(8), 1187–1197. https://doi.org/10.1016/j.clinph.2010.02.163

Bialer, M., & White, H. S. (2010). Key factors in the discovery and development of new antiepileptic drugs. *Nature Reviews Drug Discovery*, *9*(1), 68–82. https://doi.org/10.1038/nrd2997

Bookheimer, S. Y., Salat, D. H., Terpstra, M., Ances, B. M., Barch, D. M., Buckner, R. L., Burgess, G. C., Curtiss, S. W., Diaz-Santos, M., Elam, J. S., Fischl, B., Greve, D. N., Hagy, H. A., Harms, M. P., Hatch, O. M., Hedden, T., Hodge, C., Japardi, K. C., Kuhn, T. P., … Yacoub, E. (2019). The lifespan human connectome project in aging: An overview. *NeuroImage*, *185*, 335–348. https://doi.org/10.1016/j.neuroimage.2018.10.009

Bornholdt, S., & Röhl, T. (2003). Self-organized critical neural networks. *Physical Review E*, *67*(6), 066118. https://doi.org/10.1103/PhysRevE.67.066118

Bornholdt, S., & Rohlf, T. (2000). Topological evolution of dynamical networks: Global criticality from local dynamics. *Physical Review Letters*, *84*(26), 6114–6117. https://doi.org/10.1103/PhysRevLett.84.6114

Brodie, M., Barry, S., Bamagous, G., Norrie, J., & Kwan, P. (2012). Patterns of treatment response in newly diagnosed epilepsy. *Neurology*, *78*(20), 1548–1554. https://doi.org/10.1212/WNL.0b013e3182563b19

Busch, R. M., Hogue, O., Miller, M., Ferguson, L., McAndrews, M. P., Hamberger, M., Kim, M., McDonald, C. R., Reyes, A., Drane, D. L., Hermann, B. P., Bingaman, W., Najm, I. M., Kattan, M. W., & Jehi, L. (2021). Nomograms to predict verbal memory decline after temporal lobe resection in adults with epilepsy. *Neurology*, *97*(3). https://doi.org/10.1212/WNL.0000000000012221

Buzsáki, G., Anastassiou, C. A., & Koch, C. (2012). The origin of extracellular fields and currents — EEG, ECoG, LFP and spikes. *Nature Reviews Neuroscience*, *13*(6), 407–420. https://doi.org/10.1038/nrn3241

Cavagna, A., Cimarelli, A., Giardina, I., Parisi, G., Santagati, R., Stefanini, F., & Viale, M. (2010). Scale-free correlations in starling flocks. *Proceedings of the National Academy of Sciences*, *107*(26), 11865–11870. https://doi.org/10.1073/pnas.1005766107

Chialvo, D. R. (2004). Critical brain networks. *Physica A: Statistical Mechanics and its Applications*, *340*(4), 756–765. https://doi.org/10.1016/j.physa.2004.05.064

Ciliento, R., Gjini, K., Dabbs, K., Hermann, B., Riedner, B., Jones, S., Fatima, S., Johnson, S., Bendlin, B., Lam, A. D., Boly, M., & Struck, A. F. (2023). Prevalence and localization of nocturnal epileptiform discharges in mild cognitive impairment. *Brain Communications*, *5*(6), fcad302. https://doi.org/10.1093/braincomms/fcad302

Cox, R. W. (1996). AFNI: Software for analysis and visualization of functional magnetic resonance neuroimages. *Computers and Biomedical Research*, *29*(3), 162–173. https://doi.org/10.1006/cbmr.1996.0014

Dabbs, K., Jones, J., Seidenberg, M., & Hermann, B. (2009). Neuroanatomical correlates of cognitive phenotypes in temporal lobe epilepsy. *Epilepsy & Behavior*, *15*(4), 445–451. https://doi.org/10.1016/j.yebeh.2009.05.012

Dahnke, R., Yotter, R. A., & Gaser, C. (2013). Cortical thickness and central surface estimation [Publisher: Elsevier]. *Neuroimage*, *65*, 336–348.

Dakos, V., Scheffer, M., Van Nes, E. H., Brovkin, V., Petoukhov, V., & Held, H. (2008). Slowing down as an early warning signal for abrupt climate change. *Proceedings of the National Academy of Sciences*, *105*(38), 14308–14312. https://doi.org/10.1073/pnas.0802430105

De Tisi, J., Bell, G. S., Peacock, J. L., McEvoy, A. W., Harkness, W. F., Sander, J. W., & Duncan, J. S. (2011). The long-term outcome of adult epilepsy surgery, patterns of seizure remission, and relapse: A cohort study. *The Lancet*, *378*(9800), 1388–1395. https://doi.org/10.1016/S0140-6736(11)60890-8

Devulder, A., Vanderlinden, G., Van Langenhoven, L., Testelmans, D., Van Den Bossche, M., De Winter, F.-L., Vandenbulcke, M., Vandenberghe, R., Theys, T., Van Laere, K., & Van Paesschen, W. (2024). Epileptic activity on foramen ovale electrodes is associated with sleep and tau pathology in alzheimer's disease. *Brain*, awae231. https://doi.org/10.1093/brain/awae231

Ebus, S., Arends, J., Hendriksen, J., Van Der Horst, E., De La Parra, N., Hendriksen, R., Santegoeds, E., Boon, P., & Aldenkamp, B. (2012). Cognitive effects of

interictal epileptiform discharges in children. *European Journal of Paediatric Neurology*, *16*(6), 697–706. https://doi.org/10.1016/j.ejpn.2012.05.010

Eddy, C. M., Rickards, H. E., & Cavanna, A. E. (2011). The cognitive impact of antiepileptic drugs. *Therapeutic Advances in Neurological Disorders*, *4*(6), 385–407. https://doi.org/10.1177/1756285611417920

Elger, C. E., Helmstaedter, C., & Kurthen, M. (2004). Chronic epilepsy and cognition. *The Lancet Neurology*, *3*(11), 663–672. https://doi.org/10.1016/S1474-4422(04)00906-8

Fagerholm, E. D., Lorenz, R., Scott, G., Dinov, M., Hellyer, P. J., Mirzaei, N., Leeson, C., Carmichael, D. W., Sharp, D. J., Shew, W. L., & Leech, R. (2015). Cascades and cognitive state: Focused attention incurs subcritical dynamics. *The Journal of Neuroscience*, *35*(11), 4626–4634. https://doi.org/10.1523/JNEUROSCI.3694-14.2015

Fiest, K. M., Sauro, K. M., Wiebe, S., Patten, S. B., Kwon, C.-S., Dykeman, J., Pringsheim, T., Lorenzetti, D. L., & Jetté, N. (2017). Prevalence and incidence of epilepsy: A systematic review and meta-analysis of international studies. *Neurology*, *88*(3), 296–303. https://doi.org/10.1212/WNL.0000000000003509

Fisher, R. S., Acevedo, C., Arzimanoglou, A., Bogacz, A., Cross, J. H., Elger, C. E., Engel, J., Forsgren, L., French, J. A., Glynn, M., Hesdorffer, D. C., Lee, B., Mathern, G. W., Moshé, S. L., Perucca, E., Scheffer, I. E., Tomson, T., Watanabe, M., & Wiebe, S. (2014). ILAE official report: A practical clinical definition of epilepsy. *Epilepsia*, *55*(4), 475–482. https://doi.org/10.1111/epi.12550

Fisher, R. S., Cross, J. H., French, J. A., Higurashi, N., Hirsch, E., Jansen, F. E., Lagae, L., Moshé, S. L., Peltola, J., Roulet Perez, E., Scheffer, I. E., & Zuberi, S. M. (2017). Operational classification of seizure types by the international league against epilepsy: Position paper of the ILAE commission for classification and terminology. *Epilepsia*, *58*(4), 522–530. https://doi.org/10.1111/epi.13670

Fitzgerald, Z., Morita-Sherman, M., Hogue, O., Joseph, B., Alvim, M. K. M., Yasuda, C. L., Vegh, D., Nair, D., Burgess, R., Bingaman, W., Najm, I., Kattan, M. W., Blumcke, I., Worrell, G., Brinkmann, B. H., Cendes, F., & Jehi, L. (2021). Improving the prediction of epilepsy surgery outcomes using basic scalp EEG findings. *Epilepsia*, *62*(10), 2439–2450. https://doi.org/10.1111/epi.17024

Frauscher, B. (2020). Localizing the epileptogenic zone. *Current Opinion in Neurology*, *33*(2), 198–206. https://doi.org/10.1097/WCO.0000000000000790

Friedman, N., Ito, S., Brinkman, B. A. W., Shimono, M., DeVille, R. E. L., Dahmen, K. A., Beggs, J. M., & Butler, T. C. (2012). Universal critical dynamics in high resolution neuronal avalanche data. *PHYSICAL REVIEW LETTERS*, 5.

Friston, K. J. (2009). Modalities, modes, and models in functional neuroimaging. *Science*, *326*(5951), 399–403. https://doi.org/10.1126/science.1174521

Fuscà, M., Siebenhühner, F., Wang, S. H., Myrov, V., Arnulfo, G., Nobili, L., Palva, J. M., & Palva, S. (2023). Brain criticality predicts individual levels of inter-areal synchronization in human electrophysiological data. *Nature Communications*, *14*(1), 4736. https://doi.org/10.1038/s41467-023-40056-9

Gao, R., van den Brink, R. L., Pfeffer, T., & Voytek, B. (2020). Neuronal timescales are functionally dynamic and shaped by cortical microarchitecture. *eLife*, *9*, e61277. https://doi.org/10.7554/eLife.61277

Garcia-Ramos, C., Nair, V., Maganti, R., Mathis, J., Conant, L. L., Prabhakaran, V., Binder, J. R., Meyerand, B., Hermann, B., & Struck, A. F. (2022). Network phenotypes and their clinical significance in temporal lobe epilepsy using machine learning applications to morphological and functional graph theory metrics. *Scientific Reports*, *12*(1), 14407. https://doi.org/10.1038/s41598-022-18495-z

Gautam, S. H., Hoang, T. T., McClanahan, K., Grady, S. K., & Shew, W. L. (2015). Maximizing sensory dynamic range by tuning the cortical state to criticality (C. C. Hilgetag, Ed.). *PLOS Computational Biology*, *11*(12), e1004576. https://doi.org/10.1371/journal.pcbi.1004576

Glasser, M. F., Coalson, T. S., Robinson, E. C., Hacker, C. D., Harwell, J., Yacoub, E., Ugurbil, K., Andersson, J., Beckmann, C. F., Jenkinson, M., Smith, S. M., & Van Essen, D. C. (2016). A multi-modal parcellation of human cerebral cortex. *Nature*, *536*(7615), 171–178. https://doi.org/10.1038/nature18933

Goldenfeld, N. (1992). *Lectures on phase transitions and the renormalization group* (1st ed.). CRC Press. https://doi.org/10.1201/9780429493492

Golesorkhi, M., Gomez-Pilar, J., Tumati, S., Fraser, M., & Northoff, G. (2021). Temporal hierarchy of intrinsic neural timescales converges with spatial core-periphery organization. *Communications Biology*, *4*(1), 277. https://doi.org/10.1038/s42003-021-01785-z

Golesorkhi, M., Gomez-Pilar, J., Zilio, F., Berberian, N., Wolff, A., Yagoub, M. C. E., & Northoff, G. (2021). The brain and its time: Intrinsic neural timescales are key for input processing. *Communications Biology*, *4*(1), 970. https://doi.org/10.1038/s42003-021-02483-6

Gross, T. (2021). Not one, but many critical states: A dynamical systems perspective. *Frontiers in Neural Circuits*, *15*, 614268. https://doi.org/10.3389/fncir.2021.614268

Gunnarsdottir, K. M., Li, A., Smith, R. J., Kang, J.-Y., Korzeniewska, A., Crone, N. E., Rouse, A. G., Cheng, J. J., Kinsman, M. J., Landazuri, P., Uysal, U., Ulloa, C. M., Cameron, N., Cajigas, I., Jagid, J., Kanner, A., Elarjani, T., Bicchi, M. M., Inati, S., … Sarma, S. V. (2021, October 18). *Source-sink connectivity: A novel interictal EEG marker for seizure localization* (preprint). Bioengineering. https://doi.org/10.1101/2021.10.15.464594

Habibollahi, F., Kagan, B. J., Burkitt, A. N., & French, C. (2023). Critical dynamics arise during structured information presentation within embodied in vitro

neuronal networks. *Nature Communications*, *14*(1), 5287. https://doi.org/10.1038/s41467-023-41020-3

Hahn, G., Petermann, T., Havenith, M. N., Yu, S., Singer, W., Plenz, D., & Nikolić, D. (2010). Neuronal avalanches in spontaneous activity in vivo. *Journal of Neurophysiology*, *104*(6), 3312–3322. https://doi.org/10.1152/jn.00953.2009

Hahn, G., Ponce-Alvarez, A., Monier, C., Benvenuti, G., Kumar, A., Chavane, F., Deco, G., & Frégnac, Y. (2017). Spontaneous cortical activity is transiently poised close to criticality (C. C. Hilgetag, Ed.). *PLOS Computational Biology*, *13*(5), e1005543. https://doi.org/10.1371/journal.pcbi.1005543

Haldeman, C., & Beggs, J. M. (2005). Critical branching captures activity in living neural networks and maximizes the number of metastable states. *Physical Review Letters*, *94*(5), 058101. https://doi.org/10.1103/PhysRevLett.94.058101

Hardstone, R., Poil, S.-S., Schiavone, G., Jansen, R., Nikulin, V. V., Mansvelder, H. D., & Linkenkaer-Hansen, K. (2012). Detrended fluctuation analysis: A scale-free view on neuronal oscillations. *Frontiers in Physiology*, *3*. https://doi.org/10.3389/fphys.2012.00450

Harris, T. E. (1964). *The theory of branching processes* (Vol. 6) [OCLC: 931719544]. Springer-Verlag.

Helmstaedter, C., & Durwen, H. (1990). [The Verbal Learning and Retention Test. A useful and differentiated tool in evaluating verbal memory performance]. *Schweiz Arch Neurol Psychiatr (1985)*, *141*(1), 21–30. http://europepmc.org/abstract/MED/1690447

Helmstaedter, C., Elger, C., & Vogt, V. (2018). Cognitive outcomes more than 5 years after temporal lobe epilepsy surgery: Remarkable functional recovery when seizures are controlled. *Seizure*, *62*, 116–123. https://doi.org/10.1016/j.seizure.2018.09.023

Hermann, B., Conant, L. L., Cook, C. J., Hwang, G., Garcia-Ramos, C., Dabbs, K., Nair, V. A., Mathis, J., Bonet, C. N. R., Allen, L., Almane, D. N., Arkush, K., Birn, R., DeYoe, E. A., Felton, E., Maganti, R., Nencka, A., Raghavan, M., Shah, U., … Meyerand, M. E. (2020). Network, clinical and sociodemographic features of cognitive phenotypes in temporal lobe epilepsy. *NeuroImage: Clinical*, *27*, 102341. https://doi.org/10.1016/j.nicl.2020.102341

Hermann, B. P., Struck, A. F., Busch, R. M., Reyes, A., Kaestner, E., & McDonald, C. R. (2021). Neurobehavioural comorbidities of epilepsy: Towards a network-based precision taxonomy. *Nature Reviews Neurology*, *17*(12), 731–746. https://doi.org/10.1038/s41582-021-00555-z

Hesse, J., & Gross, T. (2014). Self-organized criticality as a fundamental property of neural systems. *Frontiers in Systems Neuroscience*, *8*. https://doi.org/10.3389/fnsys.2014.00166

Honey, C. J., Thesen, T., Donner, T. H., Silbert, L. J., Carlson, C. E., Devinsky, O., Doyle, W. K., Rubin, N., Heeger, D. J., & Hasson, U. (2012). Slow cortical

dynamics and the accumulation of information over long timescales. *Neuron*, *76*(2), 423–434. https://doi.org/10.1016/j.neuron.2012.08.011

Hwang, G., Dabbs, K., Conant, L., Nair, V. A., Mathis, J., Almane, D. N., Nencka, A., Birn, R., Humphries, C., Raghavan, M., DeYoe, E. A., Struck, A. F., Maganti, R., Binder, J. R., Meyerand, E., Prabhakaran, V., & Hermann, B. (2019). Cognitive slowing and its underlying neurobiology in temporal lobe epilepsy. *Cortex*, *117*, 41–52. https://doi.org/10.1016/j.cortex.2019.02.022

Ihle, M., Feldwisch-Drentrup, H., Teixeira, C. A., Witon, A., Schelter, B., Timmer, J., & Schulze-Bonhage, A. (2012). EPILEPSIAE – a european epilepsy database. *Computer Methods and Programs in Biomedicine*, *106*(3), 127–138. https://doi.org/10.1016/j.cmpb.2010.08.011

Irrmischer, M., Poil, S.-S., Mansvelder, H. D., Intra, F. S., & Linkenkaer-Hansen, K. (2018). Strong long-range temporal correlations of beta/gamma oscillations are associated with poor sustained visual attention performance. *European Journal of Neuroscience*, *48*(8), 2674–2683. https://doi.org/10.1111/ejn.13672

Jehi, L., Jette, N., Kwon, C.-S., Josephson, C. B., Burneo, J. G., Cendes, F., Sperling, M. R., Baxendale, S., Busch, R. M., Triki, C. C., Cross, J. H., Ekstein, D., Englot, D. J., Luan, G., Palmini, A., Rios, L., Wang, X., Roessler, K., Rydenhag, B., … Wiebe, S. (2022). Timing of referral to evaluate for epilepsy surgery: Expert consensus recommendations from the surgical therapies commission of the international league against epilepsy. *Epilepsia*, *63*(10), 2491–2506. https://doi.org/10.1111/epi.17350

Jehi, L., Morita-Sherman, M., Love, T. E., Bartolomei, F., Bingaman, W., Braun, K., Busch, R. M., Duncan, J., Hader, W. J., Luan, G., Rolston, J. D., Schuele, S., Tassi, L., Vadera, S., Sheikh, S., Najm, I., Arain, A., Bingaman, J., Diehl, B., … Wiebe, S. (2021). Comparative effectiveness of stereotactic electroencephalography versus subdural grids in epilepsy surgery. *Annals of Neurology*, *90*(6), 927–939. https://doi.org/10.1002/ana.26238

Jenkinson, M., Beckmann, C. F., Behrens, T. E., Woolrich, M. W., & Smith, S. M. (2012). FSL. *NeuroImage*, *62*(2), 782–790. https://doi.org/10.1016/j.neuroimage.2011.09.015

Jensen, H. J. (2021). What is critical about criticality: In praise of the correlation function. *Journal of Physics: Complexity*, *2*(3), 032002. https://doi.org/10.1088/2632-072X/ac24f2

Kaestner, E., Reyes, A., Macari, A. C., Chang, Y.-H., Paul, B. M., Hermann, B. P., & McDonald, C. R. (2019). Identifying the neural basis of a language-impaired phenotype of temporal lobe epilepsy. *Epilepsia*, *60*(8), 1627–1638. https://doi.org/10.1111/epi.16283

Kardan, O., Stier, A. J., Layden, E. A., Choe, K. W., Lyu, M., Zhang, X., Beilock, S. L., Rosenberg, M. D., & Berman, M. G. (2023). Improvements in task performance after practice are associated with scale-free dynamics of brain

activity. *Network Neuroscience*, *7*(3), 1129–1152. https://doi.org/10.1162/netn_a_00319

Karoly, P. J., Freestone, D. R., Boston, R., Grayden, D. B., Himes, D., Leyde, K., Seneviratne, U., Berkovic, S., O'Brien, T., & Cook, M. J. (2016). Interictal spikes and epileptic seizures: Their relationship and underlying rhythmicity. *Brain*, *139*(4), 1066–1078. https://doi.org/10.1093/brain/aww019

Kashyap, A., Müller, P., Miron, G., & Meisel, C. (2024). Critical dynamics and interictal epileptiform discharge: A comparative analysis with respect to tracking seizure risk cycles. *Frontiers in Network Physiology*, *4*, 1420217. https://doi.org/10.3389/fnetp.2024.1420217

Keller, S. S., Baker, G., Downes, J. J., & Roberts, N. (2009). Quantitative MRI of the prefrontal cortex and executive function in patients with temporal lobe epilepsy. *Epilepsy & Behavior*, *15*(2), 186–195. https://doi.org/10.1016/j.yebeh.2009.03.005

Kessels, R. P., Van Zandvoort, M. J., Postma, A., Kappelle, L. J., & De Haan, E. H. (2000). The corsi block-tapping task: Standardization and normative data [Publisher: Taylor & Francis]. *Applied neuropsychology*, *7*(4), 252–258.

Kinouchi, O., & Copelli, M. (2006). Optimal dynamical range of excitable networks at criticality. *Nature Physics*, *2*(5), 348–351. https://doi.org/10.1038/nphys289

Klaus, A., Yu, S., & Plenz, D. (2011). Statistical analyses support power law distributions found in neuronal avalanches. *PLoS ONE*, *6*(5), 12.

Kleen, J. K., & Kirsch, H. E. (2017). The nociferous influence of interictal discharges on memory. *Brain*, *140*(8), 2072–2074. https://doi.org/10.1093/brain/awx178

Kleen, J. K., Scott, R. C., Holmes, G. L., Roberts, D. W., Rundle, M. M., Testorf, M., Lenck-Santini, P.-P., & Jobst, B. C. (2013). Hippocampal interictal epileptiform activity disrupts cognition in humans. *Neurology*, *81*(1), 18–24. https://doi.org/10.1212/WNL.0b013e318297ee50

Kural, M. A., Duez, L., Sejer Hansen, V., Larsson, P. G., Rampp, S., Schulz, R., Tankisi, H., Wennberg, R., Bibby, B. M., Scherg, M., & Beniczky, S. (2020). Criteria for defining interictal epileptiform discharges in EEG: A clinical validation study. *Neurology*, *94*(20). https://doi.org/10.1212/WNL.0000000000009439

Kwan, P., Sills, G. J., & Brodie, M. J. (2001). The mechanisms of action of commonly used antiepileptic drugs. *Pharmacology & Therapeutics*, *90*(1), 21–34. https://doi.org/10.1016/S0163-7258(01)00122-X

Lam, A. D., Deck, G., Goldman, A., Eskandar, E. N., Noebels, J., & Cole, A. J. (2017). Silent hippocampal seizures and spikes identified by foramen ovale electrodes in alzheimer's disease. *Nature Medicine*, *23*(6), 678–680. https://doi.org/10.1038/nm.4330

Lamberink, H. J., Otte, W. M., Blümcke, I., Braun, K. P. J., Aichholzer, M., Amorim, I., Aparicio, J., Aronica, E., Arzimanoglou, A., Barba, C., Beck, J., Becker, A., Beckervordersandforth, J. C., Bien, C. G., Blümcke, I., Bodi, I., Braun, K. P., Catenoix, H., Chassoux, F., … Anciones, C. (2020). Seizure outcome and

use of antiepileptic drugs after epilepsy surgery according to histopathological diagnosis: A retrospective multicentre cohort study. *The Lancet Neurology*, *19*(9), 748–757. https://doi.org/10.1016/S1474-4422(20)30220-9

Lang, N., Rothkegel, H., Peckolt, H., & Deuschl, G. (2013). Effects of lacosamide and carbamazepine on human motor cortex excitability: A double-blind, placebo-controlled transcranial magnetic stimulation study. *Seizure*, *22*(9), 726–730. https://doi.org/10.1016/j.seizure.2013.05.010

Langton, C. G. (1990). Computation at the edge of chaos: Phase transitions and emergent computation. *Physica D: Nonlinear Phenomena*, *42*(1), 12–37. https://doi.org/10.1016/0167-2789(90)90064-V

Larivière, S., Rodríguez-Cruces, R., Royer, J., Caligiuri, M. E., Gambardella, A., Concha, L., Keller, S. S., Cendes, F., Yasuda, C., Bonilha, L., Gleichgerrcht, E., Focke, N. K., Domin, M., Von Podewills, F., Langner, S., Rummel, C., Wiest, R., Martin, P., Kotikalapudi, R., … Bernhardt, B. C. (2020). Network-based atrophy modeling in the common epilepsies: A worldwide ENIGMA study. *Science Advances*, *6*(47), eabc6457. https://doi.org/10.1126/sciadv.abc6457

Larremore, D. B., Shew, W. L., Ott, E., Sorrentino, F., & Restrepo, J. G. (2014). Inhibition causes ceaseless dynamics in networks of excitable nodes. *Physical Review Letters*, *112*(13), 138103. https://doi.org/10.1103/PhysRevLett.112.138103

Larremore, D. B., Shew, W. L., & Restrepo, J. G. (2011). Predicting criticality and dynamic range in complex networks: Effects of topology. *Physical Review Letters*, *106*(5), 058101. https://doi.org/10.1103/PhysRevLett.106.058101

Lee, H. M., Fadaie, F., Gill, R., Caldairou, B., Sziklas, V., Crane, J., Hong, S.-J., Bernhardt, B. C., Bernasconi, A., & Bernasconi, N. (2022). Decomposing MRI phenotypic heterogeneity in epilepsy: A step towards personalized classification. *Brain*, *145*(3), 897–908. https://doi.org/10.1093/brain/awab425

Li, A., Huynh, C., Fitzgerald, Z., Cajigas, I., Brusko, D., Jagid, J., Claudio, A. O., Kanner, A. M., Hopp, J., Chen, S., Haagensen, J., Johnson, E., Anderson, W., Crone, N., Inati, S., Zaghloul, K. A., Bulacio, J., Gonzalez-Martinez, J., & Sarma, S. V. (2021). Neural fragility as an EEG marker of the seizure onset zone. *Nature Neuroscience*, *24*(10), 1465–1474. https://doi.org/10.1038/s41593-021-00901-w

Li, X., Morgan, P. S., Ashburner, J., Smith, J., & Rorden, C. (2016). The first step for neuroimaging data analysis: DICOM to NIfTI conversion. *Journal of Neuroscience Methods*, *264*, 47–56. https://doi.org/10.1016/j.jneumeth.2016.03.001

Lin, J. J., Mula, M., & Hermann, B. P. (2012). Uncovering the neurobehavioural comorbidities of epilepsy over the lifespan. *The Lancet*, *380*(9848), 1180–1192. https://doi.org/10.1016/S0140-6736(12)61455-X

Linkenkaer-Hansen, K., Nikouline, V. V., Palva, J. M., & Ilmoniemi, R. J. (2001). Long-range temporal correlations and scaling behavior in human brain oscillations. *The Journal of Neuroscience*, *21*(4), 1370–1377. https://doi.org/10.1523/JNEUROSCI.21-04-01370.2001

Löscher, W., Potschka, H., Sisodiya, S. M., & Vezzani, A. (2020). Drug resistance in epilepsy: Clinical impact, potential mechanisms, and new innovative treatment options (E. L. Barker, Ed.). *Pharmacological Reviews*, *72*(3), 606–638. https://doi.org/10.1124/pr.120.019539

Lundstrom, B. N., Brinkmann, B. H., & Worrell, G. A. (2021). Low frequency novel interictal EEG biomarker for localizing seizures and predicting outcomes. *Brain Communications*, *3*(4), fcab231. https://doi.org/10.1093/braincomms/fcab231

Lynch, B. A., Lambeng, N., Nocka, K., Kensel-Hammes, P., Bajjalieh, S. M., Matagne, A., & Fuks, B. (2004). The synaptic vesicle protein SV2a is the binding site for the antiepileptic drug levetiracetam. *Proceedings of the National Academy of Sciences*, *101*(26), 9861–9866. https://doi.org/10.1073/pnas.0308208101

Mahjoory, K., Cesnaite, E., Hohlefeld, F. U., Villringer, A., & Nikulin, V. V. (2019). Power and temporal dynamics of alpha oscillations at rest differentiate cognitive performance involving sustained and phasic cognitive control. *NeuroImage*, *188*, 135–144. https://doi.org/10.1016/j.neuroimage.2018.12.001

Manning, J. R., Jacobs, J., Fried, I., & Kahana, M. J. (2009). Broadband shifts in local field potential power spectra are correlated with single-neuron spiking in humans. *Journal of Neuroscience*, *29*(43), 13613–13620. https://doi.org/10.1523/JNEUROSCI.2041-09.2009

Mariani, B., Nicoletti, G., Bisio, M., Maschietto, M., Vassanelli, S., & Suweis, S. (2022). Disentangling the critical signatures of neural activity. *Scientific Reports*, *12*(1), 10770. https://doi.org/10.1038/s41598-022-13686-0

Maschke, C., O'Byrne, J., Colombo, M. A., Boly, M., Gosseries, O., Laureys, S., Rosanova, M., Jerbi, K., & Blain-Moraes, S. (2024). Critical dynamics in spontaneous EEG predict anesthetic-induced loss of consciousness and perturbational complexity. *Communications Biology*, *7*(1), 946. https://doi.org/10.1038/s42003-024-06613-8

Maturana, M. I., Meisel, C., Dell, K., Karoly, P. J., D'Souza, W., Grayden, D. B., Burkitt, A. N., Jiruska, P., Kudlacek, J., Hlinka, J., Cook, M. J., Kuhlmann, L., & Freestone, D. R. (2020). Critical slowing down as a biomarker for seizure susceptibility. *Nature Communications*, *11*(1), 2172. https://doi.org/10.1038/s41467-020-15908-3

McDonald, C. R., Busch, R. M., Reyes, A., Arrotta, K., Barr, W., Block, C., Hessen, E., Loring, D. W., Drane, D. L., Hamberger, M. J., Wilson, S. J., Baxendale, S., & Hermann, B. P. (2023). Development and application of the international classification of cognitive disorders in epilepsy (IC-CoDE): Initial results from

a multi-center study of adults with temporal lobe epilepsy. *Neuropsychology*, *37*(3), 301–314. https://doi.org/10.1037/neu0000792

Meekes, J., & Jennekens-Schinkel, A. (2018). Effects of interictal epileptiform discharges on cognition. *Journal of Pediatric Epilepsy*, *07*(3), 082–088. https://doi.org/10.1055/s-0038-1676847

Meisel, C. (2020). Antiepileptic drugs induce subcritical dynamics in human cortical networks. *Proceedings of the National Academy of Sciences*, *117*(20), 11118–11125. https://doi.org/10.1073/pnas.1911461117

Meisel, C., Bailey, K., Achermann, P., & Plenz, D. (2017). Decline of long-range temporal correlations in the human brain during sustained wakefulness. *Scientific Reports*, *7*(1), 11825. https://doi.org/10.1038/s41598-017-12140-w

Meisel, C., & Gross, T. (2009). Adaptive self-organization in a realistic neural network model. *Physical Review E*, *80*(6), 061917. https://doi.org/10.1103/PhysRevE.80.061917

Meisel, C., Klaus, A., Kuehn, C., & Plenz, D. (2015). Critical slowing down governs the transition to neuron spiking (B. S. Gutkin, Ed.). *PLOS Computational Biology*, *11*(2), e1004097. https://doi.org/10.1371/journal.pcbi.1004097

Meisel, C., Klaus, A., Vyazovskiy, V. V., & Plenz, D. (2017). The interplay between long- and short-range temporal correlations shapes cortex dynamics across vigilance states. *The Journal of Neuroscience*, *37*(42), 10114–10124. https://doi.org/10.1523/JNEUROSCI.0448-17.2017

Meisel, C., & Kuehn, C. (2012). Scaling effects and spatio-temporal multilevel dynamics in epileptic seizures (M. Perc, Ed.). *PLoS ONE*, *7*(2), e30371. https://doi.org/10.1371/journal.pone.0030371

Meisel, C., Storch, A., Hallmeyer-Elgner, S., Bullmore, E., & Gross, T. (2012). Failure of adaptive self-organized criticality during epileptic seizure attacks (T. Behrens, Ed.). *PLoS Computational Biology*, *8*(1), e1002312. https://doi.org/10.1371/journal.pcbi.1002312

Miller, K. J. (2010). Broadband spectral change: Evidence for a macroscale correlate of population firing rate? *Journal of Neuroscience*, *30*(19), 6477–6479. https://doi.org/10.1523/JNEUROSCI.6401-09.2010

Miron, G., Müller, P. M., Hohmann, L., Oltmanns, F., Holtkamp, M., Meisel, C., & Chien, C. (2024). Cortical thickness patterns of cognitive impairment phenotypes in drug-resistant temporal lobe epilepsy. *Annals of Neurology*, *95*(5), 984–997. https://doi.org/10.1002/ana.26893

Miron, G., Müller, P. M., Holtkamp, M., & Meisel, C. (2023). Prediction of epilepsy surgery outcome using foramen ovale EEG – a machine learning approach. *Epilepsy Research*, 107111. https://doi.org/10.1016/j.eplepsyres.2023.107111

Monto, S., Vanhatalo, S., Holmes, M. D., & Palva, J. M. (2007). Epileptogenic neocortical networks are revealed by abnormal temporal dynamics in seizure-free subdural EEG. *Cerebral Cortex*, *17*(6), 1386–1393. https://doi.org/10.1093/cercor/bhl049

Müller, P. M., & Meisel, C. (2023). Spatial and temporal correlations in human cortex are inherently linked and predicted by functional hierarchy, vigilance state as well as antiepileptic drug load (P. N. Taylor, Ed.). *PLOS Computational Biology*, *19*(3), e1010919. Retrieved March 22, 2023, from https://dx.plos.org/10.1371/journal.pcbi.1010919

Müller, P. M., Miron, G., Holtkamp, M., & Meisel, C. (2024, January 1). *Critical dynamics predict cognitive performance and are disrupted by epileptic spikes, antiseizure medication and slow-wave activity* (preprint). https://doi.org/10.1101/2024.08.19.24312223

Muñoz, M. A., Juhász, R., Castellano, C., & Ódor, G. (2010). Griffiths phases on complex networks. *Physical Review Letters*, *105*(12), 128701. https://doi.org/10.1103/PhysRevLett.105.128701

Murray, J. D., Bernacchia, A., Freedman, D. J., Romo, R., Wallis, J. D., Cai, X., Padoa-Schioppa, C., Pasternak, T., Seo, H., Lee, D., & Wang, X.-J. (2014). A hierarchy of intrinsic timescales across primate cortex. *Nature Neuroscience*, *17*(12), 1661–1663. https://doi.org/10.1038/nn.3862

Nir, Y., Fisch, L., Mukamel, R., Gelbard-Sagiv, H., Arieli, A., Fried, I., & Malach, R. (2007). Coupling between neuronal firing rate, gamma LFP, and BOLD fMRI is related to interneuronal correlations. *Current Biology*, *17*(15), 1275–1285. https://doi.org/10.1016/j.cub.2007.06.066

Ossemann, M., de Fays, K., Bihin, B., & Vandermeeren, Y. (2016). Effect of a single dose of retigabine in cortical excitability parameters: A cross-over, double-blind placebo-controlled TMS study. *Epilepsy Research*, *126*, 78–82. https://doi.org/10.1016/j.eplepsyres.2016.06.004

Palva, J. M., Zhigalov, A., Hirvonen, J., Korhonen, O., Linkenkaer-Hansen, K., & Palva, S. (2013). Neuronal long-range temporal correlations and avalanche dynamics are correlated with behavioral scaling laws. *Proceedings of the National Academy of Sciences*, *110*(9), 3585–3590. https://doi.org/10.1073/pnas.1216855110

Pardoe, H. R., Cole, J. H., Blackmon, K., Thesen, T., & Kuzniecky, R. (2017). Structural brain changes in medically refractory focal epilepsy resemble premature brain aging. *Epilepsy Research*, *133*, 28–32. https://doi.org/10.1016/j.eplepsyres.2017.03.007

Parvizi, J., & Kastner, S. (2018). Promises and limitations of human intracranial electroencephalography. *Nature Neuroscience*, *21*(4), 474–483. https://doi.org/10.1038/s41593-018-0108-2

Pedregosa, F., Varoquaux, G., Gramfort, A., Michel, V., Thirion, B., Grisel, O., Blondel, M., Prettenhofer, P., Weiss, R., Dubourg, V., Vanderplas, J., Passos, A., Cournapeau, D., Brucher, M., Perrot, M., & Duchesnay, E. (2011). Scikit-learn: Machine learning in python. *Journal of Machine Learning Research*, *12*, 2825–2830.

Petermann, T., Thiagarajan, T. C., Lebedev, M. A., Nicolelis, M. A. L., Chialvo, D. R., & Plenz, D. (2009). Spontaneous cortical activity in awake monkeys composed of neuronal avalanches. *Proceedings of the National Academy of Sciences*, *106*(37), 15921–15926. https://doi.org/10.1073/pnas.0904089106

Poil, S.-S., Jansen, R., van Aerde, K., Timmerman, J., Brussaard, A. B., Mansvelder, H. D., & Linkenkaer-Hansen, K. (2011). Fast network oscillations in vitro exhibit a slow decay of temporal auto-correlations: Stability of fast network oscillations. *European Journal of Neuroscience*, *34*(3), 394–403. https://doi.org/10.1111/j.1460-9568.2011.07748.x

Poil, S.-S., Hardstone, R., Mansvelder, H. D., & Linkenkaer-Hansen, K. (2012). Critical-state dynamics of avalanches and oscillations jointly emerge from balanced excitation/inhibition in neuronal networks. *Journal of Neuroscience*, *32*(29), 9817–9823. https://doi.org/10.1523/JNEUROSCI.5990-11.2012

Premoli, I., Costantini, A., Rivolta, D., Biondi, A., & Richardson, M. P. (2017). The effect of lamotrigine and levetiracetam on TMS-evoked EEG responses depends on stimulation intensity. *Frontiers in Neuroscience*, *11*, 585. https://doi.org/10.3389/fnins.2017.00585

Priesemann, V., Valderrama, M., Wibral, M., & Le Van Quyen, M. (2013). Neuronal avalanches differ from wakefulness to deep sleep – evidence from intracranial depth recordings in humans (O. Sporns, Ed.). *PLoS Computational Biology*, *9*(3), e1002985. https://doi.org/10.1371/journal.pcbi.1002985

Quon, R. J., Meisenhelter, S., Camp, E. J., Testorf, M. E., Song, Y., Song, Q., Culler, G. W., Moein, P., & Jobst, B. C. (2022). AiED: Artificial intelligence for the detection of intracranial interictal epileptiform discharges. *Clinical Neurophysiology*, *133*, 1–8. https://doi.org/10.1016/j.clinph.2021.09.018

Raut, R. V., Snyder, A. Z., & Raichle, M. E. (2020). Hierarchical dynamics as a macroscopic organizing principle of the human brain. *Proceedings of the National Academy of Sciences*, *117*(34), 20890–20897. https://doi.org/10.1073/pnas.2003383117

Reed, C. M., Birch, K. G., Kamiński, J., Sullivan, S., Chung, J. M., Mamelak, A. N., & Rutishauser, U. (2017). Automatic detection of periods of slow wave sleep based on intracranial depth electrode recordings. *Journal of Neuroscience Methods*, *282*, 1–8. https://doi.org/10.1016/j.jneumeth.2017.02.009

Reyes, A., Kaestner, E., Bahrami, N., Balachandra, A., Hegde, M., Paul, B. M., Hermann, B., & McDonald, C. R. (2019). Cognitive phenotypes in temporal lobe epilepsy are associated with distinct patterns of white matter network abnormalities. *Neurology*, *92*(17), e1957–e1968. https://doi.org/10.1212/WNL.0000000000007370

Reyes, A., Salinas, L., Hermann, B. P., Baxendale, S., Busch, R. M., Barr, W. B., & McDonald, C. R. (2023). Establishing the cross-cultural applicability of a harmonized approach to cognitive diagnostics in epilepsy: Initial results of

the international classification of cognitive disorders in epilepsy in a spanish-speaking sample. *Epilepsia*, *64*(3), 728–741. https://doi.org/10.1111/epi.17501

Ribeiro, T. L., Copelli, M., Caixeta, F., Belchior, H., Chialvo, D. R., Nicolelis, M. A. L., & Ribeiro, S. (2010). Spike avalanches exhibit universal dynamics across the sleep-wake cycle (O. Sporns, Ed.). *PLoS ONE*, *5*(11), e14129. https://doi.org/10.1371/journal.pone.0014129

Rixecker, H., & Hartje, W. (1980). Kimura's recurring-figures-test: A normative study. *Journal of Clinical Psychology*, *36*(2), 465–467. https://doi.org/10.1002/jclp.6120360213

Rodríguez-Cruces, R., Velázquez-Pérez, L., Rodríguez-Leyva, I., Velasco, A. L., Trejo-Martínez, D., Barragán-Campos, H. M., Camacho-Téllez, V., & Concha, L. (2018). Association of white matter diffusion characteristics and cognitive deficits in temporal lobe epilepsy. *Epilepsy & Behavior*, *79*, 138–145. https://doi.org/10.1016/j.yebeh.2017.11.040

Ryvlin, P., Cross, J. H., & Rheims, S. (2014). Epilepsy surgery in children and adults. *The Lancet Neurology*, *13*(11), 1114–1126. https://doi.org/10.1016/S1474-4422(14)70156-5

Saetre, E., & Abdelnoor, M. (2018). Incidence rate of sudden death in epilepsy: A systematic review and meta-analysis. *Epilepsy & Behavior*, *86*, 193–199. https://doi.org/10.1016/j.yebeh.2018.06.037

Sankar, R., & Holmes, G. L. (2004). Mechanisms of action for the commonly used antiepileptic drugs: Relevance to antiepileptic drug-associated neurobehavioral adverse effects. *Journal of Child Neurology*, *19*(1), S6–S14. https://doi.org/10.1177/088307380401900102

Scheffer, I. E., Berkovic, S., Capovilla, G., Connolly, M. B., French, J., Guilhoto, L., Hirsch, E., Jain, S., Mathern, G. W., Moshé, S. L., Nordli, D. R., Perucca, E., Tomson, T., Wiebe, S., Zhang, Y.-H., & Zuberi, S. M. (2017). ILAE classification of the epilepsies: Position paper of the ILAE commission for classification and terminology. *Epilepsia*, *58*(4), 512–521. https://doi.org/10.1111/epi.13709

Scheffer, M., Bascompte, J., Brock, W. A., Brovkin, V., Carpenter, S. R., Dakos, V., Held, H., van Nes, E. H., Rietkerk, M., & Sugihara, G. (2009). Early-warning signals for critical transitions. *Nature*, *461*(7260), 53–59. https://doi.org/10.1038/nature08227

Sethna, J. P., Dahmen, K. A., & Myers, C. R. (2001). Crackling noise. *Nature*, *410*(6825). https://doi.org/10.1038/35065675

Shew, W. L., Yang, H., Petermann, T., Roy, R., & Plenz, D. (2009). Neuronal avalanches imply maximum dynamic range in cortical networks at criticality. *Journal of Neuroscience*, *29*(49), 15595–15600. https://doi.org/10.1523/JNEUROSCI.3864-09.2009

Shew, W. L., Yang, H., Yu, S., Roy, R., & Plenz, D. (2011). Information capacity and transmission are maximized in balanced cortical networks with neuronal

avalanches. *Journal of Neuroscience*, *31*(1), 55–63. https://doi.org/10.1523/JNEUROSCI.4637-10.2011

Shew, W. L., Clawson, W. P., Pobst, J., Karimipanah, Y., Wright, N. C., & Wessel, R. (2015). Adaptation to sensory input tunes visual cortex to criticality. *Nature Physics*, *11*(8), 659–663. https://doi.org/10.1038/nphys3370

Shew, W. L., & Plenz, D. (2013). The functional benefits of criticality in the cortex. *The Neuroscientist*, *19*(1), 88–100. https://doi.org/10.1177/1073858412445487

Simola, J., Zhigalov, A., Morales-Muñoz, I., Palva, J. M., & Palva, S. (2017). Critical dynamics of endogenous fluctuations predict cognitive flexibility in the go/NoGo task. *Scientific Reports*, *7*(1), 2909. https://doi.org/10.1038/s41598-017-02750-9

Sormunen, S., Gross, T., & Saramäki, J. (2023). Critical drift in a neuro-inspired adaptive network. *Physical Review Letters*, *130*(18), 188401. https://doi.org/10.1103/PhysRevLett.130.188401

Sorrentino, P., Rabuffo, G., Baselice, F., Troisi Lopez, E., Liparoti, M., Quarantelli, M., Sorrentino, G., Bernard, C., & Jirsa, V. (2023). Dynamical interactions reconfigure the gradient of cortical timescales. *Network Neuroscience*, *7*(1), 73–85. https://doi.org/10.1162/netn_a_00270

Sporns, O. (2010). Networks of the brain: Quantitative analysis and modeling, 7.

Steffener, J. (2021). Education and age-related differences in cortical thickness and volume across the lifespan. *Neurobiology of Aging*, *102*, 102–110. https://doi.org/10.1016/j.neurobiolaging.2020.10.034

Strogatz, S. H. (2015). *Nonlinear dynamics and chaos: With applications to physics, biology, chemistry, and engineering* (Second edition) [OCLC: ocn842877119]. Westview Press, a member of the Perseus Books Group.

Strzelczyk, A., & Schubert-Bast, S. (2022). Psychobehavioural and cognitive adverse events of anti-seizure medications for the treatment of developmental and epileptic encephalopathies. *CNS Drugs*, *36*(10), 1079–1111. https://doi.org/10.1007/s40263-022-00955-9

Sudbrack-Oliveira, P., Lima Najar, L., Foldvary-Schaefer, N., & Da Mota Gomes, M. (2019). Sleep architecture in adults with epilepsy: A systematic review. *Sleep Medicine*, *53*, 22–27. https://doi.org/10.1016/j.sleep.2018.09.004

Tagliazucchi, E., Balenzuela, P., Fraiman, D., & Chialvo, D. R. (2012). Criticality in large-scale brain fMRI dynamics unveiled by a novel point process analysis. *Frontiers in Physiology*, *3*. https://doi.org/10.3389/fphys.2012.00015

Tatum, W. O. (2022). EEG essentials. *CONTINUUM: Lifelong Learning in Neurology*, *28*(2), 261–305. https://doi.org/10.1212/CON.0000000000001129

Tononi, G. (2008). Consciousness as integrated information: A provisional manifesto. *The Biological Bulletin*, *215*(3), 216–242. https://doi.org/10.2307/25470707

Touboul, J., & Destexhe, A. (2010). Can power-law scaling and neuronal avalanches arise from stochastic dynamics? (O. Sporns, Ed.). *PLoS ONE*, *5*(2), e8982. https://doi.org/10.1371/journal.pone.0008982

Tustison, N. J., Avants, B. B., Cook, P. A., Yuanjie Zheng, Egan, A., Yushkevich, P. A., & Gee, J. C. (2010). N4itk: Improved n3 bias correction. *IEEE Transactions on Medical Imaging*, *29*(6), 1310–1320. https://doi.org/10.1109/TMI.2010.2046908

Van Essen, D. C., Smith, S. M., Barch, D. M., Behrens, T. E., Yacoub, E., & Ugurbil, K. (2013). The WU-minn human connectome project: An overview. *NeuroImage*, *80*, 62–79. https://doi.org/10.1016/j.neuroimage.2013.05.041

von Ellenrieder, N., Peter-Derex, L., Gotman, J., & Frauscher, B. (2022). SleepSEEG: Automatic sleep scoring using intracranial EEG recordings only. *Journal of Neural Engineering*, *19*(2), 026057. https://doi.org/10.1088/1741-2552/ac6829

Vyazovskiy, V. V., Olcese, U., Hanlon, E. C., Nir, Y., Cirelli, C., & Tononi, G. (2011). Local sleep in awake rats. *Nature*, *472*(7344), 443–447. https://doi.org/10.1038/nature10009

Wasmuht, D. F., Spaak, E., Buschman, T. J., Miller, E. K., & Stokes, M. G. (2018). Intrinsic neuronal dynamics predict distinct functional roles during working memory. *Nature Communications*, *9*(1), 3499. https://doi.org/10.1038/s41467-018-05961-4

Weidlich, S., & Lamberti, G. (2001). *DCS - Diagnosticum für Cerebralschädigung: ein visueller Lern- und Gedächtnistest ; nach F. Hillers ; Manual*. Huber. https://books.google.de/books?id=yAkmAAAACAAJ

Weiss, S. A., Lemesiou, A., Connors, R., Banks, G. P., McKhann, G. M., Goodman, R. R., Zhao, B., Filippi, C. G., Nowell, M., Rodionov, R., Diehl, B., McEvoy, A. W., Walker, M. C., Trevelyan, A. J., Bateman, L. M., Emerson, R. G., & Schevon, C. A. (2015). Seizure localization using ictal phase-locked high gamma: A retrospective surgical outcome study. *Neurology*, *84*(23), 2320–2328. https://doi.org/10.1212/WNL.0000000000001656

Welte, V. (1981). Der Mottier-Test, ein Prüfmittel für die Lautdifferenzierungsfähigkeit und die auditive Merkfähigkeit.

Whittingstall, K., & Logothetis, N. K. (2009). Frequency-band coupling in surface EEG reflects spiking activity in monkey visual cortex. *Neuron*, *64*(2), 281–289. https://doi.org/10.1016/j.neuron.2009.08.016

Wilting, J., & Priesemann, V. (2019). Between perfectly critical and fully irregular: A reverberating model captures and predicts cortical spike propagation. *Cerebral Cortex*, *29*(6), 2759–2770. https://doi.org/10.1093/cercor/bhz049

Wilting, J., Dehning, J., Pinheiro Neto, J., Rudelt, L., Wibral, M., Zierenberg, J., & Priesemann, V. (2018). Operating in a reverberating regime enables rapid tuning of network states to task requirements. *Frontiers in Systems Neuroscience*, *12*, 55. https://doi.org/10.3389/fnsys.2018.00055

Wodeyar, A., Chinappen, D., Mylonas, D., Baxter, B., Manoach, D. S., Eden, U. T., Kramer, M. A., & Chu, C. J. (2024). Thalamic epileptic spikes disrupt sleep

spindles in patients with epileptic encephalopathy. *Brain*, *147*(8), 2803–2816. https://doi.org/10.1093/brain/awae119

Worrell, G. A., Cranstoun, S. D., Echauz, J., & Litt, B. (2002). Evidence for self-organized criticality in human epileptic hippocampus. *NeuroReport*, *13*(16). https://doi.org/10.1097/00001756-200211150-00005

Xu, Y., Schneider, A., Wessel, R., & Hengen, K. B. (2024). Sleep restores an optimal computational regime in cortical networks. *Nature Neuroscience*. https://doi.org/10.1038/s41593-023-01536-9

Yang, H., Shew, W. L., Roy, R., & Plenz, D. (2012). Maximal variability of phase synchrony in cortical networks with neuronal avalanches. *Journal of Neuroscience*, *32*(3), 1061–1072. https://doi.org/10.1523/JNEUROSCI.2771-11.2012

Yger, P., El Boustani, S., Destexhe, A., & Frégnac, Y. (2011). Topologically invariant macroscopic statistics in balanced networks of conductance-based integrate-and-fire neurons. *Journal of Computational Neuroscience*, *31*(2), 229–245. https://doi.org/10.1007/s10827-010-0310-z

Yu, S., Klaus, A., Yang, H., & Plenz, D. (2014). Scale-invariant neuronal avalanche dynamics and the cut-off in size distributions (D. R. Chialvo, Ed.). *PLoS ONE*, *9*(6), e99761. https://doi.org/10.1371/journal.pone.0099761

Zapperi, S., Lauritsen, K. B., & Stanley, H. E. (1995). Self-organized branching processes: Mean-field theory for avalanches. *Physical Review Letters*, *75*(22), 4071–4074. https://doi.org/10.1103/PhysRevLett.75.4071

Ziemann, U., Lönnecker, S., Steinhoff, B. J., & Paulus, W. (1996). Effects of antiepileptic drugs on motor cortex excitability in humans: A transcranial magnetic stimulation study: Antiepileptic drugs and excitability of human cortex. *Annals of Neurology*, *40*(3), 367–378. https://doi.org/10.1002/ana.410400306

Zimmermann, P., & Fimm, B. (1992). *Testbatterie zur Aufmerksamkeitsprüfung:(TAP)*. Psytest.

Zimmern, V. (2020). Why brain criticality is clinically relevant: A scoping review. *Frontiers in Neural Circuits*, *14*, 54. https://doi.org/10.3389/fncir.2020.00054

Zschocke, S., & Hansen, H.-C. (Eds.). (2023). *Klinische Elektroenzephalographie*. Springer Berlin Heidelberg. https://doi.org/10.1007/978-3-662-63267-3